INFORMATION TO USERS

This dissertation was produced from a microfilm copy of the original document. While the most advanced technological means to photograph and reproduce this document have been used, the quality is heavily dependent upon the quality of the original submitted.

The following explanation of techniques is provided to help you understand markings or patterns which may appear on this reproduction.

1. The sign or "target" for pages apparently lacking from the document photographed is "Missing Page(s)". If it was possible to obtain the missing page(s) or section, they are spliced into the film along with adjacent pages. This may have necessitated cutting thru an image and duplicating adjacent pages to insure you complete continuity.

2. When an image on the film is obliterated with a large round black mark, it is an indication that the photographer suspected that the copy may have moved during exposure and thus cause a blurred image. You will find a good image of the page in the adjacent frame.

3. When a map, drawing or chart, etc., was part of the material being photographed the photographer followed a definite method in "sectioning" the material. It is customary to begin photoing at the upper left hand corner of a large sheet and to continue photoing from left to right in equal sections with a small overlap. If necessary, sectioning is continued again — beginning below the first row and continuing on until complete.

4. The majority of users indicate that the textual content is of greatest value, however, a somewhat higher quality reproduction could be made from "photographs" if essential to the understanding of the dissertation. Silver prints of "photographs" may be ordered at additional charge by writing the Order Department, giving the catalog number, title, author and specific pages you wish reproduced.

University Microfilms

300 North Zeeb Road
Ann Arbor, Michigan 48106

A Xerox Education Company

THE HALL EFFECT IN CuAu(Fe) ALLOYS

by

RANDALL CATON

A dissertation submitted to the Graduate Faculty in Physics in partial fulfillment of the requirements for the degree of Doctor of Philosophy, The City University of New York.

1972

This manuscript has been read and accepted for the Graduate Faculty in Physics in satisfaction of the dissertation requirement for the degree of Doctor of Philosophy.

12/18/72
date

Myriam P. Sarachek
Chairman of Examining Committee

12/18/72
date

Marvin H. Mittleman
Executive Officer

Harry Lipsdat
Myron Strongin
Donald R. Hamann
Philip E. Bloomfield
Supervisory Committee

The City University of New York

ACKNOWLEDGEMENTS

The author would like to acknowledge the efforts of his mentor Professor Myriam P. Sarachik. Her guidance, assistance, discussion, and enthusiastic support were most valuable and were greatly appreciated.

Further, the author wishes to acknowledge many valuable discussions with Drs. Donald Hamann and Philip Bloomfield. Also discussions with Drs. Colin Hurd, Simon Foner, and Richard More were most useful.

In designing and building the experimental apparatus, the helpful guidance, suggestions, and assistance of Dr. Robert Houghton and the suggestions and assistance of the City College machine shop were greatly appreciated.

The author would like to thank his fellow Ph.D. student Mr. James Haddad for his assistance in preparing the samples.

Finally, the author is grateful for the patience and endurance of Mrs. Nechama Block and Mrs. Bella Heimann for the typing of this thesis.

TABLE OF CONTENTS

I. INTRODUCTION

This work presents data for the Hall effect in a metal alloy system containing dilute amounts of a magnetic impurity, and examines this data in light of existing theories and ideas.

Susceptibility measurements of very dilute alloys of third-row transition metals in other metals often indicate the presence of a localized magnetic moment at each transition metal "impurity" atom. As the temperature is lowered, the localized moments gradually disappear around a characteristic temperature T_k which depends on both the impurity and the host. They can be restored by raising the temperature again or applying a magnetic field large enough that $g\mu_B H > kT_k$. Anomalous temperature dependences in the resistivities and specific heats of these alloys around T_k are other indications of the change in the state of each impurity. Theoretical calculations show that many-body effects lead to a compensation of the impurity moments by oppositely-polarized host conduction electrons at low temperatures, and give estimates for the characteristic temperature T_k. The overall correctness of the theoretical picture for the susceptibility, resistivity, and specific heat has been fairly well established. Further calculations show that this transition leads to an anomalous contribution to the Hall coefficient as a function of temperature and field. The purpose of our experiment is to observe this anomalous behavior.

The system chosen for study was Cu-Au (Fe) which has several

advantages, perhaps the most important of which is the fact that as Au is added to Cu, T_k decreases continuously from roughly 30° K to 0.3° K. This allows us to study the effect of varying T_k. Hall coefficient data was taken on the $Cu_{1-x}Au_x$ (Fe) system from $x = 0$ to $x = 1$. The measurements were made at 1.5° K and 4.2° K in fields from 0 to 60 kG. The observed variations of the Hall coefficient as a function of temperature and field are discussed in terms of a gradual transition from the spin-compensated state to the magnetic state.

II. BACKGROUND INFORMATION

We begin by summarizing, in a brief review, some of the pertinent background information. We will start with discussions of the Hall Effect (Section A) and the magnetic impurity problem (Section B) separately, and close this section with a discussion of the Hall Effect in magnetic impurity systems (Section C).

A. The Hall Effect

In 1879 E.H. Hall[1] observed that a voltage was developed transverse to an electric current passing through a plane oriented perpendicular to a magnetic field (See Fig. 1). This effect, known as the Hall Effect, has been used along with magnetoresistance measurements, to determine mobilities and carrier concentrations in semiconductors. In metals, this effect has given qualitative information about the departure from free electron behavior. Band theory has been quite successful in describing much of the Hall effect data, and we will need to draw on the concepts of this theory to discuss our results.

(1) Definition of the Hall Coefficient

The Hall coefficient is defined as $R = \frac{Vt}{IH}$, where V is the Hall voltage, t is the sample thickness, I the current, and H is the magnetic field. Practical units most often used are $\frac{\text{volt-cm}}{\text{amp-gauss}}$. Conversion to other units is discussed in Appendix F. Results on Hall effect measurements are often presented in terms of a Hall resistivity, defined by the expression $\rho_H = \frac{Vt}{I}$. Although this has the dimensions of resistivity,

it differs from ordinary resistivity in that V, t and I are all mutually perpendicular. Another quantity often quoted is the Hall angle $\tan \phi = E/E_L$, the ratio of the Hall electric field to the longitudinal electric field; then $\tan \phi = \rho_H \sigma$, where σ is the electrical conductivity.

(2) Free Electron Model

In this case, a simple derivation of the Hall effect is possible, and a simple physical picture of the mechanism emerges. If we consider the geometry shown in Fig. 1, the electrons will be deflected in the positive y direction by a magnetic field in the z direction. The electrons will tend to accumulate on the positive y surface. This will result in an electric field force acting on the electrons in the negative y direction. Equilibrium will be reached when the magnetic and electric field forces on the electrons are equal in magnitude. The electrons will then flow straight through with zero net transverse force acting on them. Thus we obtain the condition $(F_m) = (F_e)$, or $\frac{e}{c} v H = e E$. Noting that $J = nev = \frac{I}{A} = \frac{I}{Wt}$, and $E = \frac{V}{W}$ for the above charge distribution, we have

$$\frac{e}{c} \left(\frac{I}{neWt} \right) H = e \left(\frac{V}{W} \right)$$

resulting in $R = \frac{Vt}{IH} = \frac{1}{nec}$ (cgs) where n is the number of carriers in a unit volume, and e is the charge of the carrier (negative for electrons). In this simple case R is independent of field and temperature; this is not true in real materials where a more realistic model must be considered.

We can also calculate the Hall angle for this simple model. Tan ϕ =

$RH\sigma = \frac{1}{nec} H \frac{ne^2\tau}{m} = \omega_c\tau$ where ω_c is the cyclotron frequency, m is the electron mass and τ is the electronic lifetime.

(3) Hall Effect in Noble Metals

Table 1 shows observed values of R for the noble metals, and values of R calculated using the free electron model. It is clear that the free electron model does not adequately describe the noble metals. The first orderly and detailed explanation of these discrepancies was undertaken by Ziman[2]. At that time the qualitative shape of the Fermi surface had been established for the noble metals[3]. A rough sketch appears in Figs. 2 and 3. There is a marked distortion from the free electron sphere, especially along the 111 direction where it actually touches the Brillouin zone boundary. Ziman[2] constructed an eight-cone model as a crude approximation of the noble metal Fermi surface. In this approximation, assuming lifetime to be a valid concept, he calculated R to be

$$\frac{\frac{e^3}{3\pi^2 c\hbar}\int \tau_k^2\left[(v_x^2+v_y^2)M_{zz}^{-1}+(v_y^2+v_z^2)M_{xx}^{-1}+(v_z^2+v_x^2)M_{yy}^{-1}\right]\frac{dS}{v}}{\left\{\frac{e^2}{12\pi^2\hbar}\int v\tau_k\,dS\right\}^2}$$

where the integrals are over the Fermi surface, τ_k is the relaxation time, and M_{zz}^{-1}, etc. are the inverse mass tensors. The contribution from the necks (See Fig.2) to M_{zz}^{-1} is negative and this reduces the Hall coefficient from the free electron value. However, if one makes the simplifying assumption that τ_k is isotropic, then this overcompensates, and to get a correct value of R Ziman allows for variation in τ_k

over the Fermi surface. In particular, he assumes τ_k on the neck is less than τ_k on the bellies. This will reduce the negative contribution and raise R back to the proper value. A recent review by Springford[4] discusses this topic further. It has been shown by more direct measurements[5] that τ neck $< \tau$ belly at low temperatures. However, for room temperature it appears that τ_k is isotropic[6].

The electron-phonon scattering in pure metals is relatively well understood. However, the contribution to the Hall coefficient from the scattering of electrons by impurities presents yet unsolved problems in noble metals.

(4) Noble Metal-Noble Metal Alloys

We will limit our discussion to the Cu-Au and Ag-Au systems because data exist for the entire composition range of these alloys. The resistivities of disordered Cu-Au and Ag-Au alloys behave in the classical manner as a function of composition[7]. They follow the Nordheim rule which states $\rho \alpha c(1-c)$ where c is the solute concentration.

The Hall data for the two systems are not similar. The Ag-Au data have been analyzed in some detail by Hurd[8] and Heine[9]. They found that the Hall coefficient could be split into two contributions. One contribution is small and linear in concentration and is the result of a continuous change in band structure upon alloying Au into Ag. The other contributions was an impurity contribution (Au in Ag or Ag in Au) and its concentration dependence is ultimately based on the Nordeim

rule ($\tau a \frac{1}{c(1-c)}$)[9]. Unfortunately, the Hall data for Cu-Au[10] (See Fig. 10) cannot be analyzed in such a simple manner. It does not separate into two nicely analyzed contributions as for Ag-Au. Barnard, et al. used a two band[11] model, where

$$R = \frac{1}{ec} \frac{\frac{n_B \tau_B^2}{m_B^2} - \frac{n_N \tau_N^2}{m_N^2}}{\left(\frac{n_B \tau_B}{m_B} + \frac{n_N \tau_N}{m_N} \right)^2}$$

Here B refers to belly contributions and N refers to neck contributions (See Fig. 2). They ascribed the change in R to a variation in τ_N/τ_B, while n_N/n_B and m_N/m_B remained constant. However, without an explanation of the variation of τ_N/τ_B with host composition (theoretically or experimentally), this conjecture is not too useful. We can safely say that little is understood about the variation of R in Cu-Au. Certainly, the difference in lattice constants for Ag, Au and Cu must be taken into account. The lattice constants for Ag (4.08 A^o) and Au (4.07 A^o) are almost the same, while Cu (3.61 A^o)is quite different.

It is interesting to note the qualitative difference between the resistivity data and the Hall data. In the multi-band picture, the resistivity depends upon the direct sums of lifetimes. This is just an average over the Fermi surface and can be explained by a relatively simple theory. In contrast, the Hall effect is very sensitive to contributions from different parts of the Fermi surface, which may have different signs, and the resulting description is much more complex. This difference is

a general feature of resistivity versus Hall data.

Although the understanding of the Hall data is vague and incomplete, and many parameters important to the data are not known, it is clear that the lifetime is not isotropic over the Fermi surface at low temperatures and it is necessary to resort to (at least) two bands to describe the data in the Ag-Au and Cu-Au systems.

B. Magnetic Impurity Problem

Much has been written on this topic, and we will discuss only briefly the basic ideas which have led to some understanding of the problem of dilute magnetic alloys. Detailed reviews exist by Van den Berg[12], Daybell and Steyert[13], Heeger[14], and Kondo[15]. The reviews by Van den Berg and by Daybell and Steyert are from an experimental point of view; Kondo's review is theoretical in nature; and Heeger's review examines, in some detail, the data in light of existing theories.

In the present context, dilute shall be defined as the limit in which the magnetic impurities do not interact with one another. In this limit the results for n impurities can be obtained from the results for a single impurity, by superposition. Experimentally, one is guided by the concentration dependence of various physical properties to determine whether or not the above conditions are met.

We consider the effect, then, of placing an isolated magnetic impurity in a non-magnetic host. In this case the important interaction is between the impurity and the conduction electrons of the host. The

problem was first treated in the one-electron approximation, which works well in the non-magnetic case. However, in the magnetic case this approximation breaks down, and it is necessary to consider a many-body problem.

We will start by considering some of the early ideas of Friedel[16,17] as applied to impurities in general. In an isolated atom the energy levels are sharp. However, if we put this atom into a metal as an impurity, and if one of its outer atomic orbitals (d states in transition metals) falls within the conduction band, this orbital will resonate with the conduction electrons of the same energy. For transition metals this results in a state occupying a region in energy, localized on the impurity, and of strong d character. This is called a virtual bound state, for it is not truly bound like the core states, yet it does have some localization.

Friedel[17] has formulated these concepts on a more mathematical basis by treating the electrons as free and independent, and assuming the perturbation of the impurity to be spherical. He then analyzes the perturbation in terms of spherical harmonics. This results in the virtual bound state being broadened in energy (in a Lorentzian way) about the resonant energy.

In light of this, it is interesting to consider the case of transition metal impurities in Al. Measurements of the excess resistivity due to various impurities ranging from Ti to Ni show a maximum near Cr. For

Ti the impurity d level is above the Fermi energy of the Al host, and for Ni it lies below. In between (for Cr) the d level lies near the Fermi energy and thus causes strongest resonant scattering, which is evidenced as a peak in the excess resistivity. It is interesting that there is only one peak, even though for reasons outlined below, one would expect the d state to be split into several levels. Apparently, the virtual bound level is so broadened and the individual states split so little that they are not discernible.

Friedel[17] discusses three possible mechanisms for splitting the d^{10} level. The crystalline field in a cubic lattice splits the d^{10} level into two states (x^2-y^2 like and xy like). However, this splitting is observed to be very small (a fraction of an electron volt), and it is not expected to play an appreciable role. Coulomb correlations between the d states would split the d^{10} level into ten states. Finally exchange correlations split the d^{10} level into two d^5 levels of opposite spin.

A striking feature of the residual resistivity data for transition metal impurities in Cu, Au, and Ag is the existence of two peaks, one at V and the other at Fe. Friedel correctly ascribed this to a splitting of the virtual bound state into spin-up and spin-down states, where the splitting is greater than the width of the virtual state. Thus two separate resonances can be discerned.

Anderson[18] built on the ideas of Friedel and formulated the problem by starting with the Hamiltonian:

$$H = H_{0f} + H_{0d} + H_{corr} + H_{sd}$$

The first two terms are the unperturbed energies of the free electron system and the d states on the impurity, respectively. $H_{corr} = U n_\uparrow n_\downarrow$ is the Coulomb repulsive energy between two opposite spin electrons on the same d orbital. This term is responsible for the splitting of the spin states which gives rise to magnetism. H_{sd} is a mixing term between the free electrons and d states, which broadens the impurity state into a virtual level. Anderson solves the problem self-consistently in the Hartree-Fock approximation. He assumes a split d state in which one level (say spin down) is below the Fermi energy by an amount E, and the other level (spin up) is split by the Coulomb repulsion U and is above the Fermi energy by U - E. He then obtains conditions for the stability of this state. For the simple case of a single non-degenerate level, Anderson obtains a broadening of the state to width Δ through the s-d mixing term. The condition[19] for magnetism is $\frac{U}{\pi \Delta} > 1$. This, however, is also the condition for the breakdown of the Hartree-Fock approximation. As Schrieffer[20] points out, in this limit "the interaction time $\tau_U = \hbar/U$ is less than the time $\tau_\Delta = \hbar/\Delta$ required for electrons to hop on or off the impurity into the band." Hartree-Fock theory breaks down because an electron on the impurity interacts with the electrons nearby at that instant and does not see an average potential through interaction with all the electrons as assumed by Hartree-Fock. It is a true many-body problem because previous electron-impurity encounters will affect what the next conduction electron sees. Therefore, properties of these systems can only be calculated by Hartree-Fock theory

in the non-magnetic limit $U < \Delta$. A many-electron theory must be used to calculate properties in the magnetic limit. In spite of these difficulties with the theory, the concept of a local magnetic moment arising from the splitting of the spin up and spin down d levels, which are broadened in space and energy, is quite useful in describing such systems as Cu (Fe), Cu (Mn), etc.

One of the most striking features of local magnetic moment systems is the existence of a resistivity minimum as a function of temperature. Experimentally, this minimum was first connected intimately with the existence of a local moment by work of Sarachik et. al.[21,22] on Fe impurities in Nb-Mo and Mo-Re alloys. Kondo[23] gave an explanation of the minimum in a theoretical calculation of the resistivity of local magnetic moment systems. Kondo assumes that a local moment does indeed exist on the impurity, and calculates the resistivity of such a system using a $J\vec{S}\cdot\vec{s}$ Hamiltonian, where $\vec{S}$ is the impurity spin and $\vec{s}$ is the conduction electron spin. He calculates the conduction electron-impurity scattering to second Born approximation. To illustrate the important contributions to the calculation, we consider the scattering from the initial state $|k\uparrow, d\downarrow\rangle$ to the final state $|k'\uparrow, d\downarrow\rangle$, where k refers to conduction electrons and d refers to impurity electrons, and $\uparrow$ and $\downarrow$ refer to spin direction. For this initial and final state, the second order processes are as follows:

(1) $k\uparrow$ goes to $k'\uparrow$ via $k''\uparrow$

(2) The exchange of (1)

(3) $k\uparrow$ goes to $k'\uparrow$ via $k''\downarrow$. Here the impurity spin is flipped to conserve angular momentum.

Note that the exchange of (3) is not allowed because it cannot conserve angular momentum. Due to the absence of this exchange term, cancellation of the singular terms in the sum $\langle k'\uparrow, d\downarrow | H_{ex} | k'\uparrow d\downarrow \rangle$ does not occur as it does for processes (1) plus (2). This gives rise to the Kondo effect, and the contribution from (3) is often referred to as the spin-flip term. Kondo's result for the total resistivity (including first order terms) is

$$\rho = aT^5 + c\rho_A + c\rho_M \left[1 + 4JN \ln\left(\frac{k_B T}{D}\right)\right]$$

where the first term is the standard phonon term, the second arises from potential scattering from the impurity, and the last is the magnetic contribution. Note that for negative J (antiferromagnetic exchange) there will be a minimum in the resistivity. It is encouraging that Anderson's model predicts a negative J for the magnetic state, further supporting this picture.

The perturbation calculation diverges at a characteristic temperature T_k, usually referred to as the Kondo temperature, such that $kT_k = D \exp \frac{-1}{JN}$. Here D is the conduction band width and N is the density of states which is assumed constant. Much work has been done on theoretical calculations of the low temperature solution, and the reader is referred to the review articles by Kondo[15] and Heeger[14] for details. The following physical picture seems to emerge. As the temperature

is lowered below T_k a highly correlated many body state is formed in which the local moment is compensated by conduction electrons of opposite spin. As $T \to 0$ the impurity spin becomes completely compensated in the sense that the effective magnetic moment μ_{eff} in the Curie law susceptibility formula $x(T) = \mu^2_{eff}/kT$, goes to zero. The resistivity deviates from the ln T behavior given by the Kondo calculation, and saturates as the temperature is lowered. As thermal and magnetic field energies are increased, there is a transition from the spin-compensated state to a magnetic state. This transition occurs at energies of the order of kT_k. As the state breaks up, one would expect the phase transition to be gradual, because there are only a small number of particles involved, and thermal fluctuations would tend to broaden the transition in temperature.

C. Magnetic Impurities and the Hall Effect

In this section we will review those calculations of the magnetic impurity problem which specifically give results for the Hall coefficient. As pointed out in the last section, they will necessarily be based on many-electron theory. The calculations are quite involved and we will concentrate mainly on a description of the type of theory involved, the assumptions made, and the range of validity of the results. After this introduction we will discuss previous experimental results in this area.

(1) Calculations

The first calculation of the Hall coefficient in a magnetic impurity system was done by Richard More[24]. More uses the Suhl

equations, which are an application of T-matrix theory to the solid state problem of magnetic impurities. This is a scattering theory, and thus can give no information about what is happening close to the impurity.[24] This theory restricts itself to s-wave scattering only, and it is not clear how important such a restriction is for the situation in real metals. Before going further, we will list some model assumptions of the More theory (which are common to all the calculations):

(a) Small concentrations of impurities are assumed.

(b) The calculation is for a spin 1/2 impurity.

(c) The results are evaluated for a g factor, g = 2.

(d) The Hamiltonian used is:

$$H = \sum_{k,\sigma} \left(\frac{\hbar^2 k^2}{2m^*} + 2\mu_B \vec{H} \cdot \vec{S}_\sigma \right) c^\dagger_{k\sigma} c_{k\sigma} + g\mu_B \vec{S} \cdot \vec{H}$$

$$+ \frac{1}{N} \sum_{kk'} \sum_{\sigma\sigma'} \left(V \delta_{\sigma\sigma'} - J \vec{S} \cdot \vec{s}_{\sigma\sigma'} \right) c^\dagger_{k\sigma} c_{k'\sigma'}$$

where $\vec{s}$ and $\vec{S}$ are the spin operators for the conduction electrons and the impurity respectively, the c's are creation and annihilation operators, N is the number of atoms and $\vec{H}$ is the external magnetic field. The first term is the single particle energy of the electrons in a magnetic field, the second term is the Zeeman energy of the impurity, the last term is the perturbation which includes normal potential scattering and s-d exchange scattering.

More's calculation is valid at all temperatures and fields.

However, his expressions have to be evaluated on a computer, and this makes it difficult to compare his results with experiment. More considers two groups of electrons, spin up and spin down, and by including ordinary potential scattering from the magnetic impurities, he allows each spin state to have a different lifetime in a finite magnetic field. One can write an expression for the Hall coefficient arising from these two groups:

$$R = \frac{2}{nec} \quad \frac{\tau_\uparrow^2 + \tau_\downarrow^2}{(\tau_\uparrow + \tau_\downarrow)^2}$$

where $\tau\uparrow$ and $\tau\downarrow$ are the scattering lifetimes for spin up and spin down electrons respectively. This is simply a two state model where the two groups, both being electrons from the same conduction band, have the same parameters m^* and n which cancel out in the expression for R. In a single carrier host (one electron energy band) the Hall coefficient (even in the presence of magnetic impurities) will have no temperature or field dependence unless the lifetimes, $\tau\uparrow$ and $\tau\downarrow$, are different. This difference arises from an effective density of states which is skewed with respect to the Fermi level. According to More[24] one of the spin orientations has its lifetime longer than the other; which one depending on the sign of V. Using the above formula for R, More obtains the T and H dependent R plotted in Fig. 5.

Using perturbation theory, Béal-Monod and Weiner[25,26] calculated the first and second Born terms, and showed that the essential features of More's results could be obtained from first Born approximation.

Since it is a perturbation theory calculation, it is not valid at low temperatures ($T < T_k$). The calculation is carried out specifically for the case $J << V << \epsilon_F$ (where ϵ_F is the Fermi energy). They obtain results for $\tau\uparrow$ and $\tau\downarrow$, and substitute these into the same one band, two spin state formula quoted above. For $kT > g\mu_B H$ they obtain essentially the square of a Brillouin function for the dependence of R on H and T. This looks qualitatively like More's result, since the Brillouin function is linear for low arguments so that its square is an upward curving parabola, and for higher arguments it saturates. This behavior can be seen in Fig. 7 (which is a fit to P. Monod's data which will be discussed later). Note that there is little difference between the first and second Born approximations. For higher fields ($g\mu_B H > kT$) when the Brillouin function has saturated, the predominant field dependence is a $-\ln H$ term.

Finally, Bloomfield, Hecht and Sievert[27] did a Green's function calculation which generalized Nagaoka's[28] truncation procedure to finite magnetic fields. Aside from the difference in calculational approach, there is an outstanding model difference. They assume no potential scattering (V=0) and a symmetric density of states. Thus, they find $\tau\uparrow = \tau\downarrow$ and from the above formula, R = constant. These authors point out that the spin-flip process for both spin directions is being frozen out by a depopulation of levels as the magnetic field increases. As H increases there is a decrease in the populations for both the impurity spins and the conduction electron spins parallel to

the magnetic field since this is the state of higher energy. At low temperatures a magnetic field couples to the individual spins and hence prevents the spin-flip scattering from taking place; hence both $\tau\uparrow$ and $\tau\downarrow$ increase with H. With no asymmetry in the effective density of states $\tau\uparrow$ and $\tau\downarrow$ increase precisely the same way[27]. However, with V included the relaxation time of one of the spin states increases more rapidly with H.

Note that in these three calculations all scattering arises from the magnetic impurity so that all τ's are inversely proportional to the concentration. Thus R has no concentration dependence.

One of the main observations in our measurements is the strong linear concentration dependence of R. Since the Cu-Au hosts contained many defects, we first tried to explain our R behavior by including non-magnetic background scattering. In Appendix B we calculate R for a two-spin single electronic band. We find that R equals a constant plus terms of order c^2 and higher (see also section V B (2)). Bloomfield has done a further calculation which includes band structure effects. This calculation has not yet been published, and it is outlined in Appendix C. The results show that, aside from the host contribution (which is independent of field and temperature), the next largest term which results from the presence of the Fe is linear in impurity concentration , depends upon the band structure of the host, can be of opposite sign to the host Hall coefficient (this fact is a direct result of having both electron and hole-like carriers), and behaves like the magnetoresistance, ρ. Bloomfield,

Hecht and Sievert[27] have done a computer calculation of the magnetoresistance (in which $\tau\uparrow = \tau\downarrow$) for $T_k = 16^\circ$ K, shown in Fig. 6. This calculation as well as that of More[24] shows that the magnitude of ρ decreases with H. Thus Bloomfield would predict a decrease in ΔR as H increases when ΔR depends linearly on c.

These results of Bloomfield appear to be qualitatively in disagreement with those of More and of Béal-Monod and Weiner. However, the difference between $\tau\uparrow$ and $\tau\downarrow$ is influential in higher order terms of Bloomfield's formulation (Appendix C). Certainly, Bloomfield's new calculation is more realistic because it includes the effect of the band structure of the host (which is known to be quite important), while the other calculations ignore this.

(2) Previous Experimental Results

The first experiments that we will describe were done by P. Monod on 150 ppm Mn in Cu at 1.2° K in fields from 0 to 15 kG (see Ref. 25). These data fall within the range of validity for the Béal-Monod and Weiner calculation, since $T_k \sim 0.1^\circ$ K. A comparison between experiment and theory appears in Fig. 7. The agreement is quite good at low fields. The down-turn in the data at higher fields is attributed to a low field-high field transition; this will be discussed below. It is unfortunate that no data were obtained for different concentrations. This would have been most interesting, since the single band mechanism, which includes background scattering from the host,is quadratic in concentration (see Appendix B), and the leading influence in the

Bloomfield mechanism is linear in concentration (see Appendix C). Band effects should be important in this case, and it seems reasonable that Bloomfield's calculation would be more appropriate, and the concentration dependence would be linear. However, the field dependence is a separate matter, and reference to Fig. 6 shows that for temperatures well above the Kondo temperature, as is the case here, the dependence on field due to the linear Bloomfield mechanism has flattened out. Thus, it is very likely that the observed field dependence arises from the c^2 contribution. This is probably related to the mechanism of unequal lifetimes, which can enter into the single band calculation (Appendix B) or into the multiband calculation (Appendix C).

Results for Cu (Fe), Au (Fe) and Cu (Mn) for various impurity concentrations at $T = 4.2^{\circ}$ K in fields from 0 to 16 kG were obtained by Alderson and Hurd[29] (see Figs. 8 and 9). Note that they plot the Hall resistivity rather than the Hall coefficient. The data are obscured by two effects which make it impossible to observe the systematic behavior (field dependence or impurity concentration dependence) predicted by the above calculations.

The first effect is a low field-high field transition. At low fields $\omega_c\tau << 1$ the Hall coefficient is affected primarily by scattering mechanisms. This is the regime we are interested in. As the field is raised, $\omega_c\tau$ becomes comparable to 1, and the electrons can travel a full cyclotron orbit between scattering events. Thus, at fields above this ($\omega_c\tau > 1$), the topology of the Fermi surface becomes of primary importance. There

is a gradual transition between the two regimes, and it is important that this not be confused with the effects we are looking for. Under the proper conditions (i.e. pure metal hosts with small amounts of impurity so that τ is long) this transition can occur in the field region of interest and thus obscure the data. This is precisely what happens in the Alderson and Hurd data (see Figs. 8 and 9).

The second factor obscuring the data is what Alderson and Hurd refer to as a spin component. They attribute this component to superparamagnetic clustering. In support of this, they use an analogy to the well known fact that in the ferromagnetic case the anomalous Hall resistivity varies directly as the magnetization, and they fit their ρ_H data to a Langevin function (see Fig. 8). They argue against explaining the spin component by a Kondo scattering mechanism like that of More or Bloomfield. This is based on the fact that there is no correlation with a negative magnetoresistance, and that the behavior varies little between Cu (Fe) and Cu (Mn) (see Fig. 8) for which the T_k's differ by approximately two decades.

For these reasons the above systems are not good choices for investigating the Kondo effect in the Hall coefficient. However, the possibility of the above difficulties certainly must be considered when analyzing any Hall effect data.

III. OBJECT OF THESIS

The aim of the present research was to investigate the anomalous behavior in the Hall coefficient due to a dilute magnetic impurity in a metallic host.

(2) Choice of Alloy System: Cu-Au

We began by investigating Cu (Fe), Cu (Cr), and Cu (Mn). Because of the high Kondo temperature of Cu (Fe), the fields necessary to break up the spin compensated state are quite large ($\sim$200 kG), so this system was abandoned. We did preliminary measurements on Cu (Mn) and Cu (Cr), but did not continue with these systems because they have low Kondo temperatures. $T_k \sim 0.1^\circ$ K for Cu (Mn) and $T_k \sim 1^\circ$ K for Cu (Cr), and for these alloys our lowest attainable temperature was greater than T_k, so that thermal energies alone have broken up the spin-compensated state. Increasing the energy by applying a magnetic field would have little further effect.

The system finally chosen[30] was Cu-Au with Fe impurities. Loram, Whall, and Ford[31] made resistivity measurements on Cu rich alloys of Cu and Au. They found that these alloys behave as Kondo systems, and that T_k decreases as more Au is added. Their results indicate that T_k varies continuously from $\sim 24^\circ$ K for pure Cu to $\sim 0.3^\circ$ K for pure Au. Even though the exact numbers for T_k are in doubt, it is clear that somewhere between Cu and Au there is an alloy that should produce a maximum effect for our available range of temperatures (1.5° K and 4.2° K)

and fields (0 to 60 kG). Also, varying the host composition enables us to track the anomalous contributions to the coefficient as T_k is varied.

Another advantage of using the Cu-Au alloy is that the short electronic lifetime in such a binary host insures that the alloy systems will always be in the low field condition ($\omega_c\tau << 1$), so that a low field to high field transition will not occur in the available range of magnetic fields. Furthermore, interactions with impurities would tend to be reduced in a system with short lifetimes. Thus if clustering does exist, its effect is likely to be less pronounced.

Our experimental data show, however, that the Cu-Au system suffers from a different, and perhaps equally severe, disadvantage. Namely, our Hall coefficient results are very sensitive to band structure effects, and as we have seen, the band structure of Cu-Au is quite complicated. Thus, the results are not as clear-cut and conclusive as we had hoped. Although the data are found to be consistent with the theory of Bloomfield in a qualitative manner, the band structure sufficiently complicates matters so that it is not possible to extract numerical values of important parameters, such as T_k, V, and J. Furthermore, it is difficult to deduce from the data any clear-cut systematic quantitative behavior as a function of some known variation of these parameters.

The remainder of this thesis (exclusive of appendices) will discuss the experimental procedure and the results.

IV. EXPERIMENTAL PROCEDURE

The alloys were prepared from pure (99.999%) starting materials by melting the constituent elements in an argon arc furnace and quenching. Some of the ingots were cold worked. Samples were then cut to the shape shown in Fig. 35. Those samples cut from cold worked ingots were annealed for 10 days under vacuum at 830^{o} C, and quenched in a brine solution.

Hall measurements were effected as a function of magnetic field to 60 kG at 4.2^{o} K and roughly 1.5^{o} K. The magnetic field was supplied by a superconducting magnet. A constant current of 1.9 amps was used, and the resulting Hall voltage was measured with a Keithley 147 nanovolt null detector. The error in Hall measurements is estimated to be 3.5%, stemming mainly from errors in sample dimensions, magnetic field values and random thermal fluctuations in the Hall voltage. Sample compositions and homogeneity are also a major factor. The major portion of this error was systematic, however, and within a given run, changes in Hall voltage could be observed to better than 1%. A detailed description of sample preparation, apparatus, and measuring procedure is contained in Appendix A.

V. RESULTS AND DISCUSSION

In this part we will present the results and discuss them in light of existing theories and ideas. We will start by presenting the data for the Cu-Au alloys (Section A). These results are discussed first because they have a strong influence on the Cu-Au (Fe) results (Section B) which comprise the heart of the thesis.

A. Cu-Au Alloys

(1) Hall Coefficient Data

The Hall coefficient at 4.2° K is plotted as a function of atomic percent Au in Cu in Fig. 10. Included on the above plot are the data of Dugdale and Firth[32] and Barnard et. al.[10] on disordered Cu-Au alloys. The agreement is very good qualitatively, and at the Cu rich end the quantitative agreement is excellent. As was mentioned earlier (II-A), these results can be explained in terms of a variation of τ_B/τ_N as Au is alloyed into Cu. However, an explanation of the required variation of τ_B/τ_N is lacking, and values of τ_B/τ_N deduced from other types of experiments do not agree with those found from Hall coefficient data. At the present time a more basic and solid understanding of the Cu-Au system does not exist, and interesting as it may be, this was not our thesis. Thus, we did no further work and can offer no additional illumination. The importance of this data is its use in interpreting the Cu-Au (Fe) data, and the fact that it agrees with previous measurements indicates that our samples are reliable.

More extensive data was taken for "pure" Cu and "pure" Au

because a larger body of data exist for these systems. Thus quantitative agreement with previous work on Cu and Au would be the best check on the validity of our experimental data. A more detailed description appears in Appendix D. Generally, the Cu data are reproducible and in good quantitative agreement with previous results.[10,39,42-44] The Au data are not reproducible, and thus a reliable comparison cannot be attempted.

(2) Effect of Metallurgical Treatment and Structural Ordering

Most of the measurements of this thesis were done on samples directly from the arc furnace. However, a few samples were cold-worked and annealed as described in Appendix A. The "pure" Cu, "pure" Au, and Cu rich alloys seem little affected by this treatment, while there seems to be a large effect for the Au rich samples. This is possibly due to the amount of structural ordering in the samples which will be discussed below.

As a crude check on ordering in the Cu-Au alloys, we ran absolute resistivity measurements as a function of atomic percent Au, and these appear in Fig. 11. There is reason to suspect a small amount of ordering in the Au rich samples, as evidenced by the departure below the expected parabolic behavior with concentration. Resistivity data indicated that several samples were highly ordered, and the data for these were therefore disregarded. As was pointed out by Barnard et. al.[10], increasing disorder leads to an increase in the magnitude of

the Hall coefficient R. It is quite possible that the increase in the magnitude of R upon cold-working and annealing is related to an increase in the disorder. Therefore, the Au rich alloys which are more ordered to start with exhibit a greater effect when cold-worked and annealed.

(3) Field and Temperature Dependence

The field dependence for all the host data indicates that we are always in the low field condition - i.e. within experimental error the host data are independent of field. The host data appear in Figs. 14 through 17, together with data for Cu-Au (Fe). To further support this claim, we can calculate the tangent of the Hall angle ($\tan \phi = R_\sigma H$) which is equal to $\omega_c \tau$ in free electron theory. Even though we have shown that this theory does not apply, we can still get an order of magnitude estimate for $\omega_c \tau$; at most it is 0.03, and typically it is 0.005. Certainly, we remain in the low field condition throughout the entire experiment.

The Hall coefficient of the Cu-Au hosts was observed to be independent of temperature between 1.5° K and 4.2° K. Therefore, most of the host samples were measured at 4.2° K only, and these results are used in the analysis of the Cu-Au alloys containing Fe, at both 1.5 and 4.2° K.

(4) Summary of Cu-Au Alloy Data

In summary, we can conclude that the sample preparation and experimental technique are reliable, based on good agreement with

previous results. Also, we should be aware of the following factors in analyzing the Cu-Au (Fe) data:

(1) The host Hall coefficient is a strong function of composition. This must be taken into account by normalizing the data to the host value.

(2) Structural ordering in the samples can affect R considerably.

(3) The samples remain in the low-field condition throughout the experiment.

B. Cu-Au (Fe) Alloys

Before presenting and discussing the Cu-Au (Fe) data, a few preliminary measurements important to the evaluation of the data will be discussed below.

(1) Preliminaries

(a) Sample Analysis

The nominal Fe concentration in the Cu-Au (Fe) alloys was calculated from the weights of the starting materials. As a check on this, the alloys were analyzed commercially for Fe content by chemical and spectroscopic techniques. The results, which appear in Table 2, are not always in good agreement with the nominal concentrations. However, the analysis does confirm the existence of Fe in concentrations comparable to those calculated. The nominal concentrations always gave more consistent and reasonable results than did the concentrations as determined by chemical analysis. We therefore used nominal values of concentration throughout this work.

(b) Resistivity Data

As previously mentioned, Loram, Whall and Ford[31] observed Kondo behavior in the resistivity of Cu-Au (Fe) alloys. For completeness, we measured the resistivities as a function of temperature for a few of our Cu-Au (Fe) samples. The results appear in Fig. 12 on a semi-log plot. Although the error in absolute resistivity is large it is mostly systematic, and the characteristic Kondo contribution, proportional to lnT, is readily discernible in all the data. Where data exist for more than one Fe concentration, the impurity resistivity is seen to be linear in concentration at low temperatures within experimental error, and the position of the minimum shifts to higher temperatures for higher concentrations.

(c) Effect of Ru as an Impurity

In order to investigate the effect of an equivalent but non-magnetic impurity, Ru was substituted for Fe in the Cu-Au (Fe) alloys. Although its mass is different, Ru is non-magnetic and immediately below Fe in the periodic table, and should thus give us a rough idea as to what portion of the data is magnetic in origin. Measurements for the same concentrations of Fe and Ru in the same Cu-Au host appear in Fig. 13. Note that the contribution due to Ru is small and field independent. By contrast, the Fe impurity gives rise to a large contribution which is strongly field dependent. These effects due to the Fe are apparently magnetic in origin.

(d) Effect of Metallurgical Treatment and Structural Ordering

A certain number of Cu-Au (Fe) samples were cold-worked and annealed to observe the effect of this treatment on the contribution due to the Fe. The details are presented in Appendix E. The first cycle of metallurgical treatment merely shifted each data point within a particular Cu-Au (Fe) alloy series (i.e. same Au composition) by the same amount, and did not qualitatively change the results. Further cold-working and annealing produced little additional effect. For this reason, the data presented is for samples direct from the arc furnace without further treatment.

Residual resistance ratios (RRR) were measured for all the Cu-Au (Fe) samples. The RRR give a measure of the amount of structural ordering, being larger for more ordered samples. When examining Hall effect data for a Cu-Au (Fe) series of a particular Au composition, only samples which have a similar degree of order should be included, for only then will we be looking solely at the effects of the Fe. From the RRR's in Table 3 it appears that for each of the series, except $Cu\text{-}Au_{60}$ and $Cu\text{-}Au_{80}$, the amount of ordering within the series is in fact comparable. This is evidenced by the monotonic decrease in the RRR as Fe is added. Since the RRR data are not very sensitive to ordering, it is possible that there are small differences among the samples. However, it does appear that the major contribution to Hall effect changes within a series is due to Fe.

Data on the 80 at. % Au system is presented to provide a clear-

cut case of the effects of structural ordering. Notice (Fig. 17) that this is the only case where the Hall coefficient of the host alloy is less than that of the same alloy containing Fe. This change in sign could indicate a dramatic change in band structure. However, the RRR value for the host is anomalously large, and this indicates structural ordering. As pointed out in section V A2 on Cu-Au alloys, ordered samples have lower Hall coefficients. This explains the low value of the host, and we need not resort to major changes in band structure to explain this anomalous result.

(e) Effect of Composition and Temperature Differences

It should be noted that for the 1.5° K data the measuring temperatures differ by about 0.01° K for different samples. This is not a problem, because the resulting change in Hall coefficient is approximately $0.001 \times 10^{-13} \frac{\text{V-cm}}{\text{amp-gauss}}$. Also, when examining the Fe concentration data for a given host, variations of 0.1 at. % Au are not serious because they produce changes in R of only $0.02 \times 10^{-13} \frac{\text{V-cm}}{\text{amp gauss}}$.

(2) Data for Cu-Au Alloys with Fe

Most of the measurements were made on Cu rich alloys for which the T_k's are moderately high, so that the available temperature and field energies are comparable to the energy of the Kondo state. Also, sample preparation for the Cu rich alloys is more reliable.

The Hall coefficient (at 1.5° K and 4.2° K) as a function of magnetic field from 0 to 60 kG appears in Figs. 14 through 17 for all the measured alloys. Each graph presents data for different concentrations

of Fe in a particular host. Note that the vertical scale is the same for all graphs. Before going into a detailed analysis of the data, some general features are immediately apparant. Upon alloying Fe into Cu-Au, there is a strong reduction in magnitude of the Hall coefficient for small amounts of Fe (of the order of 100 ppm), and this reduction is strongly field and temperature dependent. To first order, this reduction is linear in Fe concentration c, with the possible admixture of a small c^2 term. Generally, the dependence on temperature and field is much greater for the Cu rich alloys than for the Au rich alloys. This can be understood in terms of the Kondo state as follows. T_k is of the order of degrees for Cu rich alloys, while it is a fraction of a degree for Au rich alloys. Thus, for the temperature and fields available, we span the Kondo state in energy for Cu rich alloys and see a large effect. For Au rich alloys there is little dependence on temperature and field. This is evidence of the fact that we are well above the Kondo state in energy, so that increasing temperatures and fields have little effect on the spin-compensated state. These ideas will be put on a more quantitative basis later.

(a) Dependence on Fe Concentration

One of the most striking features of the data is the concentration dependence, which is predominantly linear. The most extensive data for a single host (i.e. largest number of different Fe concentrations) was obtained for the alloy $Cu\text{-}Au_{14.3}$. This data can be nicely fit to $R = R_H - a(H,T)\,c$, where R_H is the Hall coefficient of the host alloy without Fe, and $a(H,T)$ is a phenomenological parameter derived from the data

which depends on field and temperature, but not on concentration. The data are presented in this manner in Fig. 18.

These data cannot be explained merely in terms of More's mechanism of unequal lifetimes. If we assume, as More and Béal-Monod-Weiner did, that the host's lifetime is infinite, then $\tau\uparrow$ and $\tau\downarrow$ are proportional to c, and the concentration dependence, as mentioned in Section II C, will cancel out in the expression

$$R = \frac{2}{nec} \frac{\tau\uparrow^2 + \tau\downarrow^2}{(\tau\uparrow + \tau\downarrow)^2}$$

As a first attempt at including the effect of the host, we can make a reasonable assumption, such as

$$\frac{1}{\tau\uparrow,\downarrow} = \frac{1}{\tau_o} + \frac{1}{\tau'\uparrow,\downarrow} ,$$

where $\frac{1}{\tau_o} \neq 0$ is the host's contribution and $\frac{1}{\tau'\uparrow\downarrow}$ is the impurity contribution which is linear in c. Using this to evaluate R, we obtained an expression in concentration in which the linear term in c is missing (the algebra appears in Appendix B). Thus we must go to a more realistic calculation to get even qualitative agreement with our data. Bloomfield's calculation which includes both finite host lifetime and the band structure of the host, does yield a linear term in concentration, as discussed in Part II and Appendix C. Thus we see the importance of the band structure of the host in explaining the observed concentration dependence of the data.

Bloomfield's calculation also predicts a smaller c^2 contribution. As the data for different concentrations were necessarily taken on different samples, the error in the thickness measurement was important

in comparing these results. Unfortunately this error was rather large, and a smaller c^2 term could not be reliably discerned directly. However, an indirect method was possible. If the values of $\frac{a(H,T)}{|R_H|}$ for various concentrations are set equal at a particular field and temperature (60 kG and 1.5° K in our case), then deviations in the plots of $\frac{a(H,T)}{|R_H|}$ (normalized as described) vs. H for different concentrations would indicate the presence of c^2 (and higher) terms. The presence of such a term in c^2 is clearly indicated, especially for the Cu-$Au_{5.0}$ data, in Figs. 19, 20 and 21.

(b) Dependence on Temperature and Field

The qualitative behavior of the Hall coefficient as a function of temperature and field can be compared with Bloomfield's results. Our phenomenological parameter a(H,T) is the coefficient of the linear c term in Bloomfield's expansion. Thus a(H,T) should vary directly as the magnetoresistance (see Appendix C) which is presented in Fig. 6 from the theory of Bloomfield, Hecht and Sievert[27]. In order to compare our data with the behavior predicted by Bloomfield at low fields, a careful remeasurement of one sample was undertaken including additional low field points. This appears inFig. 22, and the results for a(H,T) as a function of temperature and field are in good agreement with Bloomfield's prediction for linear c-dependence. Note that not only is the linear c-dependence different from the one-band prediction, but so is the decrease in the magnitude of ΔR with H. It is not possible to make a quantitative comparison for many reasons. The band structure and Kondo

parameters are not well enough known, and a fit would be rather meaningless with so many unknown parameters. Also, the computer calculation is too costly to warrant the undertaking of such a task.

(c) Dependence on Host Composition

We now examine the behavior of the data as a function of host composition. The quantity chosen to represent a measure of the overall field effect is $\frac{R_{60}-R_{20}}{|R_H|c}$, where R_{60} and R_{20} are the values of the Hall coefficient at 60 and 20 kG. The low value was not chosen at 0 or 10 kG, because R_0 can be deduced only by an unreliable extrapolation, and R_{10} has a large error. The difference $R_{60}-R_{20}$ was normalized to concentration and to the host value R_H, as would be indicated by Bloomfield's theory. The variation of $\frac{R_{60}-R_{20}}{|R_H|c}$ (for $T = 1.5^{\circ}$ K and $T = 4.2^{\circ}$ K) as a function of atomic percent Au appears in Fig. 23. The most prominent feature of these data is the maximum around 20 at. % Au for the 1.5° K data. This feature is consistent with the existence of a low temperature spin-compensated state through the following arguments. For high Kondo temperature alloys to the left of the maximum, the available fields are not sufficient in energy to produce a large effect on the spin-compensated state. As more Au is added and T_k decreases, the field energies become more effective in breaking up the low temperature state, the largest effect occuring at 20 at. % Au. As more Au is further added (alloys to the right), T_k is reduced further, so that the ambient temperature of 1.5° K becomes comparable with, and eventually higher than, T_k. For these alloys, the thermal energy is sufficient to break up the spin-

compensated state, and the effect of fields is progressively reduced. The data at 4.2° K fit with this explanation, because the peak shifts to the left (or higher T_k) for our higher measuring temperature. More quantitatively, if we assume that for the peak value (i.e. at 20 at. % Au for the 1.5° K data) T_k is centered in our range of field energies, then we can estimate T_k for this host. Since we are making the measurement at 1.5° K, this temperature will have to be added to our estimate. The center of our field range is 40 kG, or 4° K (using 10 kG as roughly equivalent to 1° K). Thus our estimate for T_k is 5.5° K for the $Cu\text{-}Au_{20}$ host. This agrees reasonably well with the estimate of 3° K by Loram, Whall and Ford for $Cu\text{-}Au_{20}$, considering that it is only an order of magnitude calculation.

For data far to the right in the Au rich region, we see in Fig. 17 that the slope of the Hall data as a function of field changes sign, and we get negative values. Although the Au rich data are less accurate, due to the necessarily[33] lower concentrations, the minus sign does seem to be real. For the Au rich hosts we are well above the Kondo temperature, and according to theory the contribution to the term linear in c has flattened out (see Fig. 6). Although the difference $(R_H - R)$ would still principally be linear in concentration, the field dependence would arise from the c^2 term. Bloomfield has computed the expressions involved and they indicate that the c^2 term can be opposite in sign to the c term and can increase with H. The field dependence of this term arises from the difference between $\tau\uparrow$ and $\tau\downarrow$. Thus, both the

Béal-Monod and Weiner calculation, which shows a -lnH term in this region (i.e. $T > T_k$ and $g\mu_B H > kT$), and the Bloomfield calculation are consistent with the observed dependence. However, further careful measurements would have to be made in this region to establish whether these theories describe the behavior correctly.

(d) Equivalence of Temperature and Field Energies

In order to show the equivalence of thermal energies ($k_B T$) and magnetic field energies ($g\mu_B H$) in breaking up the spin-compensated state, the Hall data obtained at both temperatures (1.5 and 4.2° K) were plotted as a function of the sum of the two energies. This procedure is expected to work below T_k, while above T_k we expect R to behave as a Brillouin function of H/T. Thus in Fig. 24 the 5 at. % Au data (for which we are below T_k) are plotted: (1) as a function of the sum of the energies treating them as scalars; (2) as a function of the square root of the sum of the squares, treating them as orthogonal vectors. The second approach produces better agreement between the two temperature runs (see Fig. 24). Still better agreement can be obtained by scaling the energies differently. We assume that $k_B T = sg\mu_B H$, where s is the scaling factor. The data are plotted in Figs. 25 through 30 for several Cu-Au (Fe) alloys using such a scaling factor. The matching of the two temperature runs is remarkably good. This scaling factor s appears in Table 4 for the various Cu-Au hosts. It is interesting to note that the value $s = 0.75$ for the 5 at. % Au data was also deduced by Fenton[34] from his magnetoresistance measurements. A possible explanation for

values of s other than unity is that we are not far enough below T_k. This conjecture is supported by the growing asymmetry of temperature and magnetic field energies (i.e. smaller s) as we go towards systems with lower T_k. Table 4 shows that s decreases between the 5 at. % and the 11.6 at. % Au alloys, corresponding to a sizable decrease in T_k between these two alloys, and then remains roughly constant within experimental error for alloys with higher Au content, for which T_k varies less rapidly.

(e) The Case of Cu-Au_5 (Fe)

The 5 at. % Au data deserve special attention. We have measured both the Hall coefficient and the magnetoresistance for this system. The parameter $\frac{a(H,T)}{|R_H|}$ from the Hall coefficient data, and $\Delta\rho/\rho_0$ from from the magnetoresistance data are plotted as a function of field in Fig. 31. At first glance, the magnetoresistance data have the qualitative behavior predicted by Bloomfield (see Fig. 6), while the Hall coefficient data do not. A possible explanation would be the existence of a large c^2 term, so that direct subtraction of the host and alloy data would not simply yield $\frac{a(H,T)}{|R_H|}$. Since data were taken for two concentrations, the coefficients of the linear and quadratic terms could be determined by solving two equations for two unknowns. The resulting coefficient of the linear term appears in Fig. 32 as a function of field. The coefficient of the linear term derived in this manner does behave as expected, so that this analysis indicates that a c^2 term may indeed exist. The reason that the c^2 contribution is so much more

important in the 5 at. % Au data is that the Fe concentration is more than a factor of two larger than for any other host, increasing the c^2 contribution roughly by a factor of five. One would expect the magnetoresistance and the linear term in the Hall effect to behave in similar ways. A close look at the magnetoresistance reveals, however, that its curvature has not changed sign at higher fields. This can arise in two ways: (1) in the Bloomfield calculation of the resistivity in impure alloys, there is a positive c^2 contribution (not related to impurity-impurity interaction effects); (2) the presence of interactions between impurities at these high concentrations would also lead to a higher resistivity. Thus, the fact that the curvature has not yet changed sign may indicate that a freezing out of these additional scattering mechanisms is still occurring.

VI. CONCLUSION

By studying the ternary alloy system Cu-Au (Fe), we were able to see manifestations of the Kondo effect in Hall coefficient data. This has yielded more information than previous experiments on binary systems such as Cu(Fe) and Au(Fe), where superparamagnetic effects and low-to-high field transitions totally obscure the results. In particular, we can make the following observations:

1. The temperature and field dependence as a function of host composition is consistent with the existence of a low temperature, spin-compensated state.

2. The contribution to the Hall coefficient due to the Fe impurity is predominantly linear in impurity concentration, and opposite in sign to the Hall coefficient of the host. This result can be derived from the theory of magnetic impurities by including the effect of the band structure of the host. Calculation shows that the field dependence arises from the fact that spin-flip scattering is "frozen out" as the magnetic field is increased. Our observed field dependence agrees well with theory.

3. In addition to the predominant linear contribution, a smaller c^2 term is observed for the samples with the largest Fe concentrations. It is quite likely that the field dependence of the

c^2 term derives from the difference between the lifetimes $\tau\uparrow$ and $\tau\downarrow$ as the magnetic field is increased.

4. We were able to relate the effects of thermal and magnetic field energies in breaking up the low temperature spin-compensated state. It appears that for all of our data, we were not far enough below T_k, so that thermal and magnetic field energies were not directly equivalent in their effect on the spin-compensated state.

The above observations are qualitative in nature. It was not possible to obtain more quantitative results (eq. Kondo temperatures) primarily because of the strong influence of band structure. Although the present experiment shows that Hall coefficient data for a system with dilute magnetic impurities can be understood in terms of existing theory, it appears that the Hall coefficient will not be a useful tool in studying magnetic impurities until more details are known about the effects of band structure of the host.

APPENDIX A: EXPERIMENTAL PROCEDURE

A. Sample Preparation

(1) Materials

The starting materials were as follows: 99.999% purity copper and gold purchased from the American Smelting and Refining Company; 99.999% purity iron and 99.999% purity ruthenium sponge purchased from the United Mineral and Chemical Corporation.

(2) Cleaning

The starting materials and copper hearth were cleaned in the following manner: The copper was etched in nitric acid diluted with water (1:1), rinsed in water, and rinsed in acetone. The gold was in the form of clean spatters and was used without etching or cleaning; the iron was etched in hydrochloric acid, rinsed in water, and rinsed in acetone; a master of gold-iron (see Section C on melting) was etched in aqua regia, rinsed in water and rinsed in acetone; the ruthenium sponge was melted into small pellets and used as such; the hearth was etched in a solution of one part HNO_3, two parts H_2SO_4, two parts water, then rinsed in water, rinsed in alcohol, and air dried with a heat gun.

(3) Melting

The starting materials for the CuAu alloys were cleaned as described above and weighed out in appropriate proportions. The dilute iron alloys were made in two steps. First, a master alloy

of about 1% iron in gold was prepared. This alloy was then diluted with appropriate amounts of copper and gold to obtain the desired Cu-Au(Fe) alloy. All samples were melted in an arc furnace (pictured in Fig. 33) under one atmosphere of argon. The arc furnace was flushed by pumping out and bleeding in argon several times before proceeding with the melt. Typical currents used were around 125 amperes. After the first melt the samples were turned over and remelted four additional times to insure homogeneity. The hearth was cooled during the melting by circulating cold water, and under these conditions the sample cooled in a matter of seconds after the arc was turned off. The sample weights ranged from 7-12 grams and the total amount of material lost was generally less than 0.03%. The atomic weights used in all determinations of atomic percent are as follows: Au-196.967, Cu-63.54, Fe-55.847, Ru-101.07.

(4) Cold Working

Cold working was accomplished by compressing the sample material between the platens of a 10 ton press. This was done in two mutually perpendicular directions (or three whenever possible). The samples were compressed until the force reached 8 or 9 tons with negligible creep. Under these conditions the samples were compressed typically to 3/4 to 1/2 of the original dimension along the axis of applied force.

(5) Cutting

The samples were cut on a surface grinder with thin alumina blades. The ingots generally were loaf shaped, approximately 1/4 inch to 1/2 inch thick. First, parallel slabs were cut (either from material directly from the arc furnace or cold worked pieces) in the range 15 to 20 mils thick. The slabs were hand lapped on sand paper to the desired thickness. Samples of the shape shown in Fig. 35 were cut from the slabs using a combination of jigs. Resistivity rods were also cut from the same material. The thickness was measured using a micrometer with the smallest division on the vernier being 0.1 mils. Readings were taken at several points between the Hall probes and an average value was obtained. The estimated error is $\pm$ 0.2 mils.

(6) Annealing

Several samples were annealed, mostly those cut from the cold-worked material. The annealing apparatus is pictured in Fig. 34. Annealing was done at 830° C in a vacuum of 10^{-6} mm. At the end of annealing, He_4 gas from a flushed-out system was bled in slowly through a cold trap until the annealing system was at atmospheric pressure. The samples were quenched as quickly as possible by dumping them into a cold brine solution.

B. Sample Geometry

The measured value of the Hall voltage can be reduced considerably by short circuiting through the current contacts if they are of high conductivity material. Isenberg, Russel, and Green [35]

have shown that this effect is negligible if the length to width ratio of the sample is 4 or greater. Also, this shorting effect can be reduced by making the current contacts small. However, this changes the current distributions, and Isenberg, et. al. tested to see if the Hall voltage was independent of the current distribution. They found that asymmetric placement of the point contact current leads, and even cutting off the corner of a sample, produced changes of only 1 to 2%.

The final [36] sample geometry used in this experiment is pictured in Fig. 35. All dimensions except AB were the same for all samples. Platinum voltage and current leads were spot welded to the sample. Care was taken to spot weld the current leads symmetrically and in roughly the same position on all samples. Since point contacts were used, the current distribution near the ends varied from sample to sample. However, using a length to width ratio of approximately 4, following Isenberg, et. al., insured that the current distribution was uniform near the center. It should be noted that with this arrangement, only 1 to 2% variations were observed when the current distributions were greatly perturbed.

It can be noticed from Fig. 35 that the voltage leads were spot welded to projecting "ears" near the center of the sample. It was felt that this placement would be less likely to perturb the measurements as the current density in the "ears" gets small

rather rapidly toward the edges of the ears. (For a quantitative example of this see C.M. Hurd.[37])

C. Experimental Apparatus and Measuring Procedure

(1) Cryogenics

The apparatus is pictured schematically in Fig. 37. Volumes "A", "B" and "C" are separated by vacuum jackets. The section labeled "A" is the outer nitrogen space. After pre-cooling, the volume "B" which contains the superconducting magnet "D", was filled with liquid He_4. The innermost volume "C" contains the sample holder "F"; this volume was pre-cooled and filled with liquid He_4. The volume "C" was pumped on until an equilibrium was reached at the lowest attainable pressure. During data taking, the temperature dropped at most $0.05^{\circ}K$, and generally much less. The pressure in volume "C" was measured by a Wallace and Tiernan pressure gauge calibrated in 0.5 mm steps. The temperature deduced from this pressure reading was compared to a previously calibrated germanium thermometer. The two differed at most by $0.01^{\circ}K$ (see Table 5).

The sample holder is pictured in Fig. 38. The sample is clamped between copper blocks "A" and "B" in a plane perpendicular to the magnetic field. "C" and "D" are insulated guides for the leads. The Ge thermometer is mounted in copper block "A" when in use.

(2) Electronics

A sample current of 1.9 amperes (See Fig. 39) was provided by a North Hills constant current/voltage reference source (Model TC602CR). The current regulation was better than one part in 10^5. The voltage was measured by a Keithley nanovolt null detector (Model 147). The voltage leads from the sample were # 30 high purity copper wire and were continuous from a point one inch above the sample. Contact was made by spot welding platinum wires to the "ears" of the sample; this was then soldered to the continuous Cu lead. The leads were brought outside the pumping space though epoxy bonds (this was found to be superior to soldering to glass-to-metal feed-throughs which caused thermal noise of approximately 1μv). The amplified signal from the Keithley nanovolt null detector was observed on a Moseley X-Y recorder (Model 2D-2). The resolution of the voltage measurement was a few nanovolts. Both the North Hills current supply and the Keithley null detector were calibrated against a Leeds and Northrup 6-dial potentiometer (Model 7556-1). For current calibration, the voltage was measured across a standard 1Ω resistor.

(3) Magnetic Field

The magnetic field was provided by a Westinghouse 60 kilogauss superconducting magnet. The magnet was energized by a Magnion CFC100 power supply. The current output for a

particular dial setting on the power supply would not repeat, and therefore the current through the magnet was measured at every data point (See Fig. 40 for circuitry). Westinghouse reports a coil constant of 1.428 kilogauss/ampere with an accuracy of 1%. The coil constant and linearity of the magnet were checked using a snatch coil method. Two coils of different sensitivity were constructed. One was used to investigate lower fields, the other was used at higher fields. From the results shown in Fig. 41, one can see that within the error, the field is linear in current. Also a coil constant of 1.41 ± 0.03 is a good average for the two coils. This is not inconsistent with the Westinghouse value, so 1.428 kilogauss/ampere was used throughout to compute field values.

(4) Resistivities

Resistivities as a function of temperature, absolute resistivities, and residual resistivity ratios were measured on the apparatus of M.P. Sarachik. The technique and apparatus are described elsewhere.[38]

D. Data Taking Procedure

Data was generally taken using the following procedure. After the liquid He_4 was transferred, as previously described, the sample current was applied and the zero offset on the Keithley 147 was adjusted to buck out the voltage resulting from misalighment of the voltage probes. This voltage ranged from 0.01μ volts for pure

metals up to 30μ volts for alloys. The system was allowed to come to equilibrium - typically one hour - after transferring or pumping so that the thermal drift rate was low. The thermal drifts, being somewhat erratic, were the major source of error in the voltage measurement. At most, the drifts were a few percent of the total signal from zero to 60 kilogauss and usually they were below 1%. For each sample (excepting most of the hosts where the behavior was fairly constant) data was taken for each of the four possible permutations of field and current directions. This would correct for any change of misalignment voltage because of a magnetoresistance effect. (Magnetoresistance is an even function of magnetic field and the Hall voltage is odd. For a given current direction the difference in measured voltage for the two different field directions would give twice the Hall voltage, and the magnetoresistance contribution would cancel out.) However, the magnetoresistance of these alloys is so small that there was little difference (a few percent at most) between the four sets of data. (That is, once the peculiar low field behavior mentioned earlier [36] was eliminated.) For each set of measurements, data points were taken in roughly 10 kG steps in the sequence 0, 10, 20, 30, 40, 50, 60, 10, 0 kG. From this data an overall drift correction could be made, except for random fluctuations which tended to be smoothed out when the four sets of data were added together. As previously stated, the

current through the magnet for a particular dial setting did not repeat, so an average field point was obtained from the four sets of data. The variation was only a few percent and the data could be assumed linear in that region. An additional source of complication was that the zero kilogauss reading was not really zero because of a leakage current in the magnet power supply which existed when the dial was set at zero. The field due to this current was about 300 gauss. (The remanent field was not measured carefully, but it was at least an order of magnitude smaller and therefore it was neglected.) Thus, the measured quantity was the change in Hall voltage from 0.3 to 10 kG. To obtain the change in Hall voltage from 0 to 10 kG, the Hall constant was assumed to be the same throughout this region (an assumption that would be incorrect by 5% at most), and the measured value was multiplied by the factor $\frac{10.3}{10}$. This is a correction of 3%. If it is off by 5%, the resulting error in the Hall constant at 10 kG would be 0.15% This is considerably less than other errors in the experiment.

E. Errors

(1) Hall Constant

The Hall constant $R = \frac{V_H t}{IH} = \frac{V_H t}{I K_m I_m}$.

Here K_m is the coil constant of the magnet, I_m the current in the magnet. I is the current through the sample, t is

the thickness and V_H is the Hall voltage. V_H and I were calibrated to one part in 1000 against the same Leeds and Northrup six-dial potentiometer, so that calibration errors in those quantities would cancel out. The shunt used to measure I_m was also calibrated to one part in 1000 against the same potentiometer, so the error from I_m would be negligible compared with others in the expression for R. The main sources of error are t, K_m and random thermal fluctuations in V_H. The measurement error in t was typically $\pm$ 1.5%. It was systematic within a given field run but random when comparing samples. The error in K_m was already quoted at $\pm$ 1% and is systematic throughout the data. The error from random thermal fluctuations in V_H was typically 1% of the voltage change for 10 kilogauss change in field - this was random throughout the data. Note that at higher fields the percentage error was reduced because it is the sum of several such 10 kilogauss intervals. For example, the percentage error at 60 kilogauss would be reduced to 0.4%. Figures 42 and 43 show reruns of data on the same sample. As can be seen, they agree within our error estimates for thermal fluctuations in V_H. To summarize, when looking at the data of a particular sample, there is a random error from point to point of at most 1%, and when comparing two samples there can be a random error between them of about 2.5%; finally, any one data point can be off as much as 3.5% in absolute value.

One other large source of error not yet mentioned is the preparation of samples. Sample preparation is very difficult to do consistently, and the resulting error is hard to measure. The metallurgy of the three component systems under study here is complicated and not well understood. Given this situation, it would not be worthwhile to improve the measuring error without improving the sample preparation - both of which would take considerable effort. Attempts to produce identical samples resulted in measured differences in the Hall coefficient of 2% in one case and 6% in another. The poor reproducibility of the latter is related to structural ordering.

In some cases, if the plane of the sample and magnetic field are not perfectly perpendicular, the measured Hall voltage can be altered dramatically. The apparatus was aligned carefully, but no allowance was made for small (less than one degree) adjustments. To check how sensitive the measurement was to angle, the sample holder was rotated 90° and 180° which would change the angle slightly because of slight misalignments in the apparatus. No change was observed in Hall voltage - so errors from this effect can be ignored.

Also, thermal galvanomagnetic effects could be superimprosed on the Hall voltage. However, all measurements took place in liquid He_4 which is an excellent thermal conductor, and the sample was thermally anchored to a large Cu block. This would make the thermal galvanomagnetic effects negligible.

(2) Resistivities

RRR's were limited in accuracy by thermal fluctuations in voltage. This produced errors in RRR's of about $\pm$ 0.5%. Absolute resistivities involve three geometrical measurements, and the error is high for each. The error is typically $\pm$ 5%. If great care was taken to make samples of uniform cross-section, and careful measurements were taken of the cross-section, and many samples were run, the error could be reduced to one or two percent. The random relative error within a given resistivity temperature run was much smaller.

APPENDIX B: CONCENTRATION DEPENDENCE OF R WITHOUT BAND EFFECTS

In this appendix we present the details of the algebra which show that without considering band effects (i.e. electron - like and hole - like contributions), it is not possible to obtain a linear c term in the expansion of R in concentration.

A reasonable assumption for the effect of the host on the relaxation time, τ, is to take $\frac{1}{\tau_{\uparrow,\downarrow}} = \frac{1}{\tau_o} + \frac{1}{\tau'_{\uparrow,\downarrow}}$ where $\frac{1}{\tau_o}$ is the host contribution and $\frac{1}{\tau'_{\uparrow,\downarrow}}$ is the impurity contribution, which will be linear in c in the dilute limit. Thus we can say $\frac{1}{\tau_{\uparrow,\downarrow}} = A + c B_{\uparrow,\downarrow}$, where A and B are independent of concentration. Putting this into the single band two spin formula, which assumes $\omega_c \tau << 1$,

$$R = \frac{2}{nec} \frac{\tau_\uparrow^2 + \tau_\downarrow^2}{(\tau_\uparrow + \tau_\downarrow)^2} ,$$

yields

$$R = \frac{2}{nec} \frac{\left(\frac{1}{A + B_\uparrow c}\right)^2 + \left(\frac{1}{A + B_\downarrow c}\right)^2}{\left(\frac{1}{A + B_\uparrow c} + \frac{1}{A + B_\downarrow c}\right)^2} .$$

Simplifying,

$$R = \frac{2}{nec} \frac{(A + B_\downarrow c)^2 + (A + B_\uparrow c)^2}{(A + B_\downarrow c + A + B_\uparrow c)^2}$$

or

$$R = \frac{2}{nec} \frac{2A^2 + 2A(B\uparrow + B\downarrow)c + (B\uparrow^2 + B\downarrow^2)c^2}{(2A + (B\uparrow + B\downarrow)c)^2} .$$

For our alloys A >> Bc so that, expanding the denominator, we obtain:

$$R \approx \frac{2}{nec} \left(2A^2 + 2A(B\uparrow + B\downarrow)c + (B\uparrow^2 + B\downarrow^2)c^2\right)\left(\frac{1}{4A^2}\right) \times$$

$$\times \left(1 - 2\frac{B\uparrow + B\downarrow}{2A}c + 3\frac{(B\uparrow + B\downarrow)^2 c^2}{4A^2} + O(c^3)\right),$$

and to order c^2

$$R = \frac{2}{nec}\frac{1}{4A^2}\left(2A^2 + 2A(B\uparrow + B\downarrow)c - 2A(B\uparrow + B\downarrow)c + \right.$$

$$\left. + \frac{c^2}{2}(B\uparrow - B\downarrow)^2 + O(c^3)\right)$$

Thus we see that the term linear in c drops out, and we are left with a constant plus terms of order c^2 and higher. Note that the coefficient of c^2 depends on the square of the difference between the spin up and spin down scattering frequencies.

APPENDIX C: BLOOMFIELD'S CALCULATION OF R, INCLUDING BAND EFFECTS

Bloomfield has calculated the Hall coefficient for a magnetic impurity in a host with an arbitrary number of bands. We can generalize the two band model to obtain

$$R = \frac{2}{ec} \frac{\sum_{i,\sigma} (\pm) \frac{n_i (\tau^{i,\sigma})^2}{m_i^2}}{\left(\sum_{i,\sigma} \frac{n_i \tau^{i\sigma}}{m_i} \right)^2} \qquad (1)$$

where i refers to the different bands, σ refers to the two spin directions, and the + and - refer to electron-like and hole-like bands respectively. Bloomfield approximates each band by a sphere so that we can use the relation $m_i = \frac{\hbar^2}{8\varepsilon_F} \left(\frac{3 n_i}{\pi} \right)^{2/3}$. A more realistic assumption would give different geometric factors for the different bands. However, this would not change the results qualitatively so the simplifying assumption is retained. Substituting for m_i in (1) we obtain:

$$R = \frac{2}{ec} \frac{\sum_{i,\sigma} (\pm) \frac{(\tau^{i,\sigma})^2}{(n_i)^{1/3}}}{\left(\sum_{i,\sigma} \tau^{i,\sigma} (n_i)^{1/3} \right)^2} \cdot \qquad (2)$$

Bloomfield now supposes that $\frac{1}{\tau^{i,\sigma}} = \frac{1}{\tau_o^i} + \frac{1}{\tau_K^\sigma}$ where $\frac{1}{\tau_o^i}$ is the host contribution and $\frac{1}{\tau_K^\sigma}$ is the impurity contribution which is linear in concentration. Assuming a common mean free path for

all carriers $\ell = v_F^i \tau_o^i$, we have

$$\tau_o^i = \ell \sqrt{\frac{m_i}{2\mathcal{E}_F}} = \frac{h\ell}{2\mathcal{E}_F} \left(\frac{3}{8\pi}\right)^{1/3} (n_i)^{1/3} \equiv T\ell (n_i)^{1/3} \tag{3}$$

We also assume $\frac{1}{\tau_K^\sigma} = c\,\alpha_K^\sigma$. We now expand τ_i^σ in terms of the smaller contribution $c\,\alpha_K^\sigma$.

$$\tau^{i,\sigma} = \tau_o^i \left[1 - c\alpha_K^\sigma \tau_o^i + (c\alpha_K^\sigma \tau_o^i)^2 + \ldots\ldots\right]$$

and

$$(\tau^{i,\sigma})^2 = (\tau_o^i)^2 \left[1 - 2c\alpha_K^\sigma \tau_o^i + 3(c\alpha_K^\sigma \tau_o^i)^2 + \ldots\ldots\right]$$

Before substituting these expansions into the expression (2) for R, we make the following definitions:

$$\sum_\sigma \alpha_K^\sigma = A$$
$$\sum_\sigma (\alpha_K^\sigma)^2 = B \tag{4}$$

$$\gamma_0 = \sum_i (\pm)(n_i)^{1/3} \qquad \eta_1 = \sum_i (n_i)^{2/3}$$
$$\gamma_1 = \sum_i (\pm)(n_i)^{2/3} \qquad \eta_2 = \sum_i n_i \tag{5}$$
$$\gamma_2 = \sum_i (\pm) n_i \qquad \eta_3 = \sum_i (n_i)^{4/3}$$

With these definitions Bloomfield obtains the following result for R (to terms of order c^2):

$$R = \frac{1}{ec}\frac{\gamma_0}{\eta_1^2}\left[1 + cAT\ell\left(\frac{\eta_2}{\eta_1} - \frac{\gamma_1}{\gamma_0}\right) + c^2(T\ell)^2\left(\frac{3A^2\eta_2^2}{4\eta_1^2} - \frac{B\eta_3}{\eta_1} + \frac{3}{2}\frac{B\gamma_2}{2\gamma_0} - \frac{A^2\gamma_1\eta_2}{\gamma_0\eta_1}\right)\right]$$

For the case of one electron-like band (i = 1) and one hole-like band (i = 2), we can show that $\frac{\eta_2}{\eta_1} - \frac{\gamma_1}{\gamma_0}$ is negative. Defining $\chi_i = (n_i)^{1/3}$ we have

$$\frac{\eta_2}{\eta_1} = \frac{\chi_1^3 + \chi_2^3}{\chi_1^2 + \chi_2^2} = (\chi_1 + \chi_2)\left[1 - \frac{\chi_1\chi_2}{\chi_1^2 + \chi_2^2}\right]$$

and

$$\frac{\gamma_1}{\gamma_0} = \frac{\chi_1^2 - \chi_2^2}{\chi_1 - \chi_2} = \chi_1 + \chi_2 \quad .$$

Thus

$$\frac{\eta_2}{\eta_1} - \frac{\gamma_1}{\gamma_0} = (\chi_1 + \chi_2)\left[1 - \frac{\chi_1\chi_2}{\chi_1^2 + \chi_2^2} - 1\right] < 0 .$$

Note that for two electron-like bands, $\frac{\eta_2}{\eta_1} - \frac{\gamma_1}{\gamma_0} > 0$.

Bloomfield's calculation shows that the predominant contribution to the Hall coefficient due to the impurity is linear in impurity concentration, with higher order terms in concentration being progressively less important. For one electron-like band and one hole-like band, the linear contribution has a sign opposite to that of the Hall

coefficient of the host. The magnetic field and temperature dependence of the linear term derives from the sum A, which also appears in the magnetoresistance. Bloomfield, Hecht and Sievert[27] have calculated the magnetoresistance for the magnetic impurity problem and the result appears in Fig. 6. Note that this result must be multiplied by a minus sign when compared with the Hall coefficient data.

The mechanism for the linear term is simply the freezing out of the spin-flip scattering. As the magnetic field is increased, both one of the impurity spin levels and one of the conduction electron spin levels involved in the spin-flip scattering process become depopulated and the spin flip scattering will decrease.[27] Thus, the linear contribution does not depend upon $\tau\uparrow$ and $\tau\downarrow$ being different. However, this difference is important in the magnetic field dependence of the c^2 term. (Bloomfield has discussed the H-dependence of the c^2 term in a private communication.)

APPENDIX D: "PURE" Cu AND "PURE" Au DATA

The Hall coefficient of Cu at 4.2° K as a function of field appears in Fig. 44 for three different samples. Field dependences have been observed[39, 40, 41] for Cu samples prepared in various ways, and as there are many variables to consider (i.e. impurities, defects, low-field to high-field transition, etc.) it is not possible to give a clear-cut explanation of our field dependence. However, it is encouraging that the values seem to converge at higher fields, and we can make a reasonable estimate for R in Cu of $-6.55 \pm .20 \times 10^{-13}$ $\frac{\text{V-cm}}{\text{amp-gauss}}$ at $T = 4.2^{\circ}$ K. This number agrees well with the results shown in Table 6.

The Au data appear in Fig. 45. Unfortunately, the reproducibility is very poor, and this could be connected with the low RRR's. Using spectrographic techniques, sample No. 118 was found to contain 7 at.ppm of Fe. This alone does not explain the low RRR's. As further experimental work would have to be done to obtain reliable values for Au, we cannot obtain a comparison with other experiments.

APPENDIX E: EFFECT OF COLD-WORKING AND ANNEALING ON Cu-Au (Fe) ALLOYS

The effect of cold-working and annealing (hereafter referred to as CWA) was observed for various Cu-Au (Fe) alloys. Plots of R vs H for various Fe concentrations in $CuAu_{14.3}$ appear in Fig. 46, where data is presented for both untreated samples and CWA samples for comparison. In addition the results for a series of untreated and CWA Cu-Au hosts containing Fe appear in Fig. 47. The CWA treatment merely shifts each data point by the same amount and the qualitative behavior of the data is unaffected. Note that for the one sample which was annealed without cold-working, the effect of the treatment was not as large as for those that had been cold-worked also.

Successive CWA treatments were carried out on two pieces of Cu-Au (Fe) alloy obtained from the same starting material. Samples A and D were cut from material that had undergone CWA once, B and E from material that had undergone two successive CWA treatments, and C and F from material treated by CWA three times. Hall coefficient data for the samples described above appear in Figs. 48 and 49. Beyond the first treatment, successive CWA treatments have no systematic effect on the Hall coefficient, and the randomness in the data is within experimental error.

In addition to the above described samples, two other samples C' and D' were subjected to a long anneal after being cut from their respectively treated materials, C and D. For both of these

samples (see Figs. 48 and 49) there is a small decrease in Hall coefficient (which is greater than experimental error in one case). Thus, results appearing in the first paragraph of this appendix are for samples that had been annealed after cutting.

Along with the Hall data for samples A, B, and C, we obtained resistance data as a function of temperature. From these data we obtained the temperature of the resistance minimum, T_{min}, and a measure of the strength of the Fe impurity contribution, $\frac{R(2^{o})-R(T_{min})}{R(T_{min})}$. These quantities appear in Table 7 and, again, there is little systematic effect due to the successive CWA treatments. One sample, A_{outer} gave results which were quite different. This sample was cut from the surface and was very probably strongly oxidized. Note that we corrected for this problem in the preparation of succeeding samples.

APPENDIX F: CONVERSION FACTORS

Practical units are commonly used, but they are a conglomeration of other systems. The conversion factors, from practical units($\frac{\text{V-cm}}{\text{a-G}}$) to other systems are listed below.

To Obtain	Multiply Practical Units by
MKS Units ($\frac{\text{m}^3}{\text{coul}}$)	$\times 10^2$
Gaussian Units	$\times \frac{1}{9 \times 10^{11}}$
cgsm	$\times 10^9$
emu	$\times 10^9$

NOTES

1. E.H. Hall, Am. J. Math. 2, 287 (1879).

2. J.M. Ziman, Adv. Phys. 10, 1 (1961).

3. For a recent review of the Fermi Surface of Noble Metals, see A.P. Cracknell, Adv. Phys. 20, 1 (1971).

4. M. Springford, Adv. Phys. 20, 493 (1971).

5. In particular, Azbel-Kaner Cyclotron Resonance and Magnetic Field Induced Surface States measurements.

6. J.S. Dugdale and L.D. Firth, J. Phys. C. (Solid State Phys.) 2, 1272 (1969). They have calculated room temperature Hall coefficients consistent with isotropic scattering using new data on the Fermi surface for Ag and Cu due to M.R. Halse, Phil. Trans. R. Soc. 265, 507 (1969).

7. For example see F. Seitz, Modern Theory of Solids, McGraw Hill, New York, 1940, p. 40.

8. C.M. Hurd, Phil. Mag. 12, 47 (1965).

9. V. Heine, Phil. Mag. 12, 53 (1965).

10. R.D. Barnard, et. al., Phys. Rev. 176, 761 (1968).

11. We use the word "Band" because it is a commonly used term from semiconductor physics. However, as C.M. Hurd (The Hall Effect in Metals and Alloys, Plenum Press, 1972, p. 87.) points out we are really talking about two groups of carriers which could possibly belong to the same band of the metal and the resulting equations have the same form as for band theory. In addition it should be noted that a two band model is just a first approximation to describing the anisotropy of τ_k over the Fermi surface because τ_k is continuously varying. However, the two band model is the easiest to handle mathematically and it most probably gives qualitatively correct results. Therefore it is often used.

12. G.J. Van den Berg in 'Progress in Low Temperature Physics' (G. J. Gorter Ed.) vol. 4, Chapt. 4, North Holland Publishing Company, Amsterdam, 1964.

13. M.D. Daybell and W.A. Steyert, Rev. Mod. Phys. 40, 380, (1968).

14. A.J. Heeger in 'Solid State Physics' (F. Seitz, D. Turnbull, H. Ehrenreich, Eds.) Vol. 23, p. 283, Academic Press, New York, 1969.

15. J. Kondo in 'Solid State Physics' (F. Seitz, D. Turnbull, H. Ehrenreich, Eds.) Vol. 23, p. 183, Academic Press, New York, 1969.

16. J. Freidel, Nuovo Cimento Supplement 7, 287 (1958).

17. J. Freidel in 'Metallic Solid Solution' (J. Friedel and A. Guinier, Eds.) Benjamin, New York, 1963.

18. P.W. Anderson, Phys. Rev. 124, 41 (1961).

19. There is a nice plausibility argument, originally due to Blandin [A. Blandin and J. Friedel, J. Phys. Rad. 20, 160 (1959).] for the criterion of magnetism. Picture the degenerate density of states diagram in Fig. 4. If we move a group (X) of electrons from below the Fermi energy to above the Fermi energy (Y), we can ask under what condition this magnetic state will be stable. It will be stable if the energy decreases upon transition to this state. The change in kinetic energy will be $\Delta KE = \Delta E_\nu$, where ν is the number of electrons moved. However $\rho \Delta E = \nu$ so $\Delta KE = \nu^2/\rho$. The initial potential energy will be Un^2 since $n\uparrow = n\downarrow$. The final potential energy will be $U(n+\nu)(n-\nu)$ so the change will be $-U\nu^2$. We want the total change in energy $\Delta W = \nu^2(1/\rho - U) < 0$ or $U\rho > 0$. The density of states ρ is at most $1/\pi\Delta$ so we obtain $U/\pi\Delta > 0$.

20. J. Schrieffer, J. Appl. Phys. 38, 1143 (1967).

21. M.P. Sarachik, J. Appl. Phys. 35, 1094 (1964).

22. M.P. Sarachik, et. al., Phys. Rev. 135, A1041 (1964).

23. J. Kondo, Prog. Theor. Phys. 32, 37 (1964).

24. R. More, Solid State Comm. 7, 237 (1969), and R. More's Thesis.

25. M.T. Béal-Monod and R.A. Weiner, Phys. Rev. 3, B3056 (1971).

26. M.T. Béal-Monod and R.A. Weiner, Phys. Rev. 3, B145 (1971).

27. P.E. Bloomfield, R. Hecht, and P.R. Sievert, Phys. Rev. 2, B3714 (1970).

28. Y. Nagaoka, Phys. Rev. 138, A1112 (1965).

29. A.E. Alderson and C.M. Hurd, J. Phys. Chem. Solids 32, 2075 (1971).

30. We are indebted to S. Foner for this suggestion.

31. J.W. Loram, T.E. Whall, P.J. Ford, Phys. Rev. 2, B857 (1970).

32. J.S. Dugdale and L.D. Firth, J. Phys. C. (Solid State Phys.) 2, 1272 (1969).

33. For lower Kondo temperatures (as in the Au-rich alloys) it is necessary to make measurements on lower concentrations to avoid interactions. This results in a correspondingly smaller effect and thus a larger percentage error.

34. E.W. Fenton, Phys. Rev. 5, B3788 (1972).

35. I. Isenberg, B.R. Russel, R.F. Green, Rev. Sci. Inst. 19, 685 (1948).

36. Pressure contacts with knife edges were used in the first attempt to measure the Hall voltage. The current leads were soldered. Peculiar, slightly nonreproducible effects were observed at low fields (i.e. below 15 kG.). A typical example of these is shown in Fig. 36. It should be noted that in spite of this peculiar effect, the average value of the Hall voltage, V_H, from the four possible permutations of current and magnetic field behaved sensibly (i.e. the peculiar effect cancelled out). The behavior improved as the set screws which applied pressure for contact, were changed from iron to brass to nylon. It is possible that the contacts were moving in a slightly non-reproducible way as a result of magnetic forces on the set screws. At any rate, the method was abandoned. When the voltage leads were spot welded the above effect was reduced considerably. However, there was a small remanent of the effect which disappeared around 0.5 kilogauss, and this was completely eliminated by spot welding the current leads as well.

37. C.M. Hurd, The Hall Effect in Metals and Alloys, Plenum Press, New York, 1972, pp. 184-189.

38. M.P. Sarachik, E. Corenzwit and L.D. Longinotti, Phys. Rev. 135, A1041 (1964).

39. R.G. Chambers Proc. Roy. Soc. (London) A238, 344 (1957).

40. W. Huppmann and F. Stangler, Phys. Stat. Sol. 35, K161 (1969).

41. J.E.A. Alderson, T. Farrell, C.M. Hurd, Phys. Rev. 1, 3904 B (1970).

42. R.D. Barnard and L. Sumner, Phil. Mag. 20, 399 (1969).

43. T.G. Berlincourt, Phys. Rev. 112, 381 (1958).

44. J.E.A. Alderson, T. Farrell, C.M. Hurd, Phys. Rev. 174, 729 (1968).

FIGURE CAPTIONS

Fig. 1. Geometry and conditions for observing the Hall effect: An electron current I is passed along the length L of a thin slab of thickness t in a magnetic field H which is perpendicular to the slab. Under these conditions a voltage V, referred to as the Hall voltage, is developed across the width W of the sample.

Fig. 2. A rough sketch of the Fermi surface of noble metals. The neck (N) and belly (B) orbits are shown.

Fig. 3. Illustration of the relative distortions of the Fermi surfaces (solid lines) of: (a) Cu, (b) Ag and (c) Au from the free electron model (dashed lines).

Fig. 4. Degenerate density of states diagram for spin-up and spin-down electrons.

Fig. 5. The Hall coefficient (in units such that e = n = 1) as a function of magnetic field and temperature (in units normalized to the Fermi energy, i.e. gu_BH/ϵ_F and kT/ϵ_F) from a calculation by R. More (see Ref. 24). These curves are for the case J = 0.025 and V = 0.10. For comparison, J = 0.4 in Cu (Fe) (see Ref. 31).

Fig. 6. Resistivity as a function of external magnetic field for a number of temperatures. The calculation is specifically for T_k= 16° K. (see Ref. 27).

Fig. 7. $\Delta R/R(0)$ vs gu_BH/kT where $\Delta R \equiv R(H) - R(H=0)$. The symbols 0 represent the data of P. Monod (see Ref. 25) for 150 PPM Fe in Mn at T = 1.2° K. The solid curves represent Béal-Monod and Weiner's second Born fit (a) and first born fit (b) to the data.

Fig. 8. Field dependence at 4.2° K of $\Delta\rho_H \equiv \rho_H$(alloy) $- \rho_H$(host) for polycrystalline Au (Fe) samples. The dash-dot lines are Langevin functions obtained for the arguments indicated.

Fig. 9. Field dependence at 4.2° K of $\Delta\rho_H = \rho_H$(alloy) $- \rho_H$(host) for polycrystalline Cu (Fe) and Cu (Mn).

Fig. 10. The Hall coefficient R as a function of host composition. The solid line is only for purposes of delineating our data. The treated samples were prepared as follows:

The material was cold-worked. A Hall sample was cut and then annealed for ten days (see Appendix A for details). For comparison, data of Barnard, et. al.[11] and Dugdale and Firth[32] appear on the plot.

Fig. 11. Resistivity ρ as a function of host composition at T = 4.2° K and T = 300° K. The solid lines are only for purposes of delineating the data. The dashed lines are a symmetric continuation of the data on the Cu rich side. Typical error bars are included for a sampling of points.

Fig. 12. Resistivity ρ vs. T for a selection of Cu-Au (Fe) alloys.

Fig. 13. R vs. H. Typical error bars are shown on the host data. Note that we have included only random error; the systematic error is larger (see Appendix A).

Figs. 14-17. R as a function of field at 1.5° K and 4.2° K (grouped by Cu-Au host composition) for Cu-Au (Fe) alloys and their corresponding hosts.

Fig. 18. R as a function of Fe concentration at T = 1.5° for the Cu $Au_{14.3}$ (Fe) alloy series. The different plots are for various magnetic fields. For details of host composition and measuring temperature refer to Fig. 15.

Fig. 19. $a'(H,T)R_H$ vs. H for $CuAu_{5.0}$ (Fe) alloys. The values of $a(H,T)/R_H$ are set equal at H = 60 kG and T = 1.50° K for all concentrations. The resulting normalized values of $a(H,T)/R_H$ are referred to as $a'(H,T)/R_H$.

Fig. 20. $a'(H,T)/R_H$ vs. H for $CuAu_{14.3}$ (Fe) alloys.

Fig. 21. $a'(H,T)/R_H$ vs. H for $CuAu_{17.5}$ (Fe) alloys.

Fig. 22. $a(H,T)$ vs. H for 252 PPM in $CuAu_{14.2}$. The typical error bars do not include systematic error because all the data is for the same sample.

Fig. 23. $\frac{R_{60}-R_{20}}{c\,R_H}$ vs. alloy composition at 4.2° and 1.5° K.

Fig. 24. R vs. $\frac{gu_BH}{k_B}+T$ and R vs. $\left[T^2+\left(\frac{gu_BH}{k_B}\right)^2\right]^{\frac{1}{2}}$ for 801 PPM Fe in $CuAu_{5.0}$. Notice energies appear in units of temperature. For this and succeeding plots we take g = 2.

Figs. 25-30. R vs. $\left[T^2 + \left(s \frac{gu_B H}{k_B}\right)^2\right]^{\frac{1}{2}}$ for the alloys labeled on the figure. Notice energies appear in units of temperature. Also the value of s used to obtain the best matching of the two temperature runs appears on the figure.

Fig. 31. $\frac{a(H,T)dir}{R_H}$ and $\Delta\rho/\rho_0$ vs. H for 801 PPM Fe in $CuAu_{5.0}$ at 1.5° K. $\frac{a(H,T)dir}{R_H}$ was obtained by direct subtraction without correcting for a c^2 term.

Fig. 32. $\frac{a(H,T)corr}{R_H}$ vs. H for 801 PPM Fe in $CuAu_{5.0}$ at 1.5° K. $\frac{a(H,T)\ corr}{R_H}$ was obtained after correcting for a c^2 term.

Fig. 33. Schematic of the arc furnace.

Fig. 34. Schematic of the annealing apparatus.

Fig. 35. Sample geometry and dimensions.

Fig. 36. ΔV_H vs. H for 373 PPM Fe in $CuAu_{14.3}$. The voltage ΔV_H was measured with pressure contacts. ΔV_H is the change in Hall voltage and for convenience the change is measured from the 4.34 kG value for all curves. The four different curves are for the four permutations of field and current directions.

Fig. 37. Schematic of the cryogenic apparatus.

Fig. 38. Schematic of the sample holder.

Fig. 39. Schematic of the measuring circuit.

Fig. 40. Schematic of the magnetic field circuit.

Fig. 41. Magnet coil constant (H/I) as a function of magnetic field. The error bars include systematic error. The random error is obviously much less.

Figs. 42-43. R vs. H for two runs on the same sample (see the figures for details.) The error bars shown are for the random thermal fluctuations only.

Fig. 44. R vs. H for several Cu samples. The sample labelled CWA was cut from cold-worked material and then annealed for 10 days. The typical error bar includes systematic error.

Fig. 45. R vs. H for several Au samples. The sample labelled CWA was cut from cold-worked material and then annealed for 10 days. Note for one ingot the starting material was etched. This was not the usual procedure for Au (see Appendix A). The error bars include systematic error.

Fig. 46. R vs. H for $CuAu_{14.3}$ (Fe) alloys. The solid curves are for untreated samples. The dashed curves are for samples which were cut from cold-worked material and then annealed for 10 days. The dot-dash curve is for a sample which was annealed for 10 days without previous cold working.

Fig. 47. R vs. H for Fe in various Cu-Au alloys. The solid curves are for untreated samples. The dashed curves are for samples which were cut from cold-worked material and then annealed for 10 days.

Fig. 48. R vs. H for sample material (from the first half of an ingot) which underwent successive treatments. Sample A was cut from material which was cold-worked and annealed for 2 hours. Sample B was from the same material after reworking and reannealing 10 hours. Sample C was from the reworked material of B after again reworking and reannealing for 7 hours. Finally sample C', in addition to the treatment of sample C, was reannealed (10 days) after cutting.

Fig. 49. R vs. H for sample material (from the second half of the ingot mentioned in the figure caption of Fig. 48) which underwent successive treatments. Sample D was cut from material which was cold-worked and annealed for 15 hours. Sample D' was from the same material; however, it was reannealed (10 days) after it was cut. Sample E came from the material of D after reworking and reannealing for 12 hours. Finally sample F was from the reworked material of E which was again reworked and reannealed for 18 hours.

TABLE CAPTIONS

Table 1 Hall coefficients for the noble metals (from Reference 4).

Table 2 Analysis of samples for Fe content. The nominal Fe concentrations were obtained from the weights of the starting materials. The analysis was generally carried out using chemical techniques. An asterisk appears by those values obtained by spectrographic techniques.

Table 3 Residual resistance ratios ($R(300^{\circ}\ K)/R(4.2^{\circ}\ K)$) for Cu-Au (Fe) alloys, Cu-Au alloys, Cu, and Au.

Table 4 Values of the scaling parameter s for various Cu-Au (Fe) alloys.

Table 5 A comparison of temperatures measured by pressure readings over liquid helium ($T_{pressure}$) and a germanium thermometer ($T_{therm.}$).

Table 6 Observed values of the Hall coefficient of Cu and the appropriate reference in the text.

Table 7 Resistance data for the samples treated as described in figure caption 48. The quoted parameters are discussed in Appendix E.

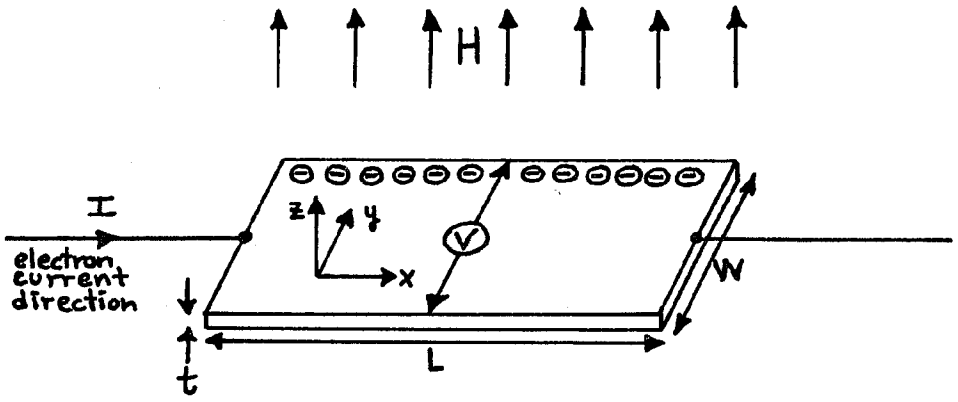

FIGURE 1

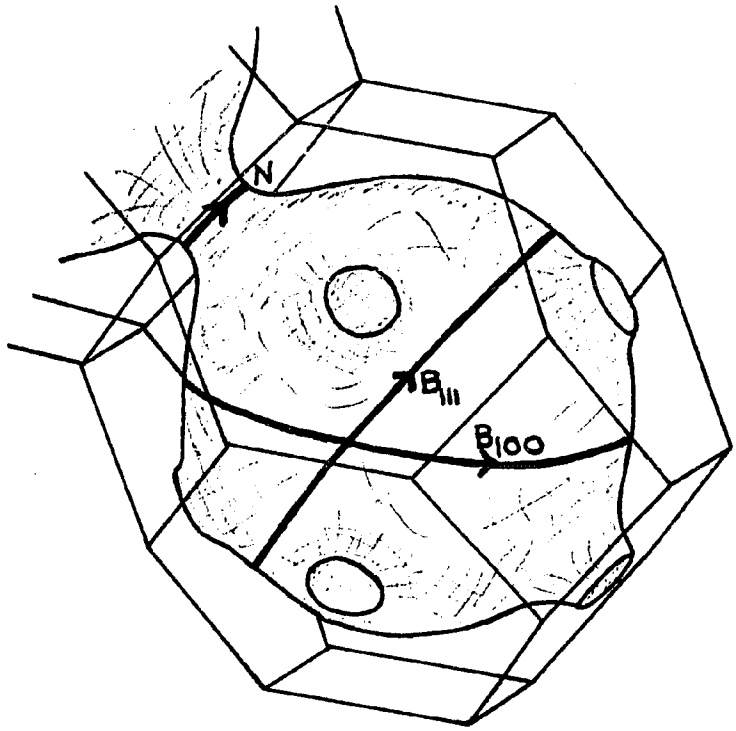

FIGURE 2

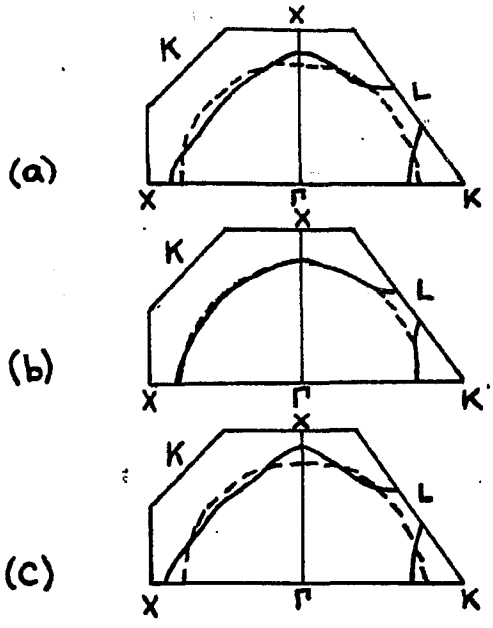

FIGURE 3

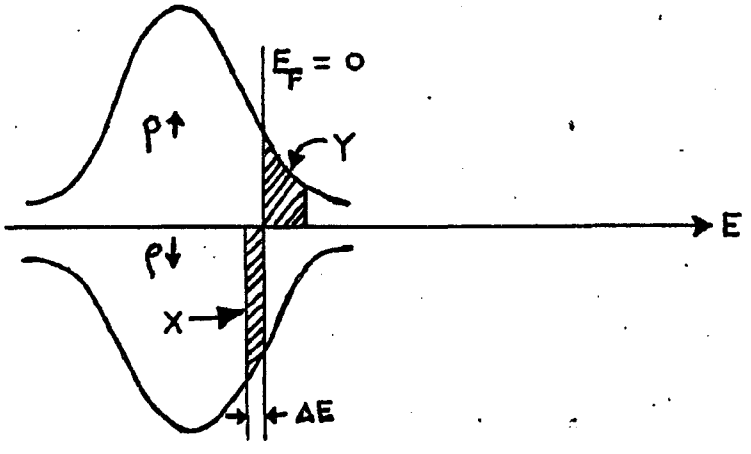

FIGURE 4

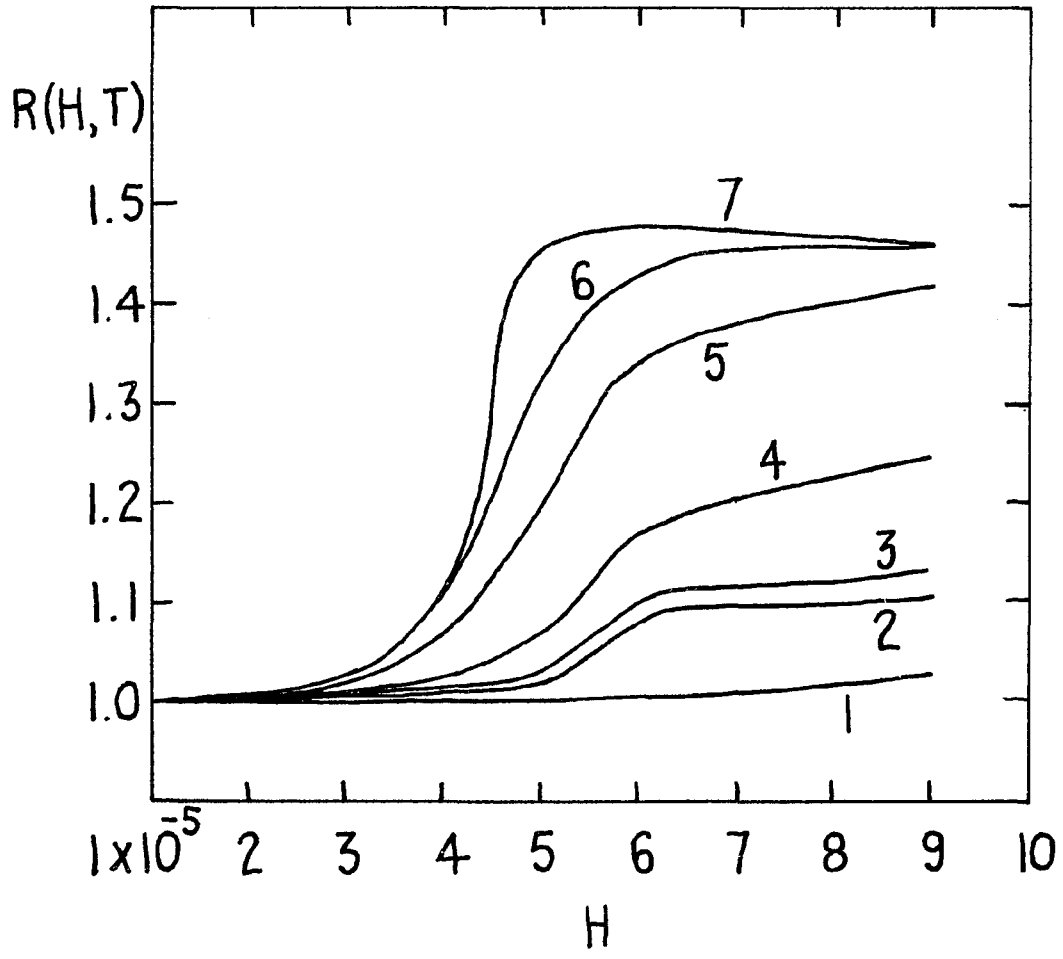

THE TEMPERATURES FOR THESE CURVES ARE:

	NORMALIZED TO E_F (I.E. $k_B T/E_F$)	IN °K FOR Cu (E_F = 7ev)
(1)	2×10^{-4}	16°K
(2)	1×10^{-5}	.8°K
(3)	4×10^{-6}	.32°K
(4)	2×10^{-6}	.16°K
(5)	1×10^{-6}	.08°K
(6)	7×10^{-7}	.06°K
(7)	5×10^{-7}	.04°K

ONE FIELD DIVISION IS EQUIVALENT TO 12 KILOGAUSS IN THE CASE OF Cu (E_F = 7 eV)

FIGURE 5

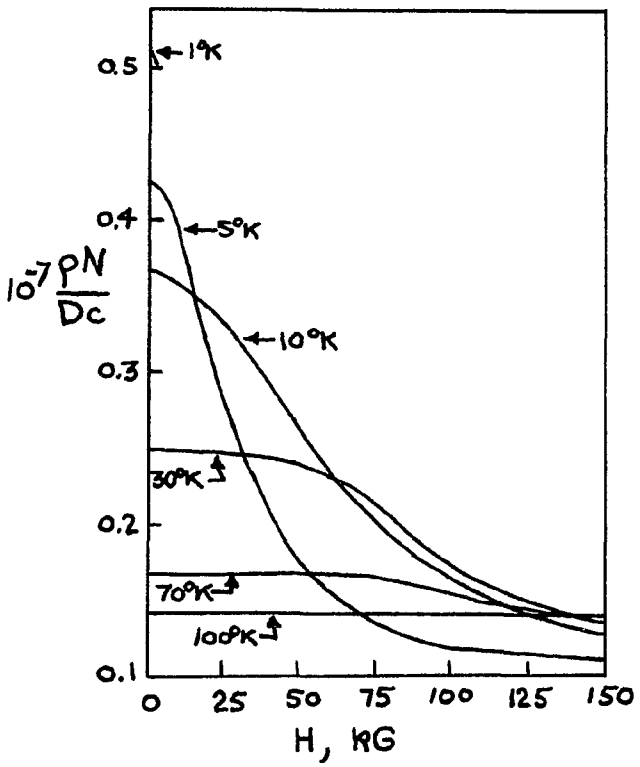

ρ IS THE RESISTIVITY

N IS THE NUMBER OF UNIT CELLS IN THE LATTICE

D IS THE BAND WIDTH OF THE CONDUCTION ELECTRONS

c IS THE IMPURITY CONCENTRATION

H IS THE MAGNETIC FIELD

FIGURE 6

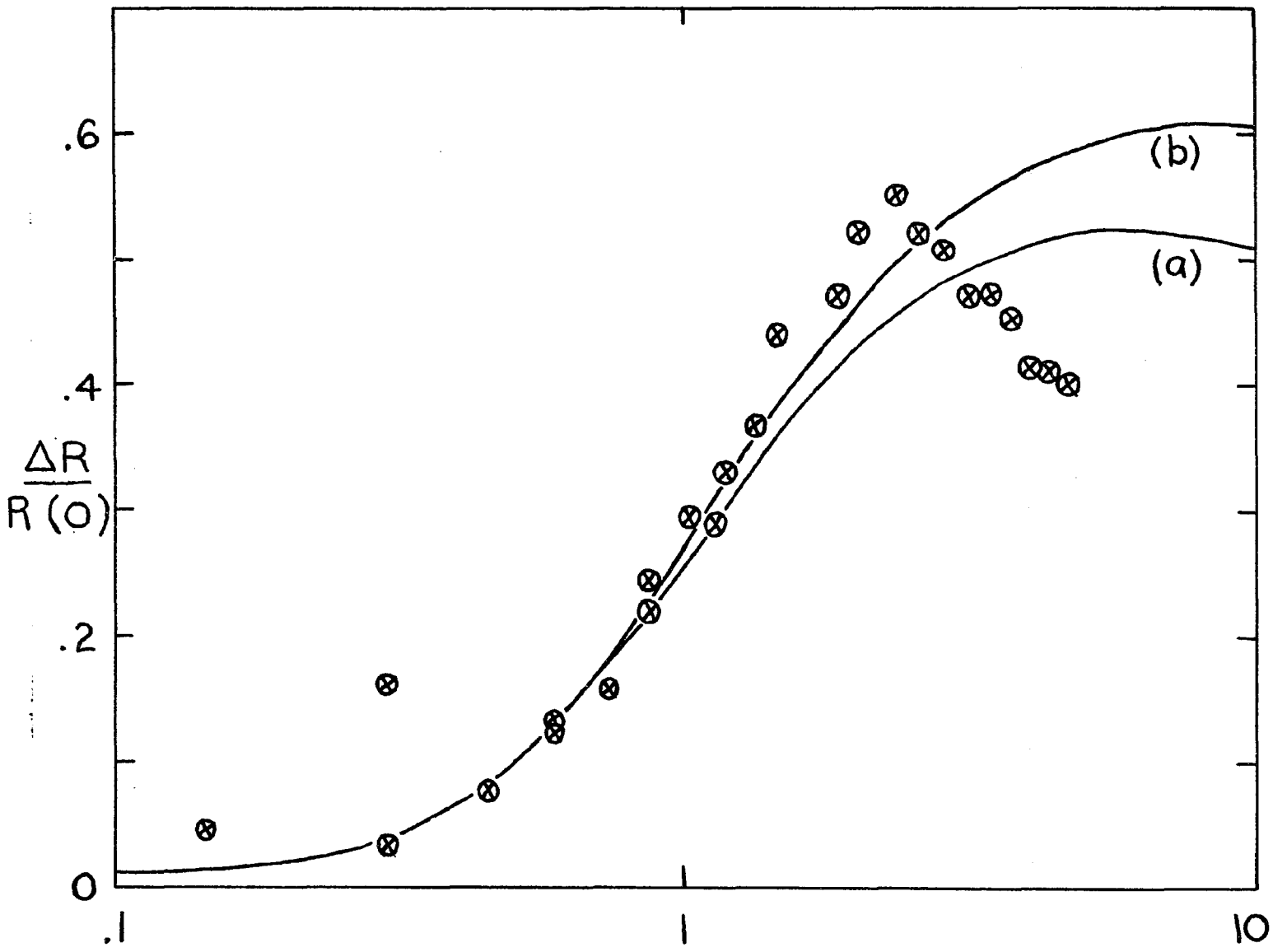

FIGURE 7

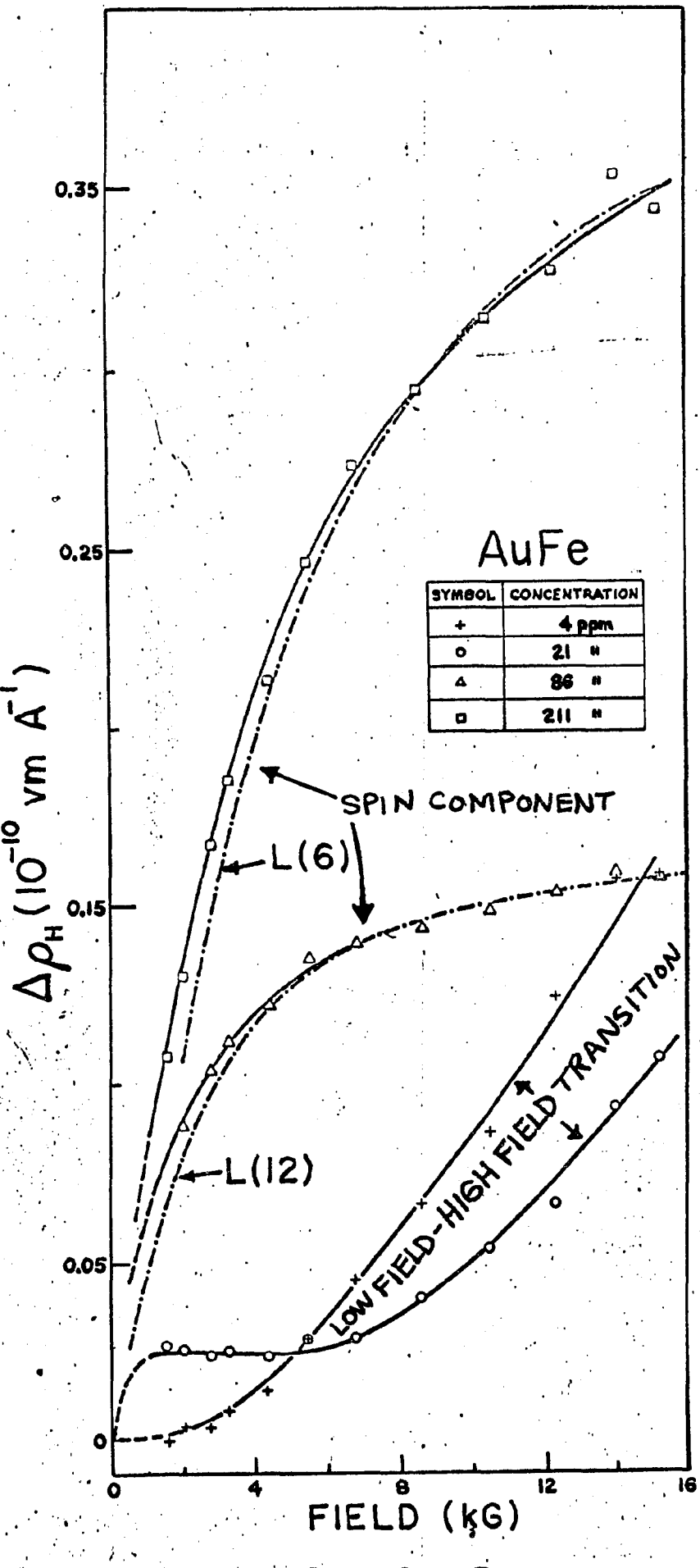
AuFe
SYMBOL | CONCENTRATION
+ | 4 ppm
o | 21 "
Δ | 86 "
□ | 211 "
SPIN COMPONENT
L(6)
L(12)
LOW FIELD-HIGH FIELD TRANSITION
Δρ_H (10^-10 vm A^-1)
0.35
0.25
0.15
0.05
0
0
4
8
12
16
FIELD (kG)

FIGURE 8

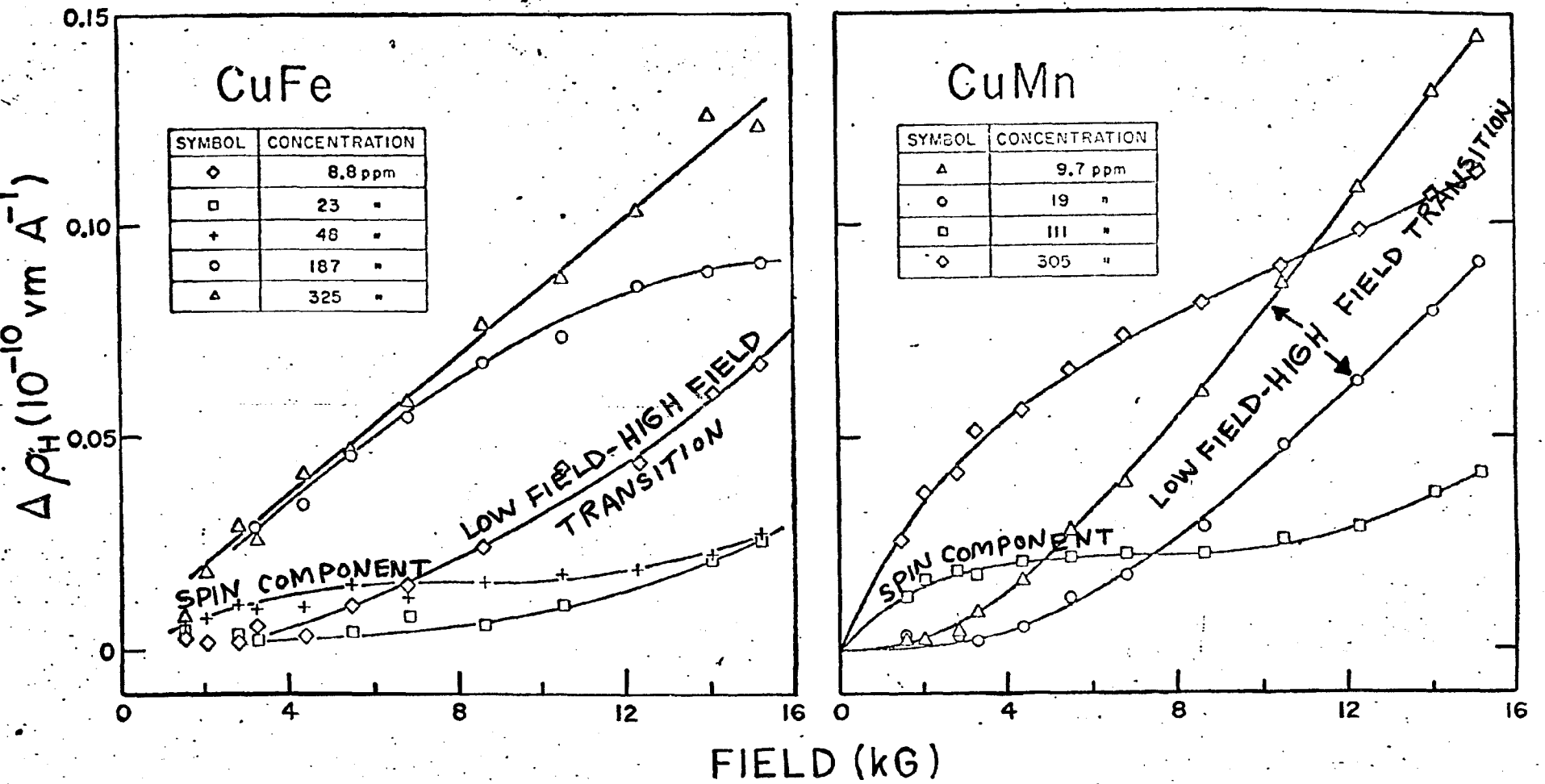
CuFe
SYMBOL
CONCENTRATION
8.8 ppm
23 "
48 "
187 "
325 "
SPIN COMPONENT
LOW FIELD-HIGH FIELD TRANSITION
CuMn
SYMBOL
CONCENTRATION
9.7 ppm
19 "
111 "
305 "
SPIN COMPONENT
LOW FIELD-HIGH FIELD TRANSITION
$\Delta\rho_H (10^{-10}$ vm $A^{-1})$
0.15
0.10
0.05
0
0
4
8
12
16
FIELD (kG)

FIGURE 9

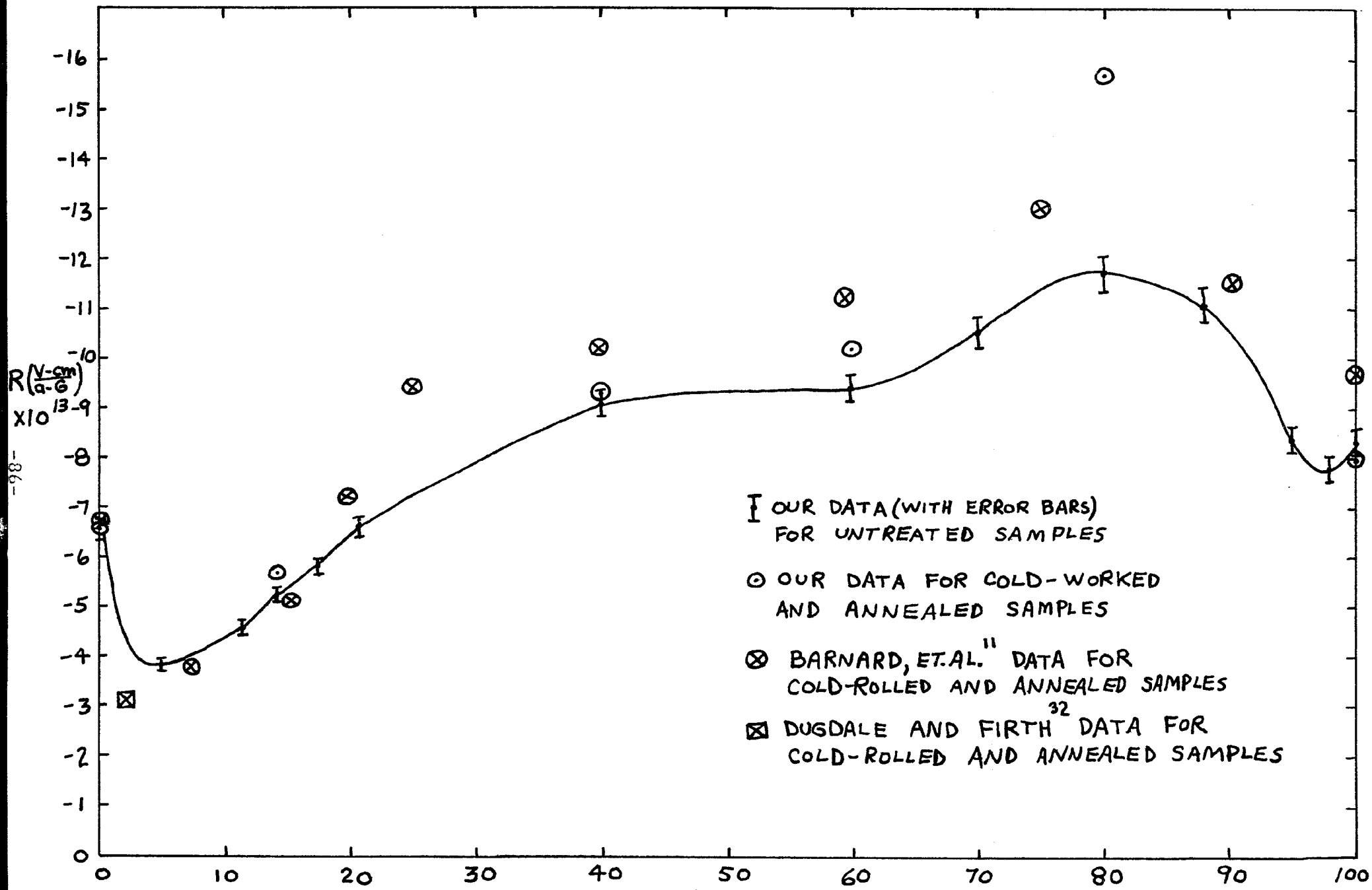
-16
-15
-14
-13
-12
-11
-10
-9
-8
-7
-6
-5
-4
-3
-2
-1
0
R(V-cm/a-G) X10^13
0
10
20
30
40
50
60
70
80
90
100
at. % Au
I OUR DATA (WITH ERROR BARS) FOR UNTREATED SAMPLES
⊙ OUR DATA FOR COLD-WORKED AND ANNEALED SAMPLES
⊗ BARNARD, ET.AL.[11] DATA FOR COLD-ROLLED AND ANNEALED SAMPLES
⊠ DUGDALE AND FIRTH[32] DATA FOR COLD-ROLLED AND ANNEALED SAMPLES

FIGURE 10

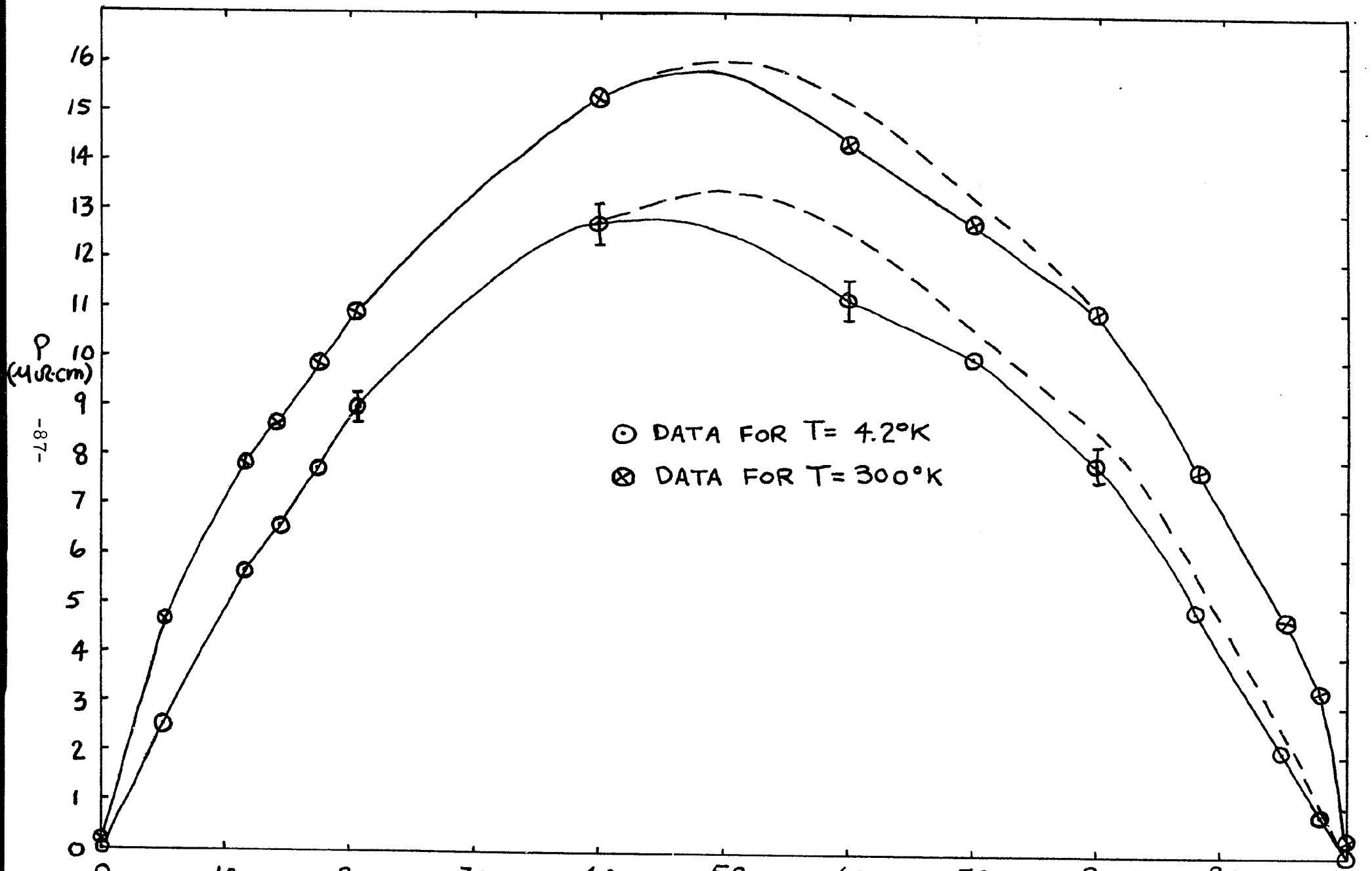
ρ (μΩ·cm)
0
1
2
3
4
5
6
7
8
9
10
11
12
13
14
15
16
0
10
20
30
40
50
60
70
80
90
100
at. % Au
⊙ DATA FOR T= 4.2°K
⊗ DATA FOR T= 300°K

FIGURE 11

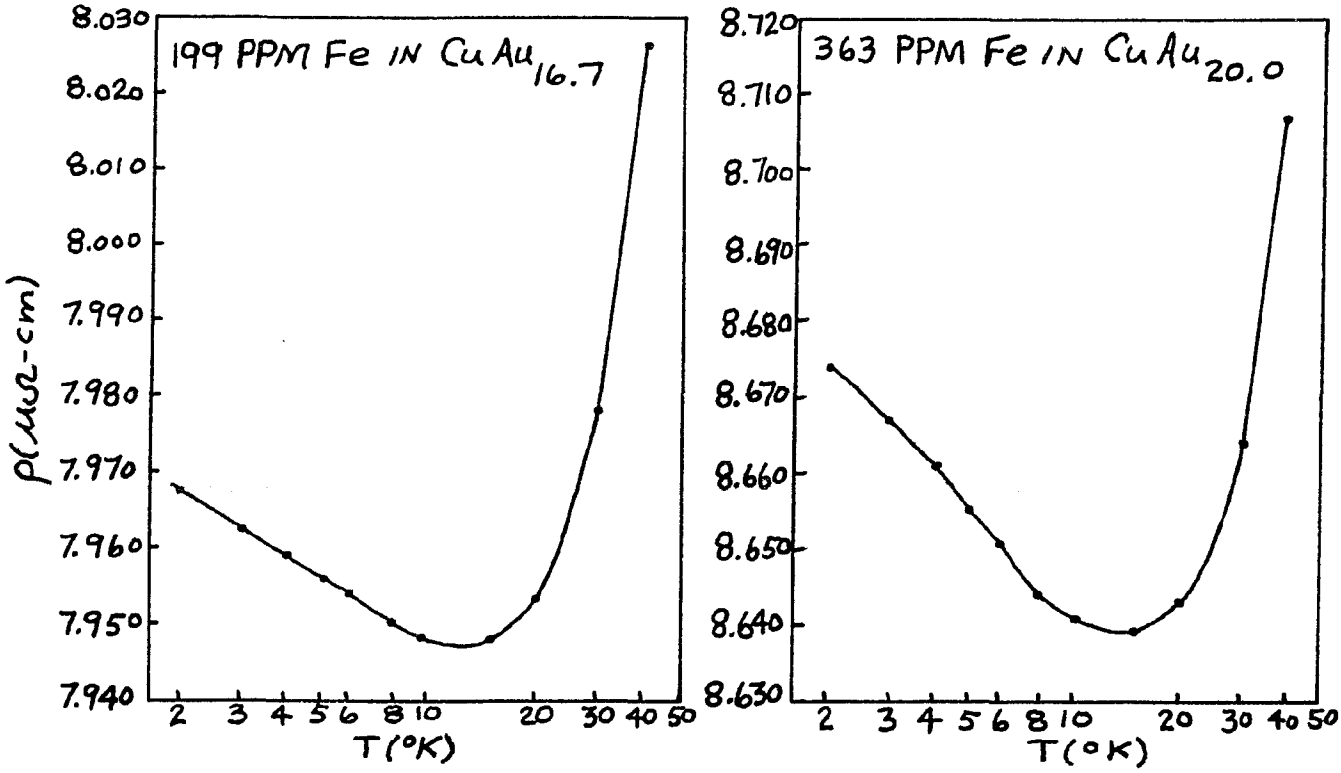
199 PPM Fe IN CuAu16.7
363 PPM Fe IN CuAu20.0
ρ(μΩ-cm)
T(°K)
8.030
8.020
8.010
8.000
7.990
7.980
7.970
7.960
7.950
7.940
8.720
8.710
8.700
8.690
8.680
8.670
8.660
8.650
8.640
8.630
2 3 4 5 6 8 10 20 30 40 50

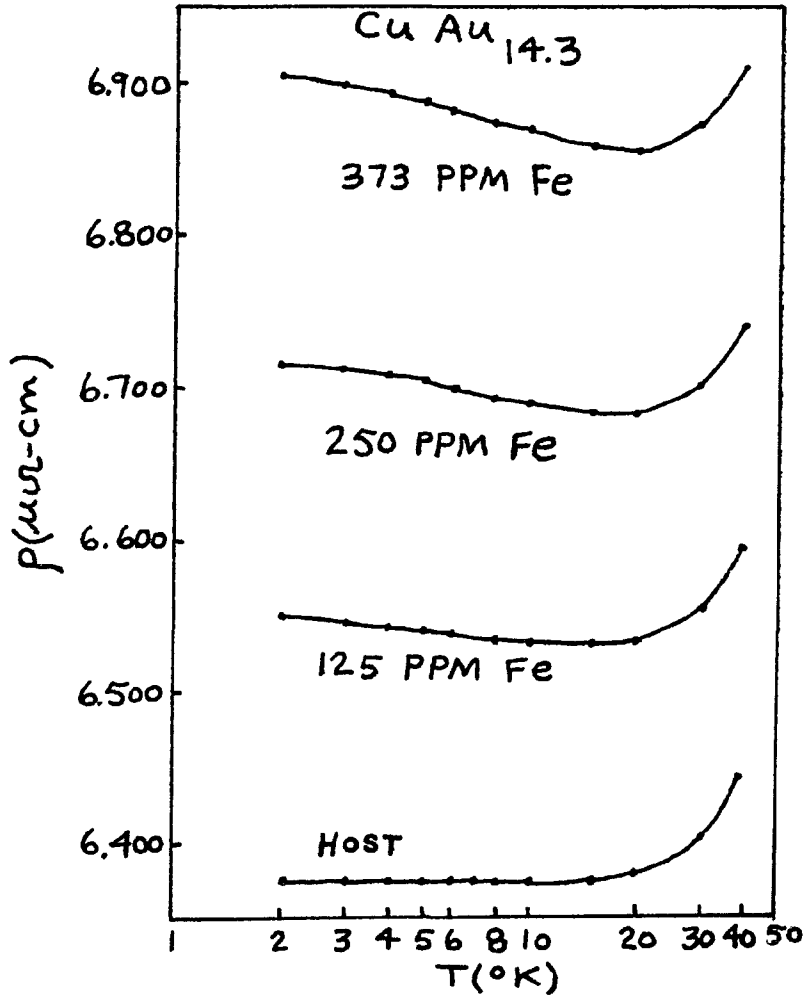
Cu Au14.3
373 PPM Fe
250 PPM Fe
125 PPM Fe
HOST
ρ(μΩ-cm)
T(°K)
6.900
6.800
6.700
6.600
6.500
6.400
1 2 3 4 5 6 8 10 20 30 40 50

FIGURE 12

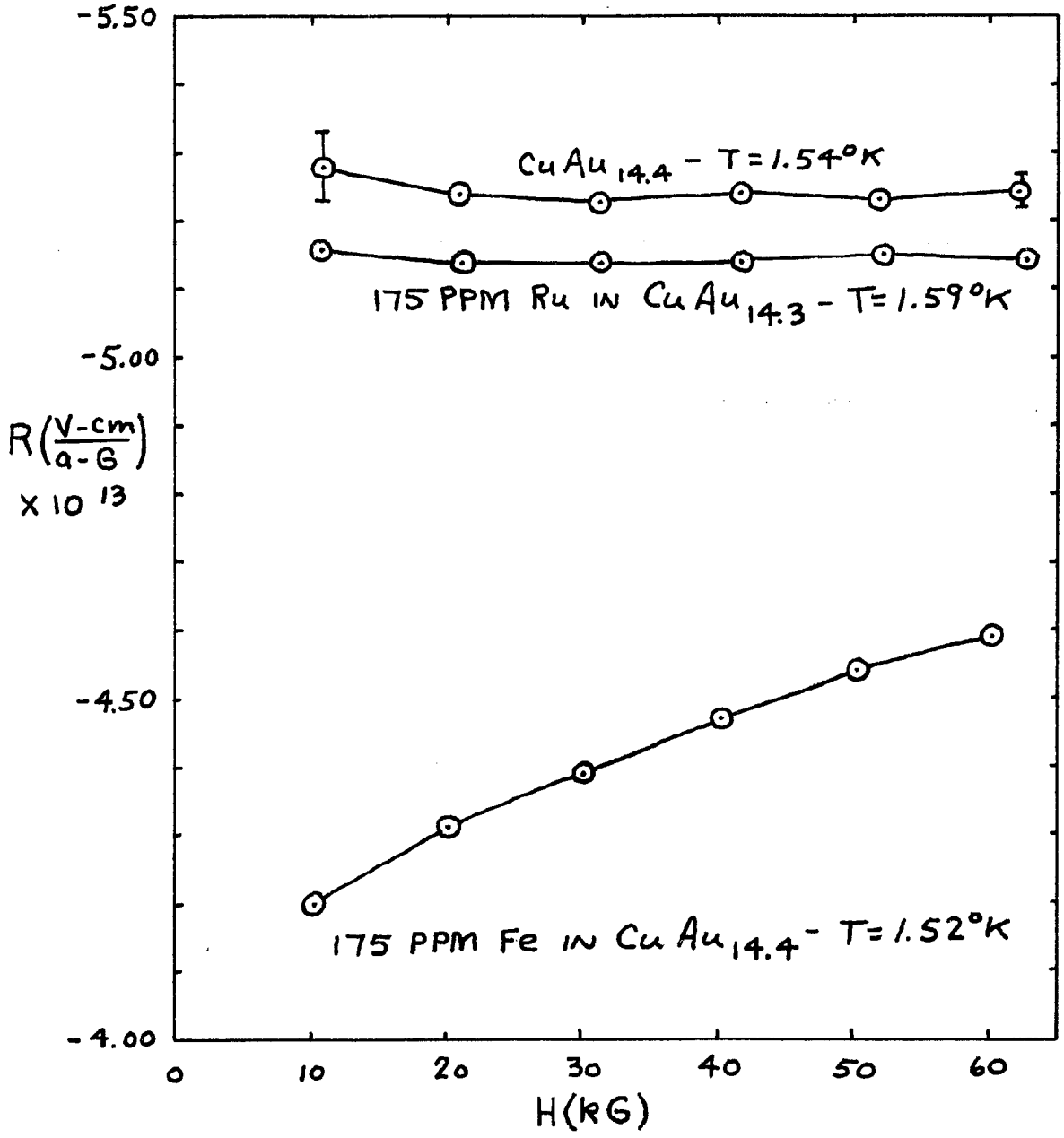
-5.50
-5.00
-4.50
-4.00
R(V-cm/a-G)
X 10 13
CuAu 14.4 - T = 1.54°K
175 PPM Ru IN CuAu 14.3 - T = 1.59°K
175 PPM Fe IN CuAu 14.4 - T = 1.52°K
0
10
20
30
40
50
60
H(kG)

FIGURE 13

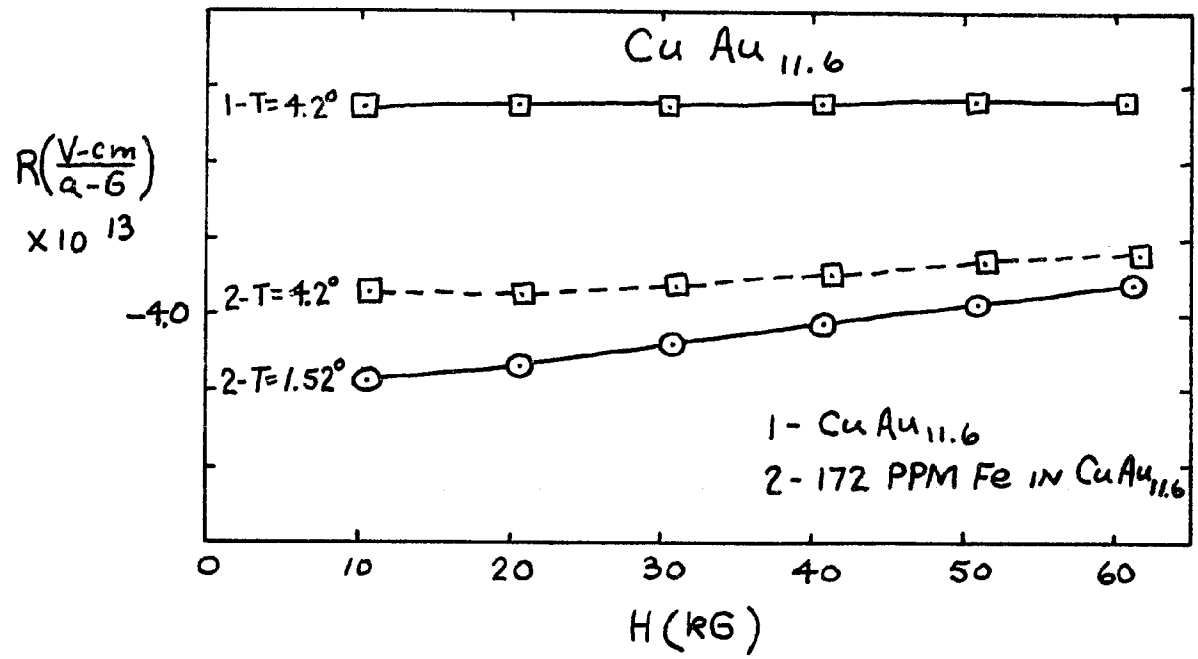
Cu Au 11.6
1-T=4.2°
2-T=4.2°
2-T=1.52°
R(V-cm/a-G)
X10 13
-4.0
1 - Cu Au 11.6
2 - 172 PPM Fe IN Cu Au 11.6
0
10
20
30
40
50
60
H(kG)

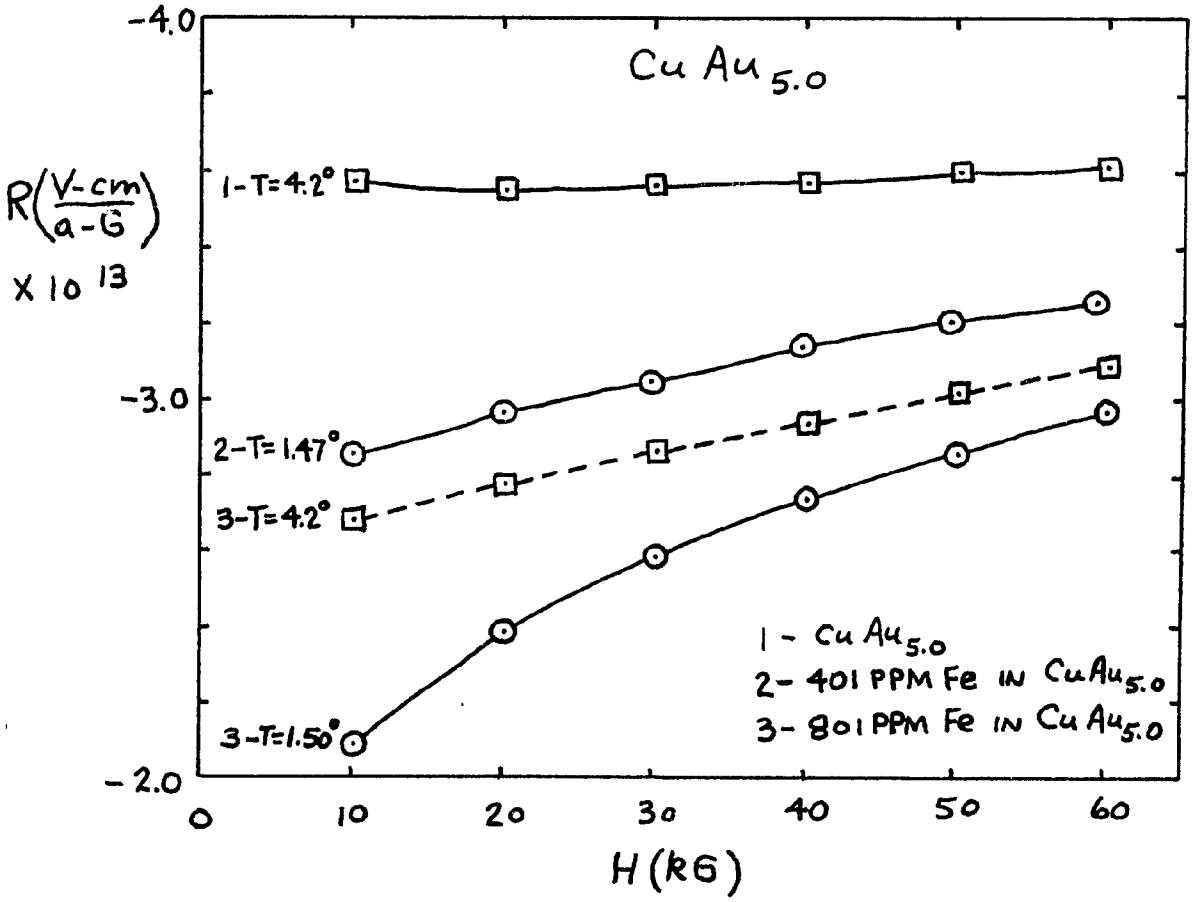
Cu Au 5.0
1-T=4.2°
2-T=1.47°
3-T=4.2°
3-T=1.50°
R(V-cm/a-G)
X10 13
-4.0
-3.0
-2.0
1 - Cu Au 5.0
2 - 401 PPM Fe IN Cu Au 5.0
3 - 801 PPM Fe IN Cu Au 5.0
0
10
20
30
40
50
60
H(kG)

FIGURE 14

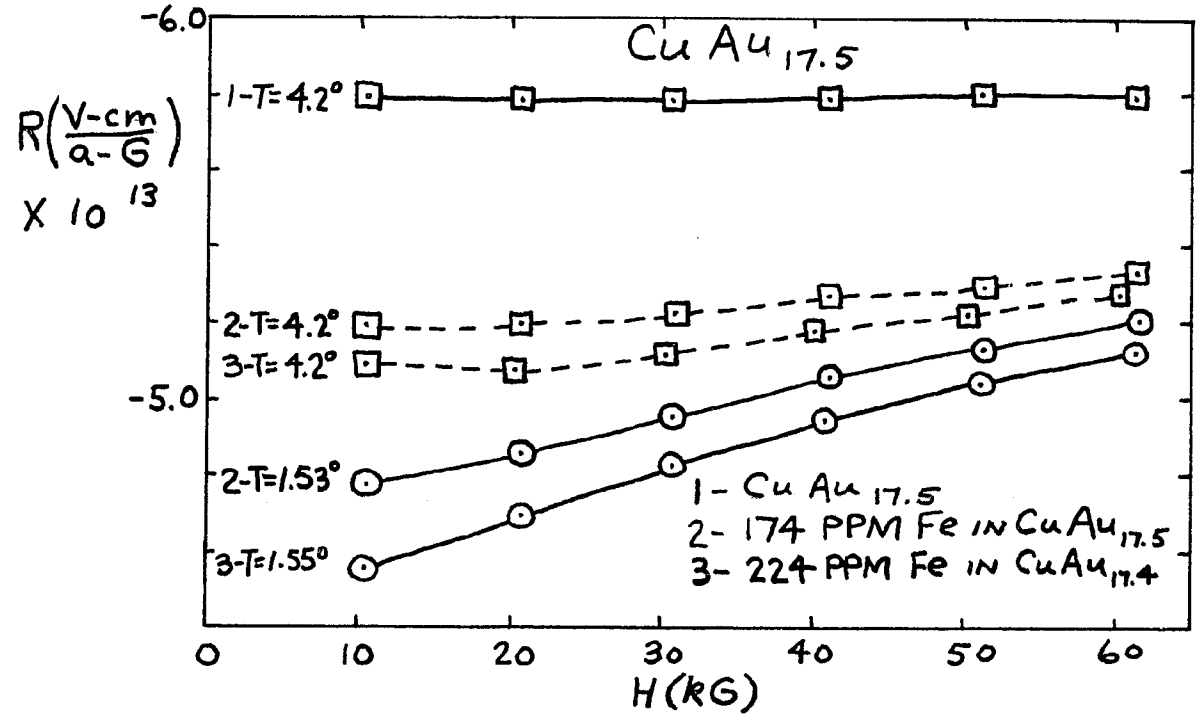
Cu Au 17.5
R(V-cm/a-G)
X 10 13
-6.0
-5.0
1-T=4.2°
2-T=4.2°
3-T=4.2°
2-T=1.53°
3-T=1.55°
1- Cu Au 17.5
2- 174 PPM Fe IN CuAu 17.5
3- 224 PPM Fe IN CuAu 17.4
0
10
20
30
40
50
60
H(kG)

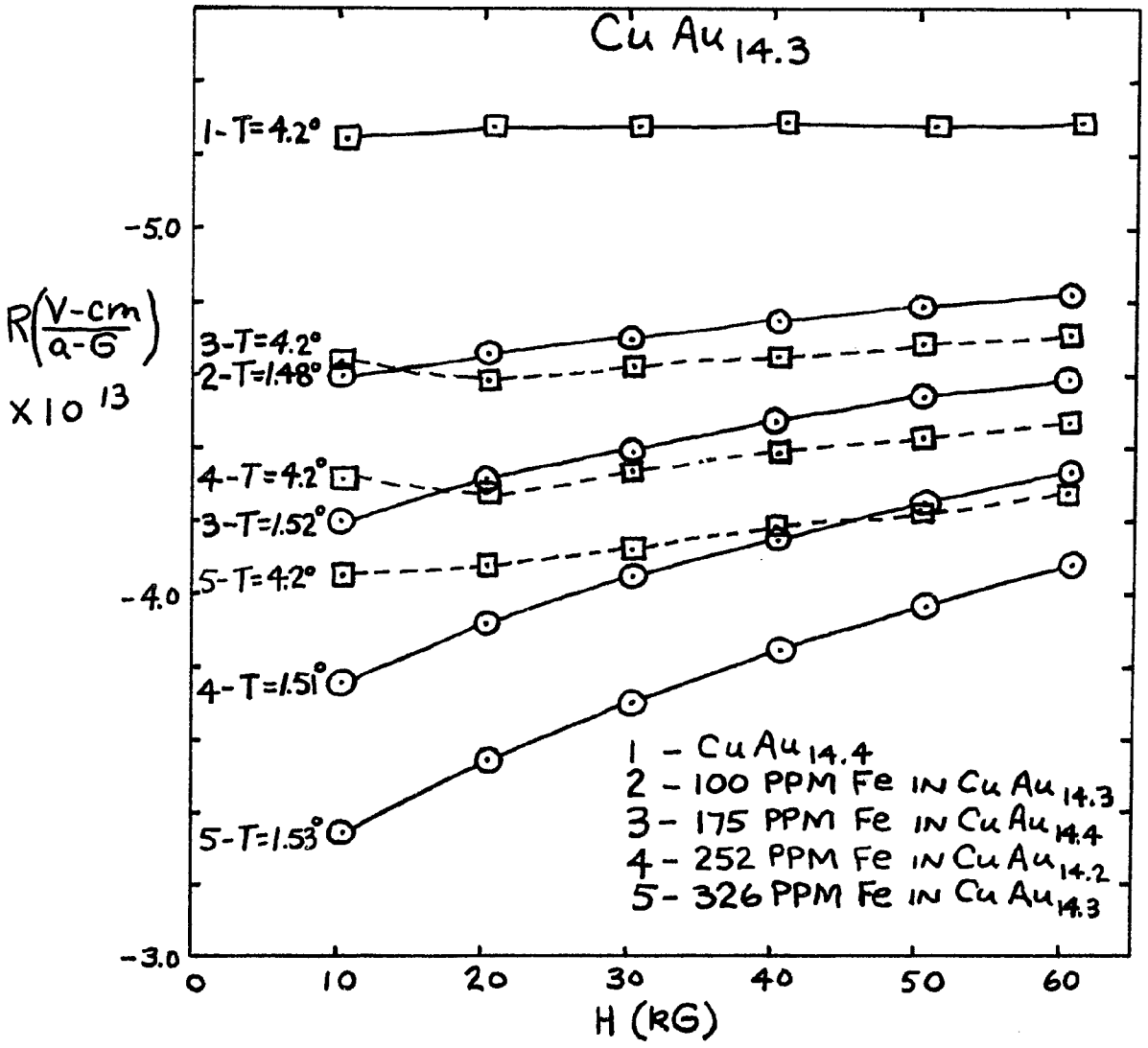
Cu Au 14.3
R(V-cm/a-G)
X10 13
-5.0
-4.0
-3.0
1-T=4.2°
3-T=4.2°
2-T=1.48°
4-T=4.2°
3-T=1.52°
5-T=4.2°
4-T=1.51°
5-T=1.53°
1 - Cu Au 14.4
2 - 100 PPM Fe IN Cu Au 14.3
3 - 175 PPM Fe IN Cu Au 14.4
4 - 252 PPM Fe IN Cu Au 14.2
5 - 326 PPM Fe IN Cu Au 14.3
0
10
20
30
40
50
60
H (kG)

FIGURE 15

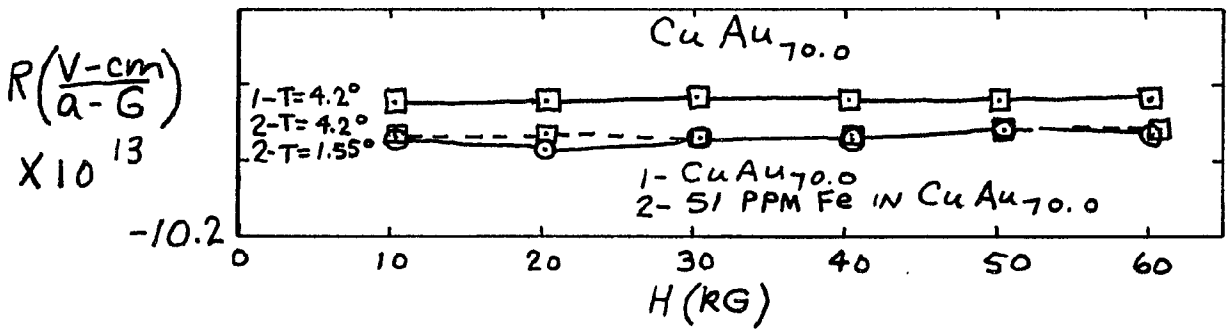
Cu Au70.0
R(V-cm/a-G)
X10 13
1-T=4.2°
2-T=4.2°
2-T=1.55°
-10.2
1- Cu Au70.0
2- 51 PPM Fe IN Cu Au70.0
0
10
20
30
40
50
60
H(KG)

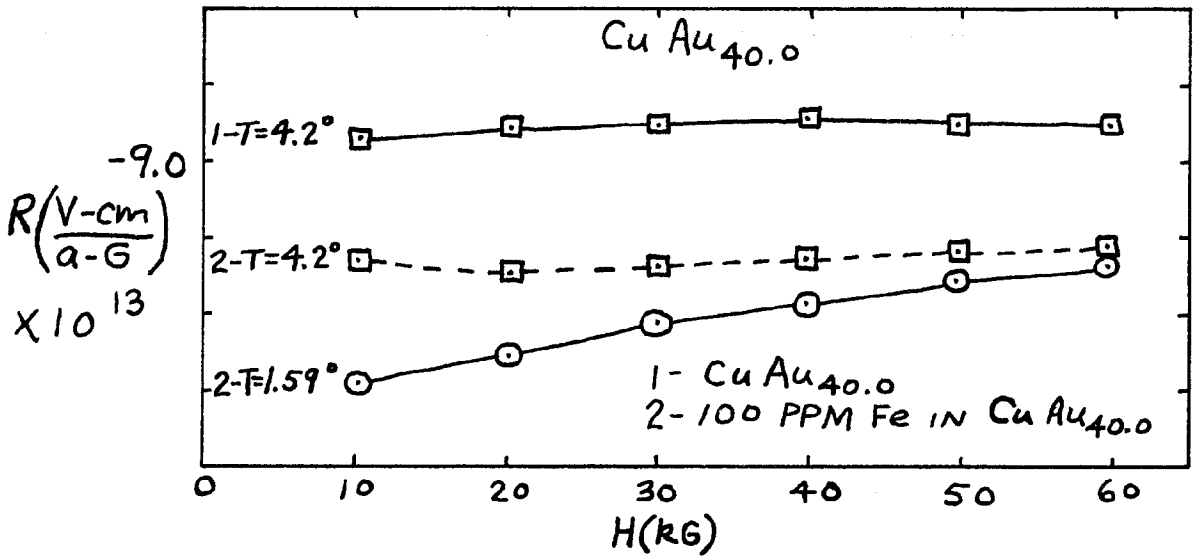
Cu Au40.0
-9.0
R(V-cm/a-G)
X10 13
1-T=4.2°
2-T=4.2°
2-T=1.59°
1- Cu Au40.0
2- 100 PPM Fe IN Cu Au40.0
0
10
20
30
40
50
60
H(KG)

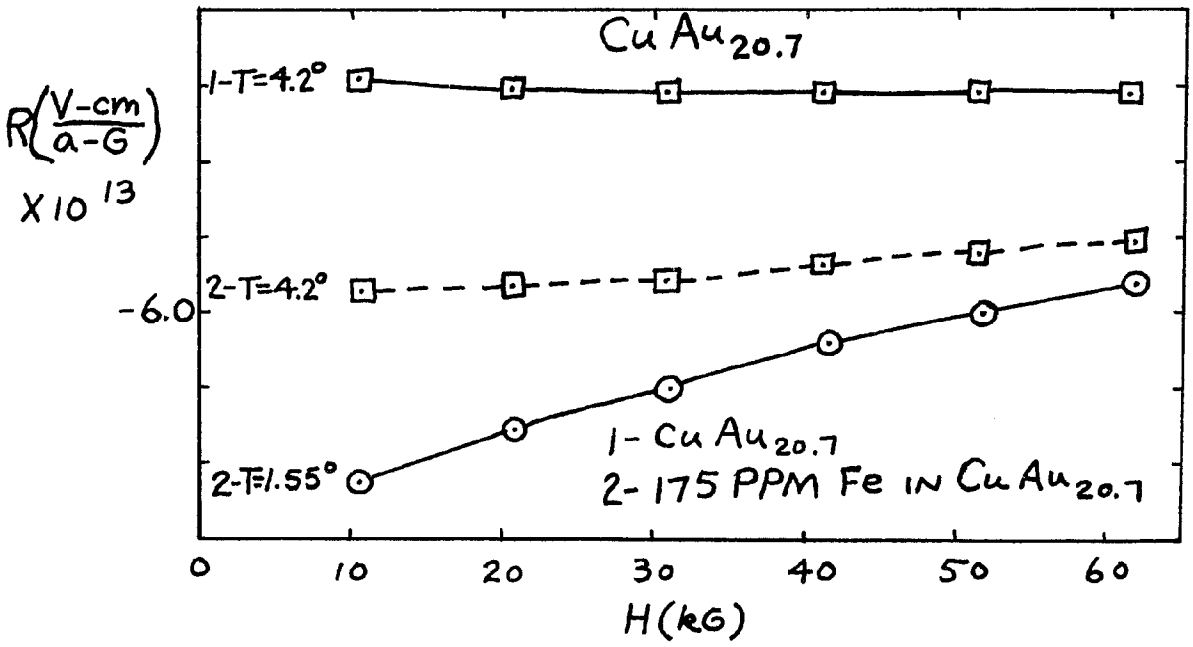
Cu Au20.7
R(V-cm/a-G)
X10 13
1-T=4.2°
2-T=4.2°
-6.0
2-T=1.55°
1- Cu Au20.7
2- 175 PPM Fe IN Cu Au20.7
0
10
20
30
40
50
60
H(kG)

FIGURE 16

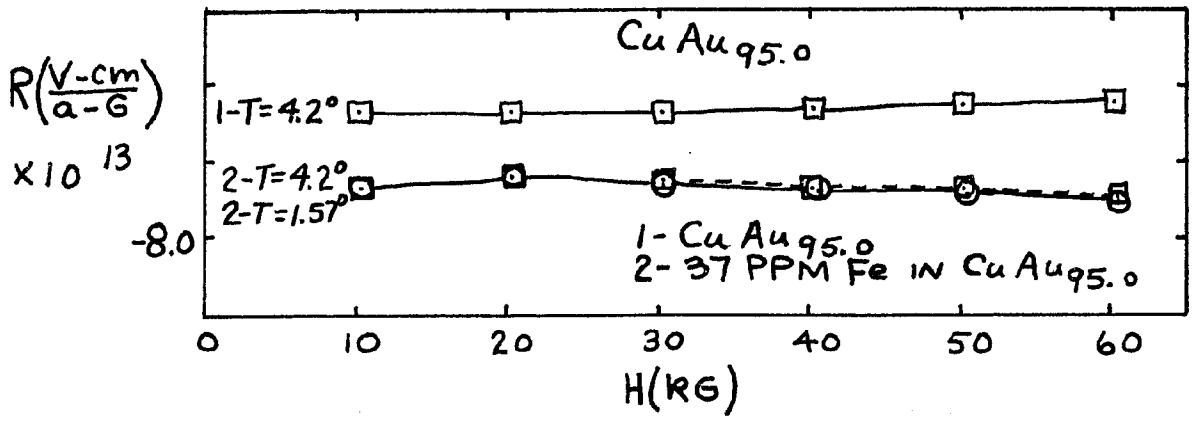
Cu Au 95.0
R(V-cm/a-G)
X10 13
1-T=4.2°
2-T=4.2°
2-T=1.57°
-8.0
1- Cu Au 95.0
2- 37 PPM Fe IN Cu Au 95.0
0
10
20
30
40
50
60
H(KG)

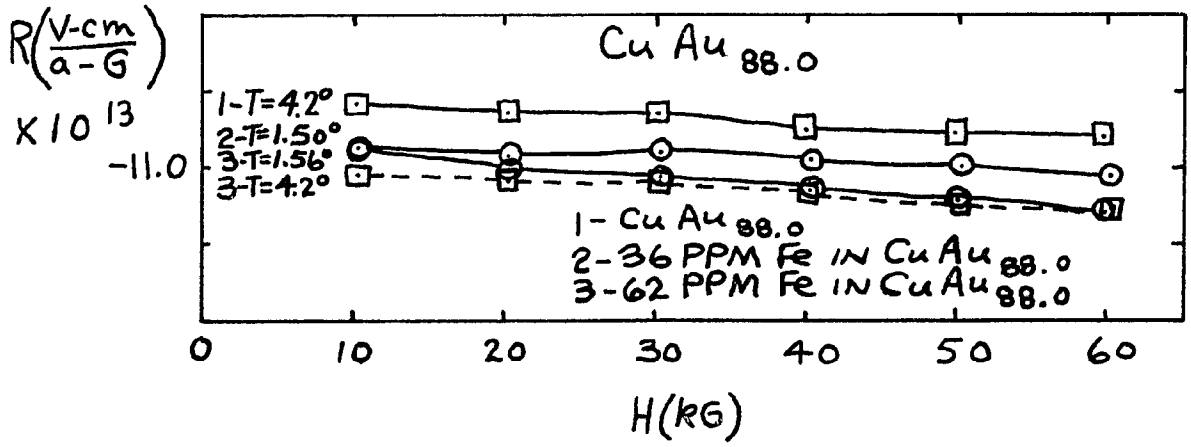
Cu Au 88.0
R(V-cm/a-G)
X10 13
1-T=4.2°
2-T=1.50°
3-T=1.56°
3-T=4.2°
-11.0
1- Cu Au 88.0
2-36 PPM Fe IN Cu Au 88.0
3-62 PPM Fe IN Cu Au 88.0
0
10
20
30
40
50
60
H(KG)

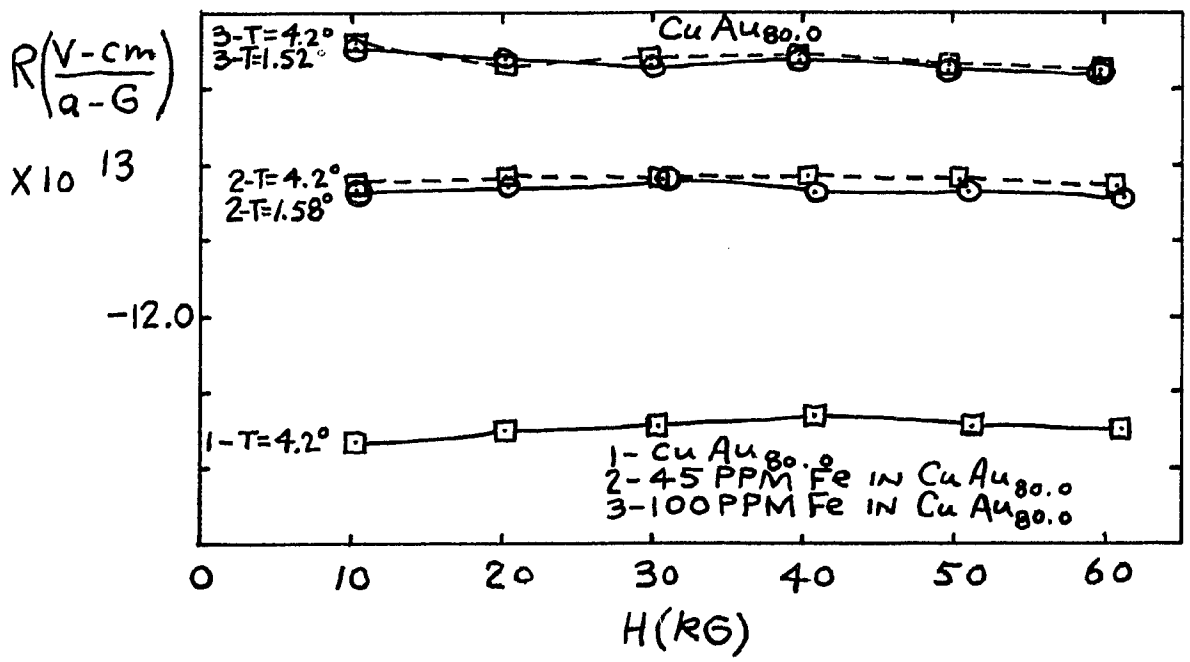
Cu Au 80.0
R(V-cm/a-G)
X10 13
3-T=4.2°
3-T=1.52°
2-T=4.2°
2-T=1.58°
-12.0
1-T=4.2°
1- Cu Au 80.0
2-45 PPM Fe IN Cu Au 80.0
3-100 PPM Fe IN Cu Au 80.0
0
10
20
30
40
50
60
H(KG)

FIGURE 17

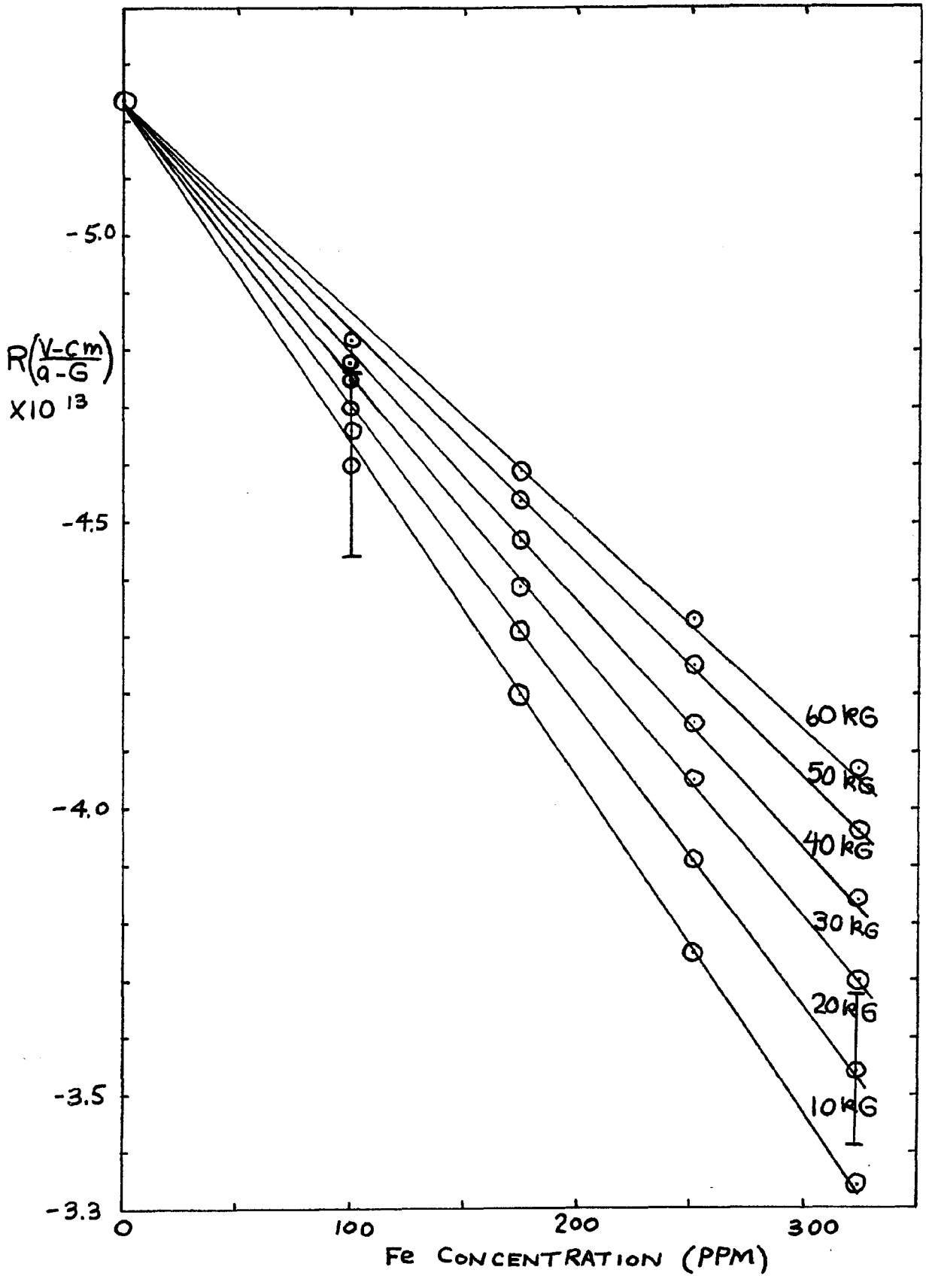
-5.0
-4.5
-4.0
-3.5
-3.3
R(V-cm/a-G)
X10 13
0
100
200
300
Fe CONCENTRATION (PPM)
60 KG
50 KG
40 KG
30 KG
20 KG
10 KG

FIGURE 18

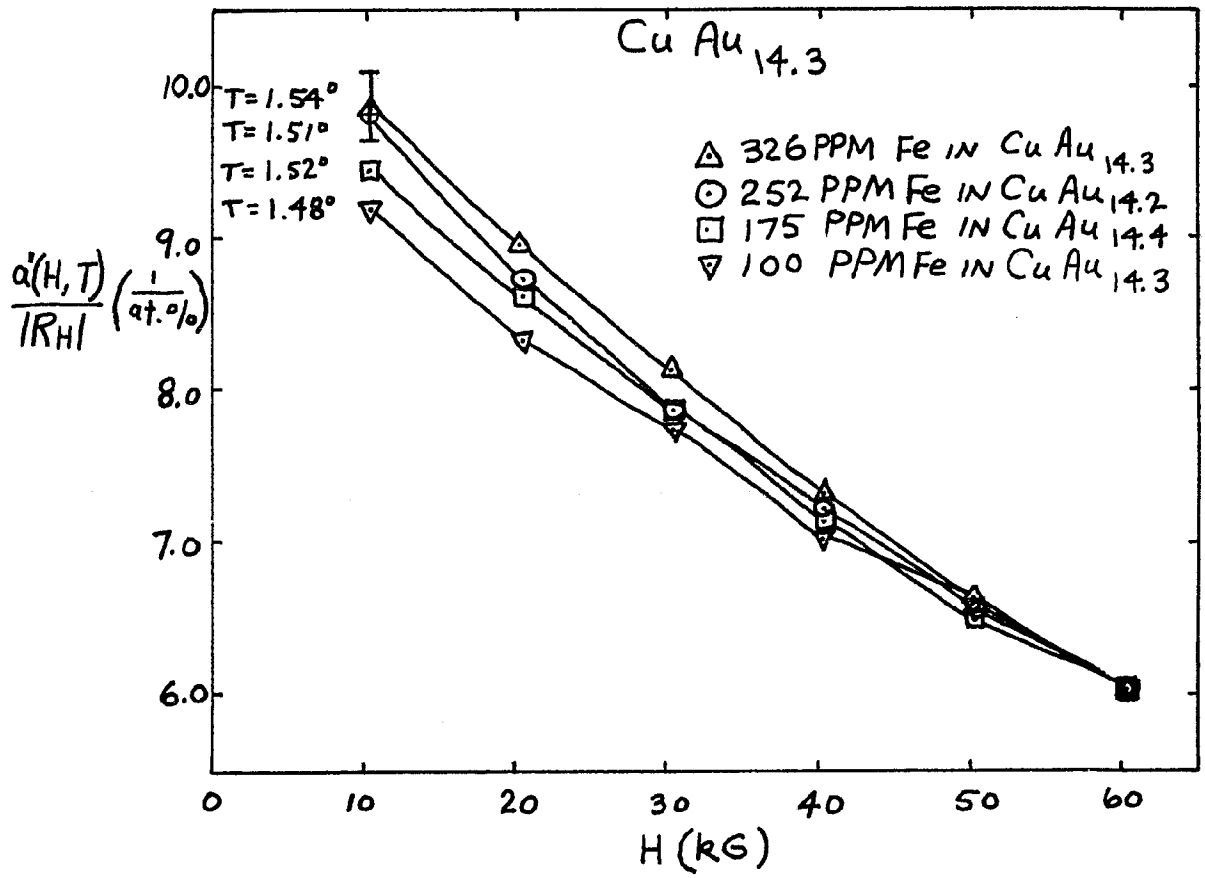

FIGURE 20

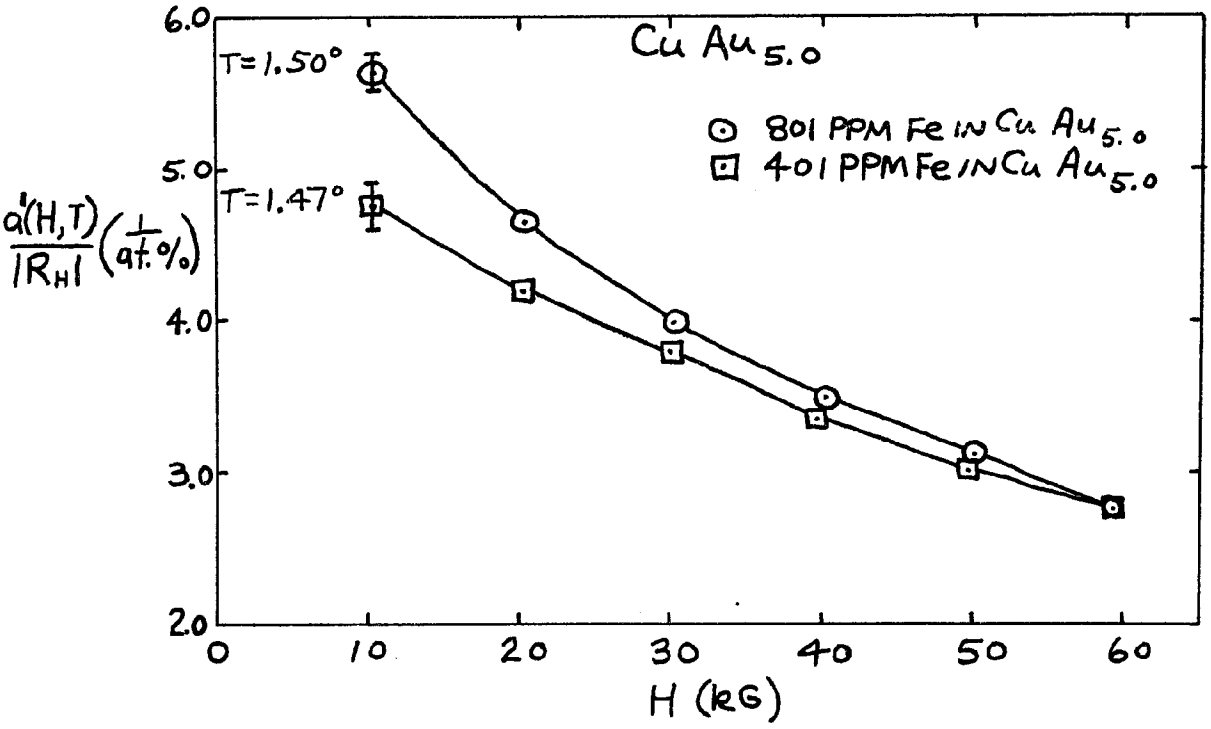

FIGURE 19

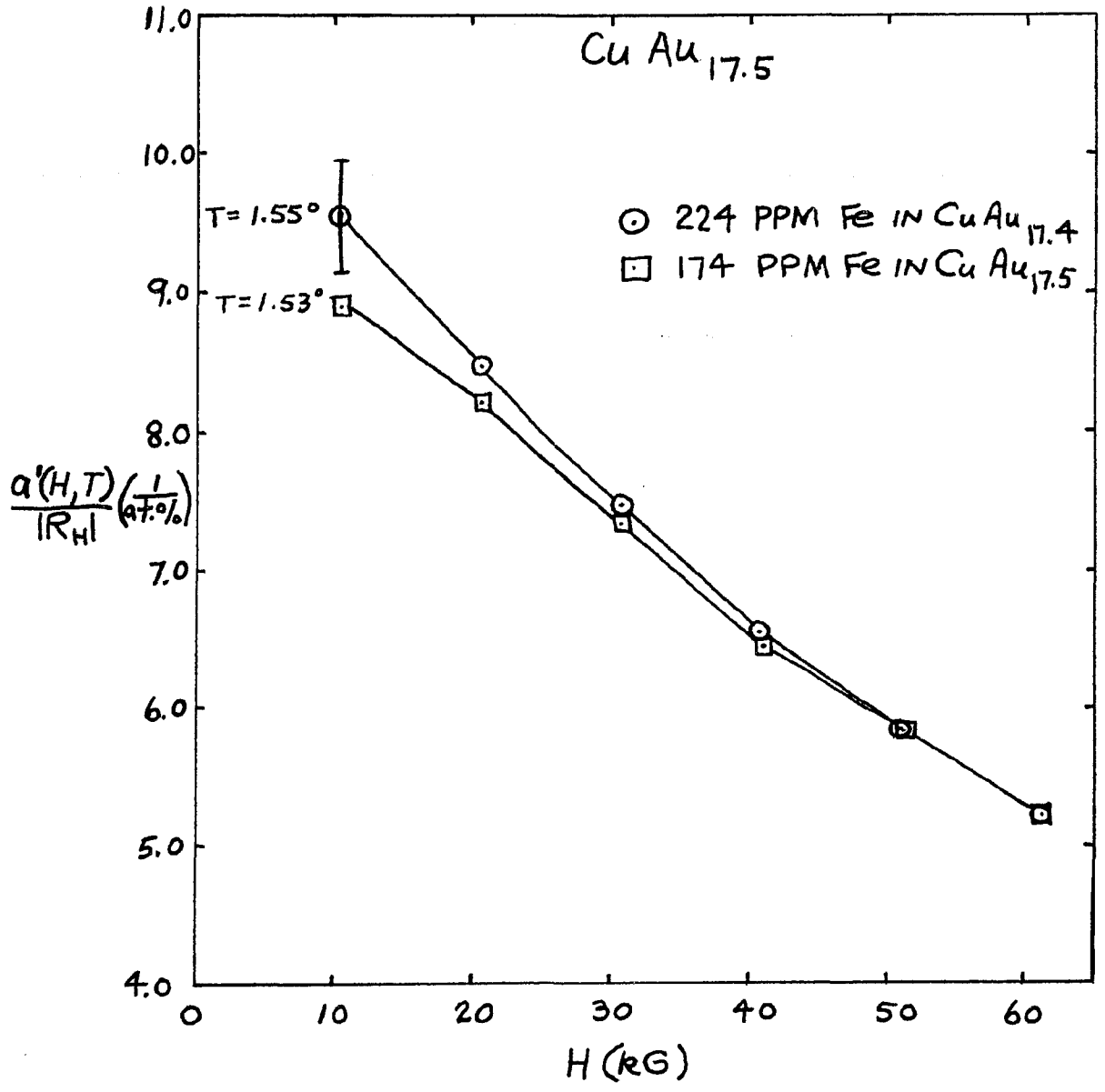
Cu Au 17.5
224 PPM Fe IN Cu Au 17.4
174 PPM Fe IN Cu Au 17.5
T= 1.55°
T= 1.53°
11.0
10.0
9.0
8.0
7.0
6.0
5.0
4.0
0
10
20
30
40
50
60
H (kG)
a'(H,T)/|R_H| (1/at.%)

FIGURE 21

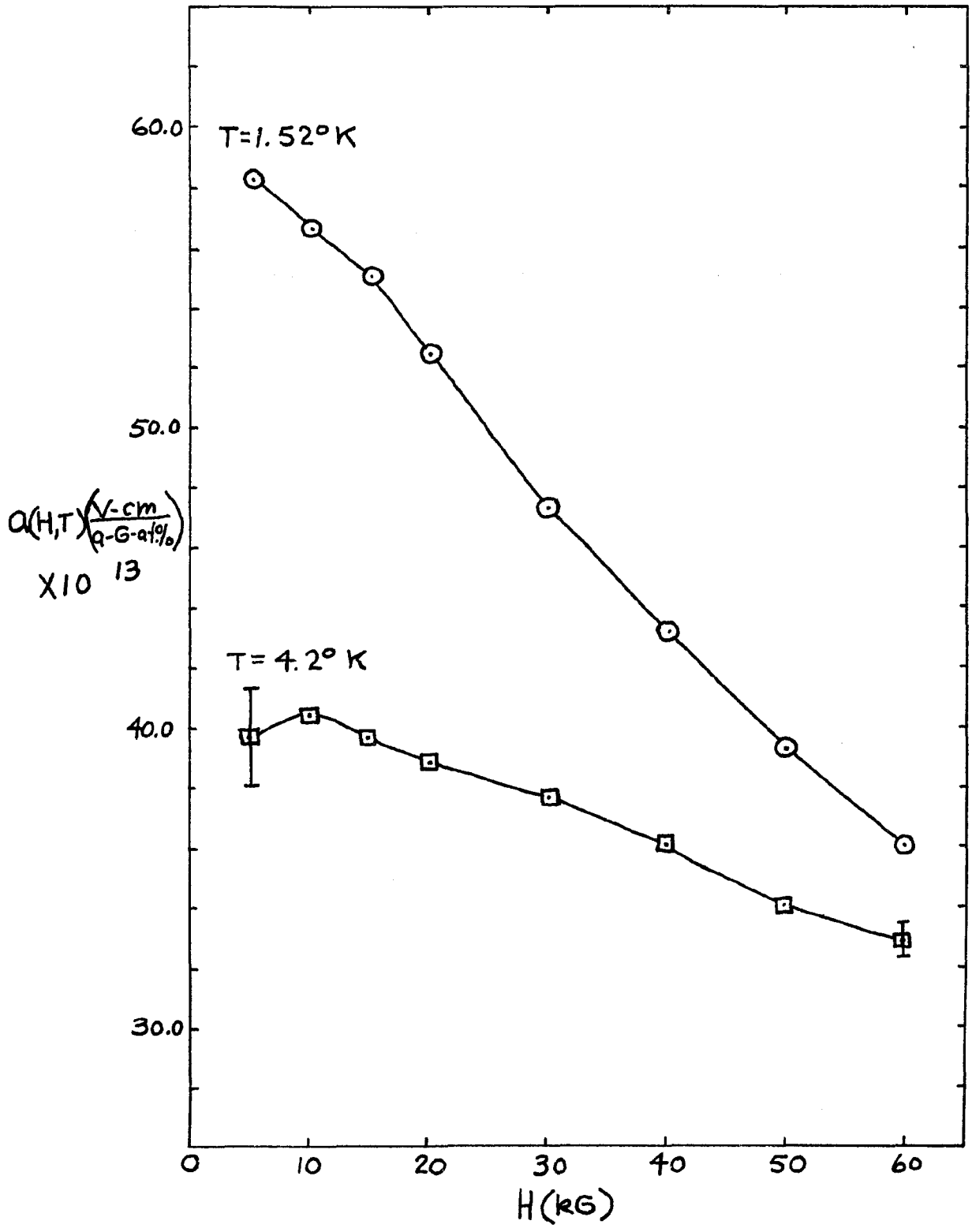
60.0
50.0
40.0
30.0
T=1.52° K
T=4.2° K
Q(H,T) (V-cm / a-G-at%)
X10 13
0
10
20
30
40
50
60
H(kG)

FIGURE 22

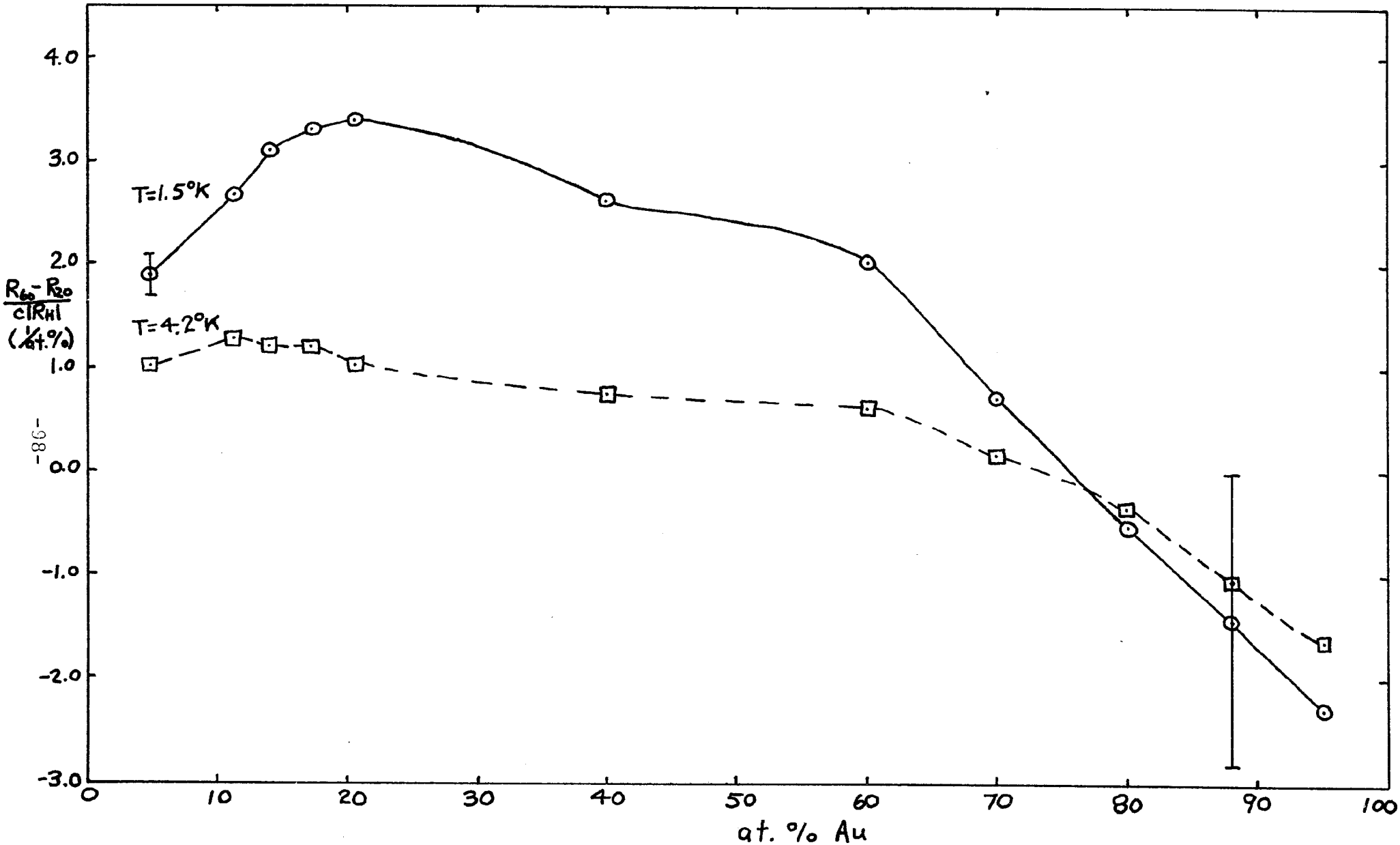
4.0
3.0
2.0
1.0
0.0
-1.0
-2.0
-3.0
T=1.5°K
T=4.2°K
$\frac{R_{60}-R_{20}}{c|R_{H1}|}$ ($\frac{1}{at.\%}$)
0
10
20
30
40
50
60
70
80
90
100
at. % Au

FIGURE 23

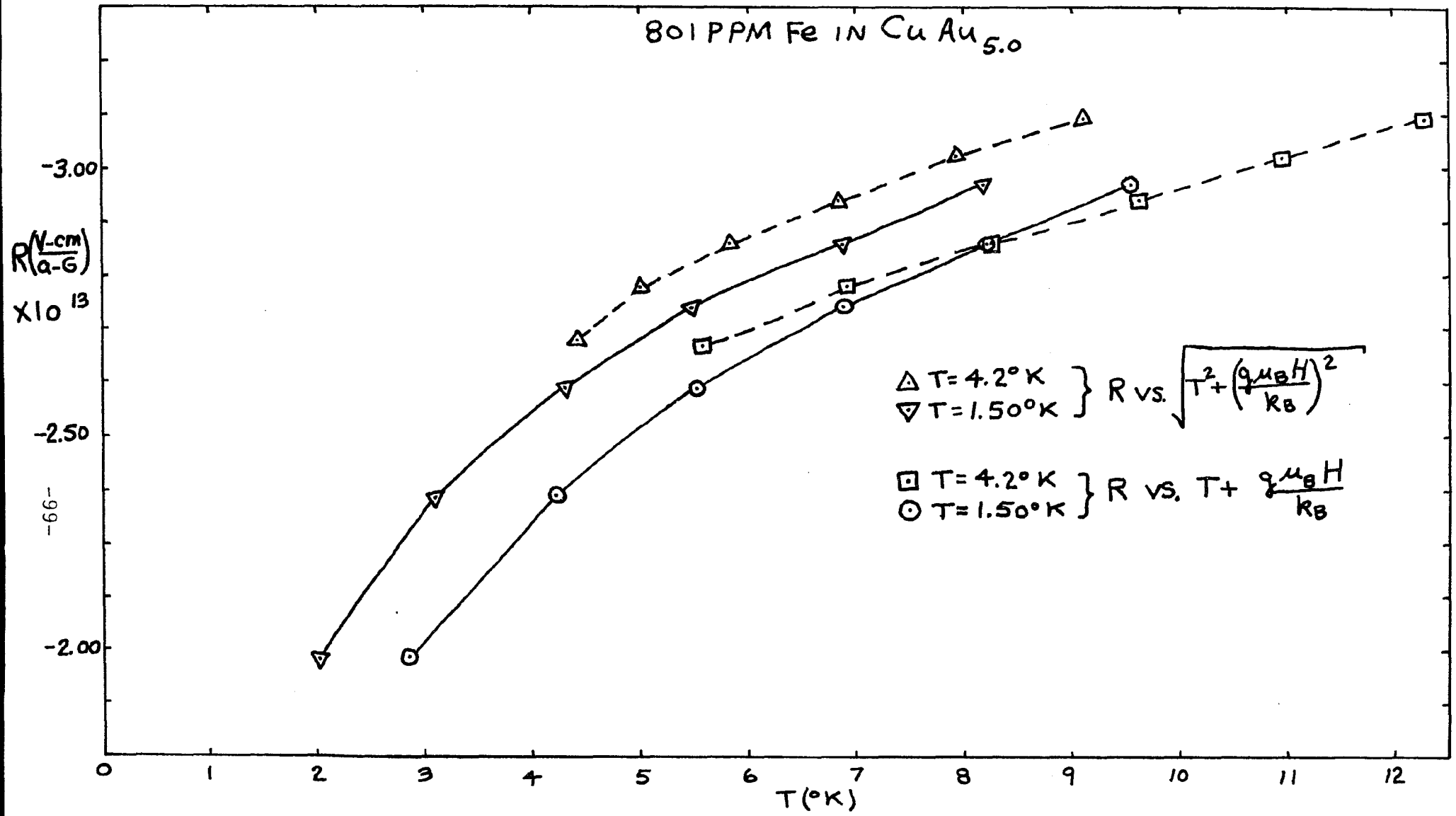
801 PPM Fe IN Cu Au 5.0
-3.00
-2.50
-2.00
R (V-cm / a-G)
X10 13
△ T= 4.2° K
▽ T= 1.50° K
} R vs. √T² + (gμB H / kB)²
□ T= 4.2° K
⊙ T= 1.50° K
} R vs. T + gμB H / kB
0
1
2
3
4
5
6
7
8
9
10
11
12
T(°K)

FIGURE 24

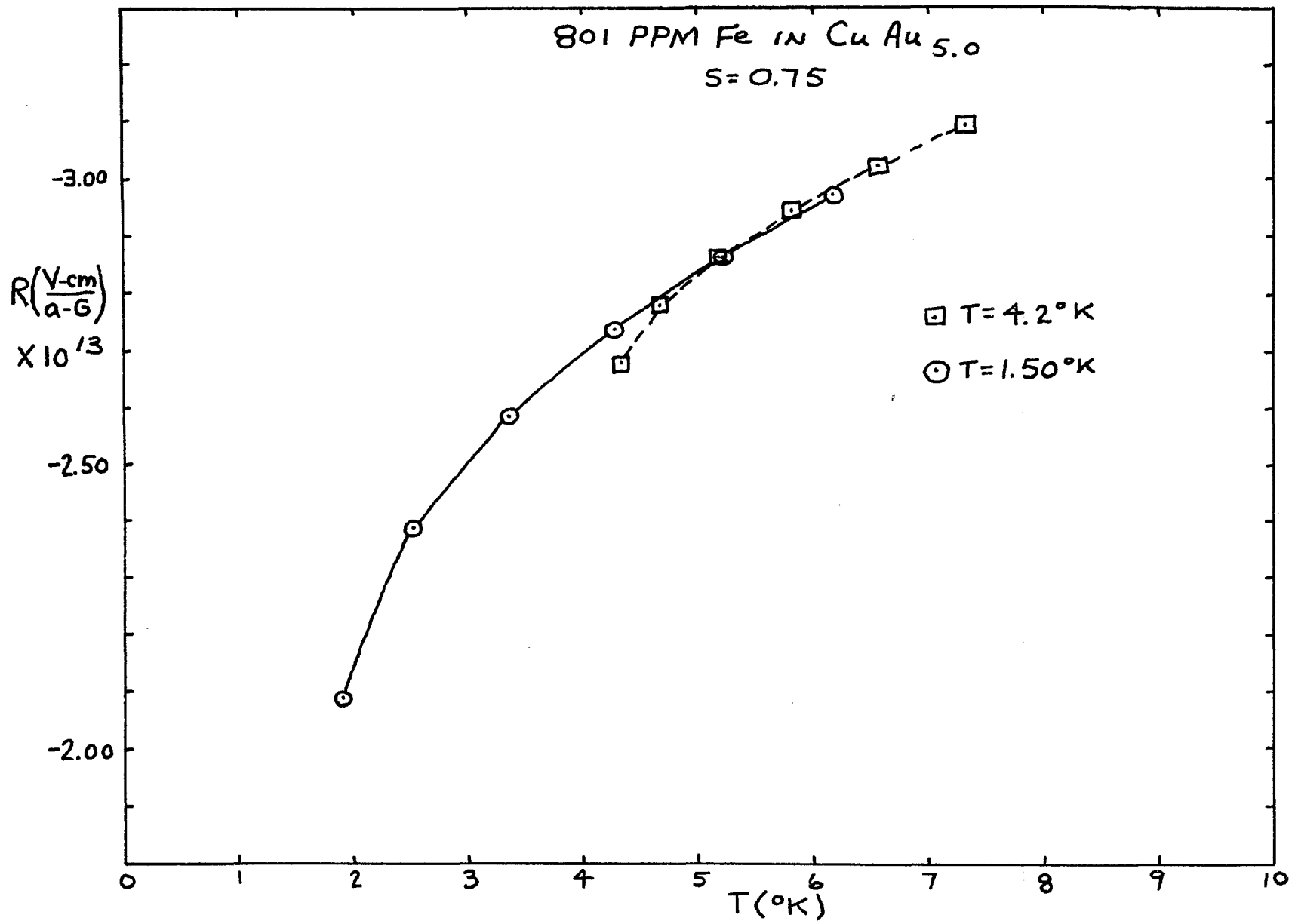
801 PPM Fe IN Cu Au 5.0
S = 0.75
-3.00
-2.50
-2.00
R(V-cm/a-G)
X 10 13
T = 4.2° K
T = 1.50° K
0
1
2
3
4
5
6
7
8
9
10
T(°K)

FIGURE 25

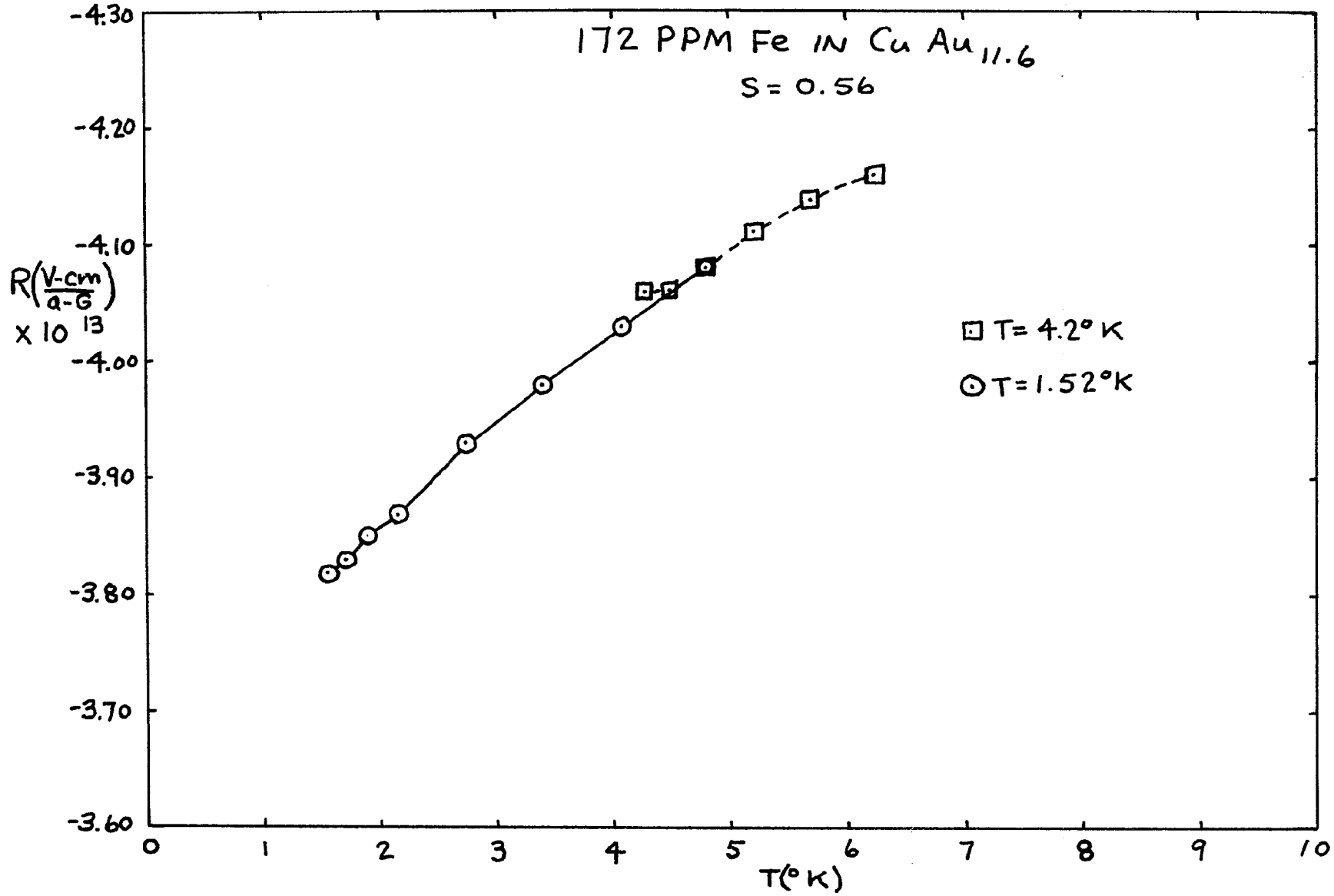
172 PPM Fe IN Cu Au 11.6
S = 0.56
R(V-cm/a-G)
X 10 13
-4.30
-4.20
-4.10
-4.00
-3.90
-3.80
-3.70
-3.60
T = 4.2° K
T = 1.52° K
0
1
2
3
4
5
6
7
8
9
10
T(° K)

FIGURE 26

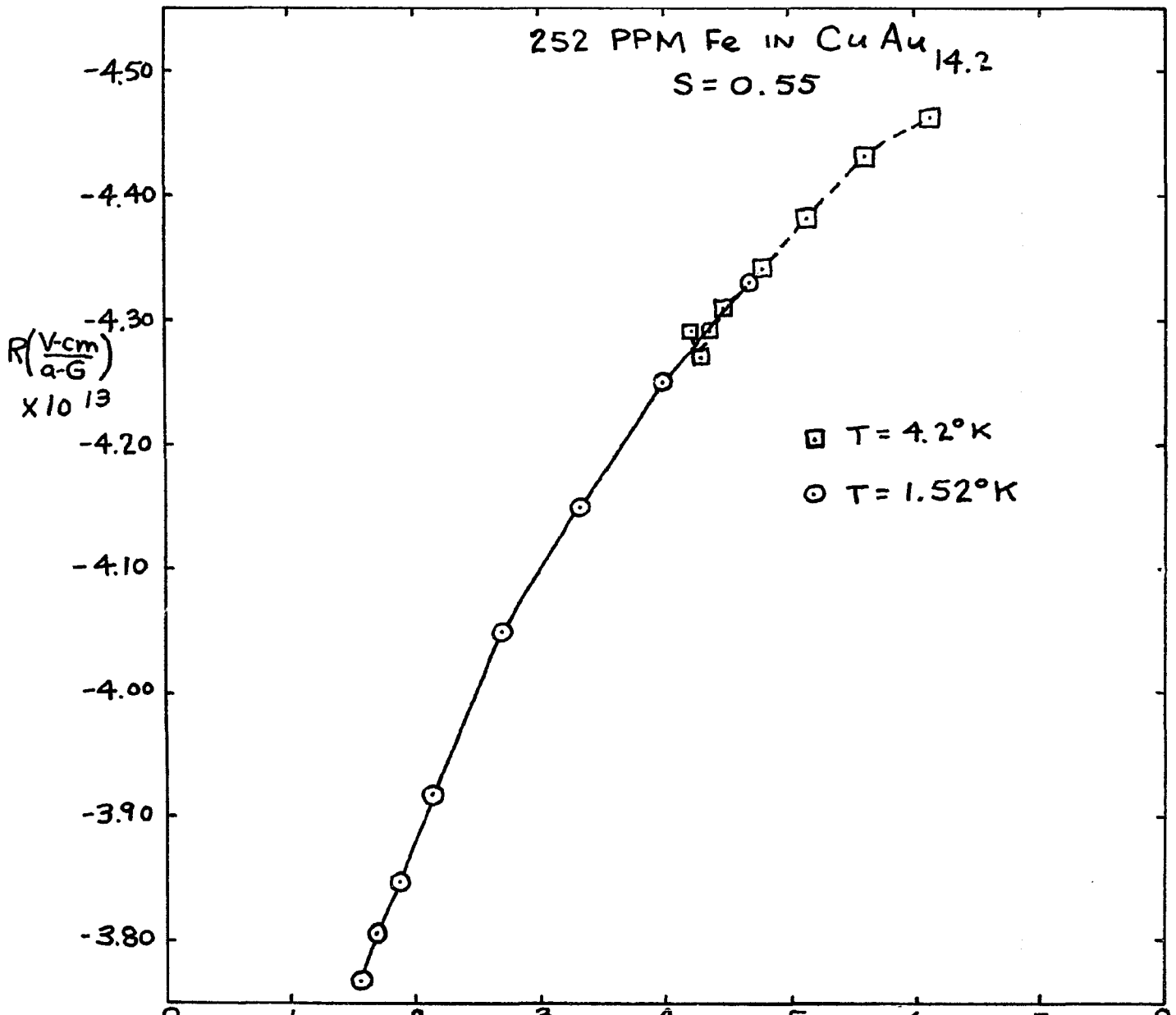
252 PPM Fe IN Cu Au 14.2
S = 0.55
-4.50
-4.40
-4.30
-4.20
-4.10
-4.00
-3.90
-3.80
R(V-cm/a-G) X 10 13
T = 4.2°K
T = 1.52°K
0
1
2
3
4
5
6
7
8
T(°K)

FIGURE 27

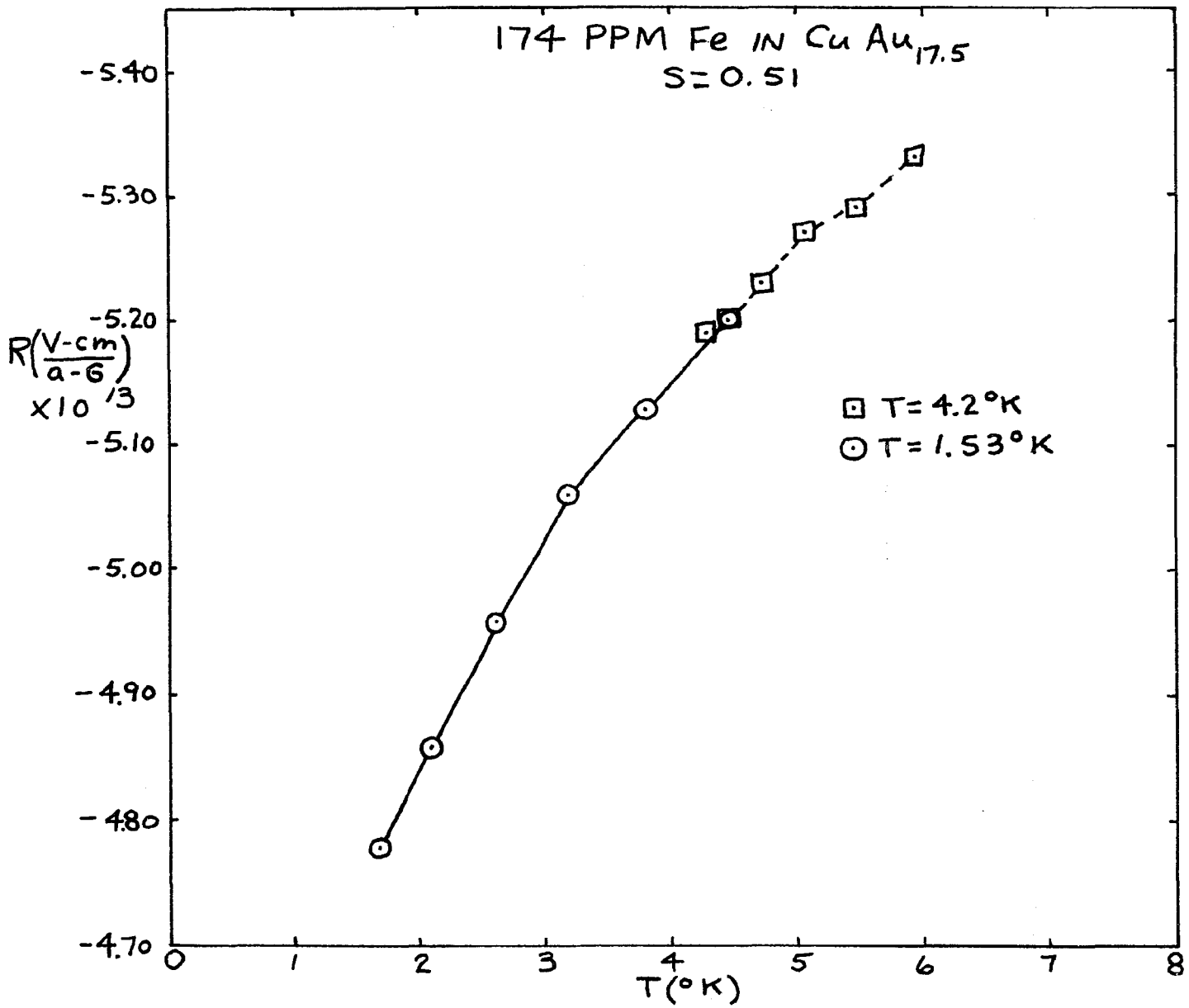
174 PPM Fe IN Cu Au17.5
S=0.51
-5.40
-5.30
-5.20
-5.10
-5.00
-4.90
-4.80
-4.70
R(V-cm/a-G) X10 13
T=4.2°K
T=1.53°K
0
1
2
3
4
5
6
7
8
T(°K)

FIGURE 28

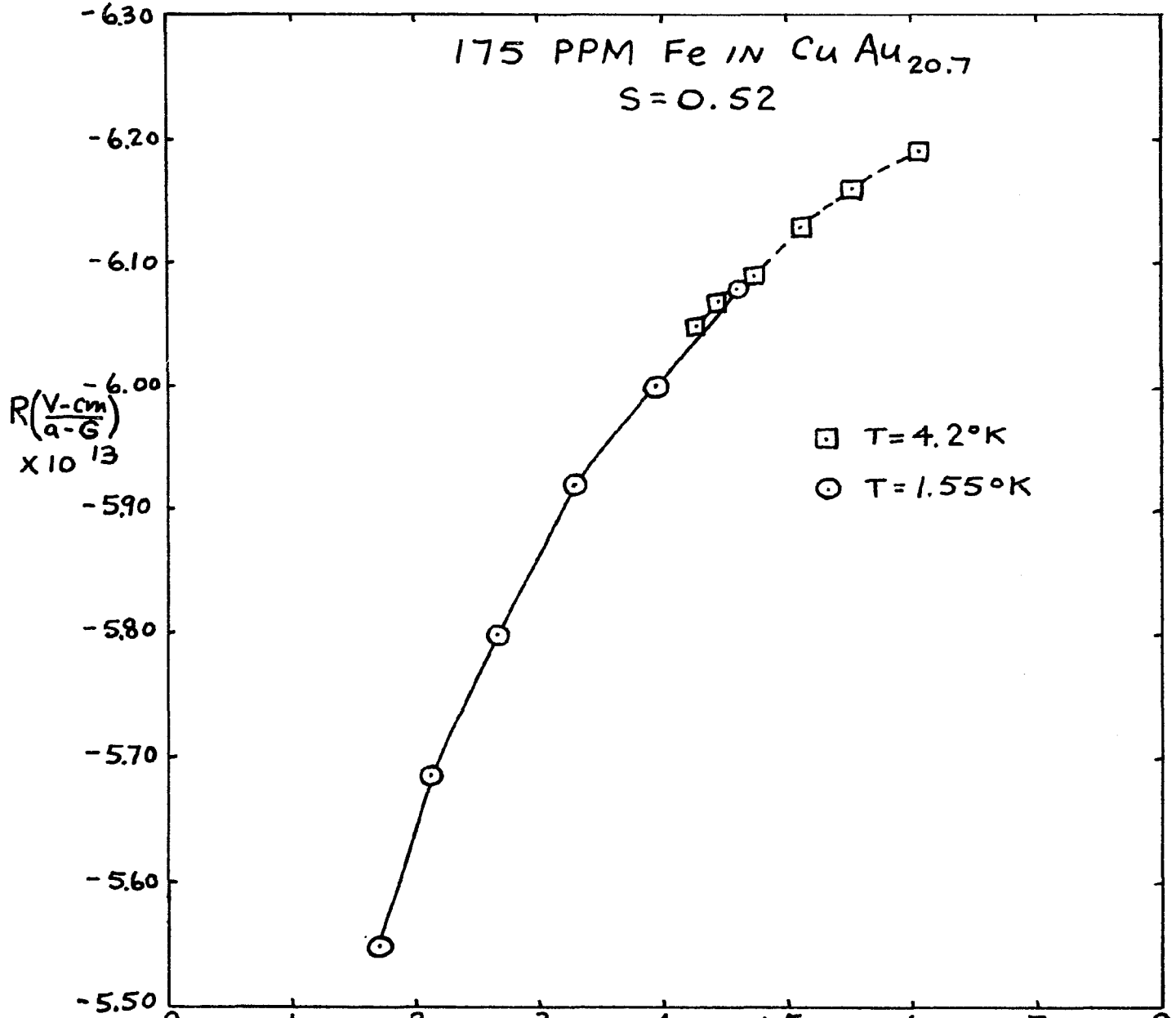
175 PPM Fe IN Cu Au20.7
S = 0.52
-6.30
-6.20
-6.10
-6.00
-5.90
-5.80
-5.70
-5.60
-5.50
R(V-cm/a-G) X 10 13
T = 4.2°K
T = 1.55°K
0
1
2
3
4
5
6
7
8
T(°K)

FIGURE 29

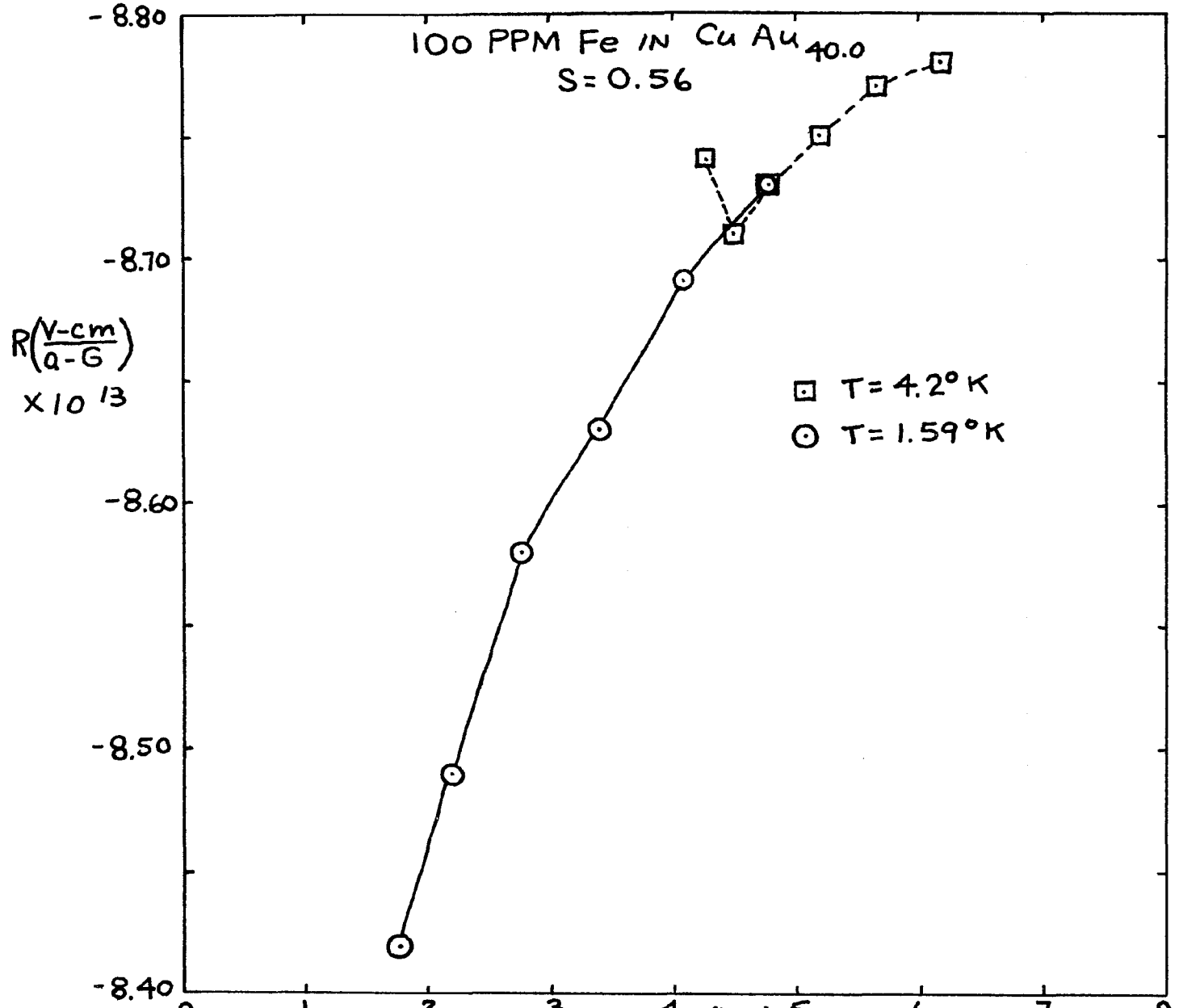
100 PPM Fe IN Cu Au 40.0
S = 0.56
T = 4.2° K
T = 1.59° K
R(V-cm/a-G)
X 10 13
-8.80
-8.70
-8.60
-8.50
-8.40
0
1
2
3
4
T(° K)
5
6
7
8

FIGURE 30

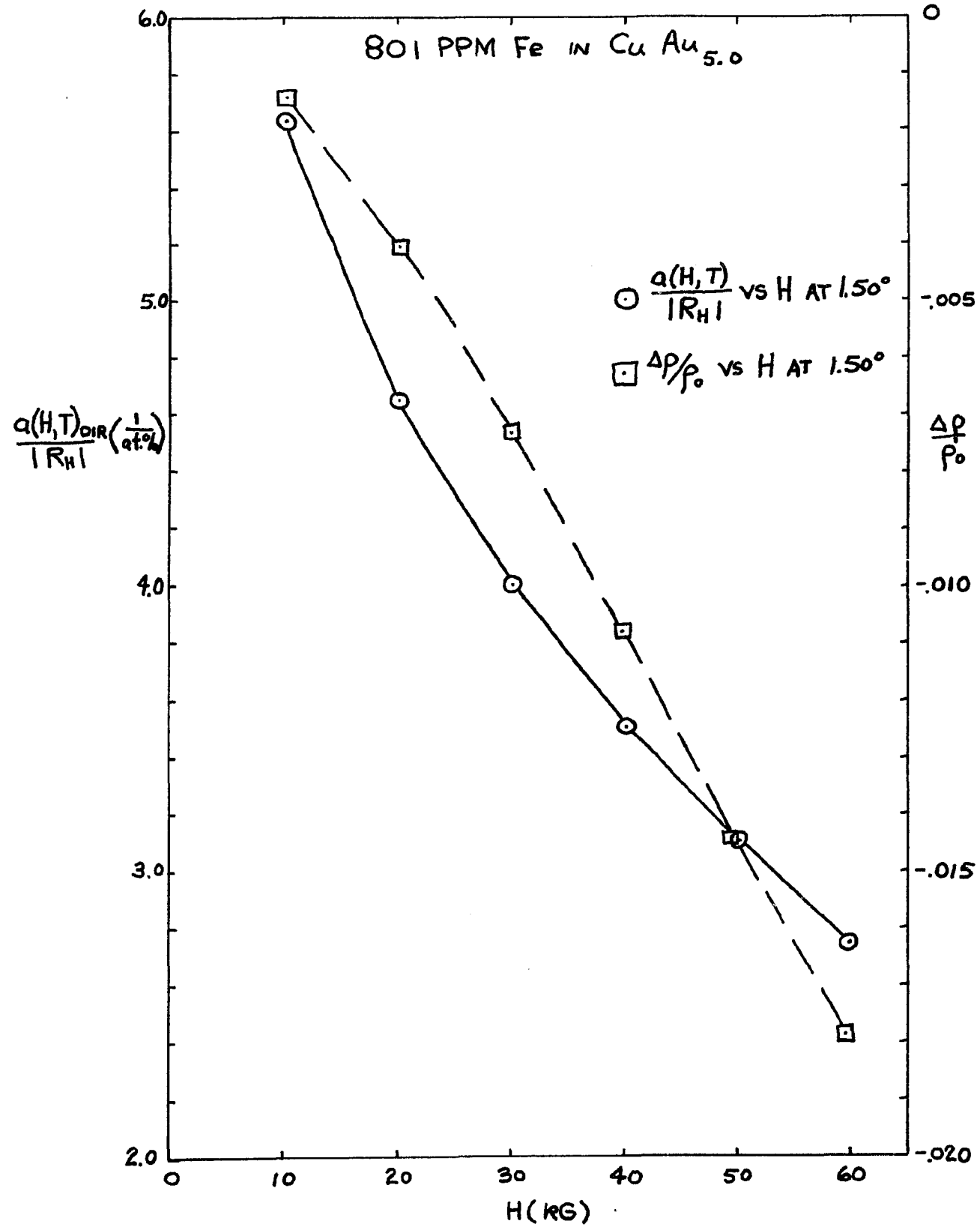
801 PPM Fe IN Cu Au 5.0
○ a(H,T)/|RH| vs H AT 1.50°
□ Δρ/ρo vs H AT 1.50°
a(H,T)/|RH| (1/at.%)
Δρ/ρo
6.0
5.0
4.0
3.0
2.0
0
-.005
-.010
-.015
-.020
0
10
20
30
40
50
60
H(KG)

FIGURE 31

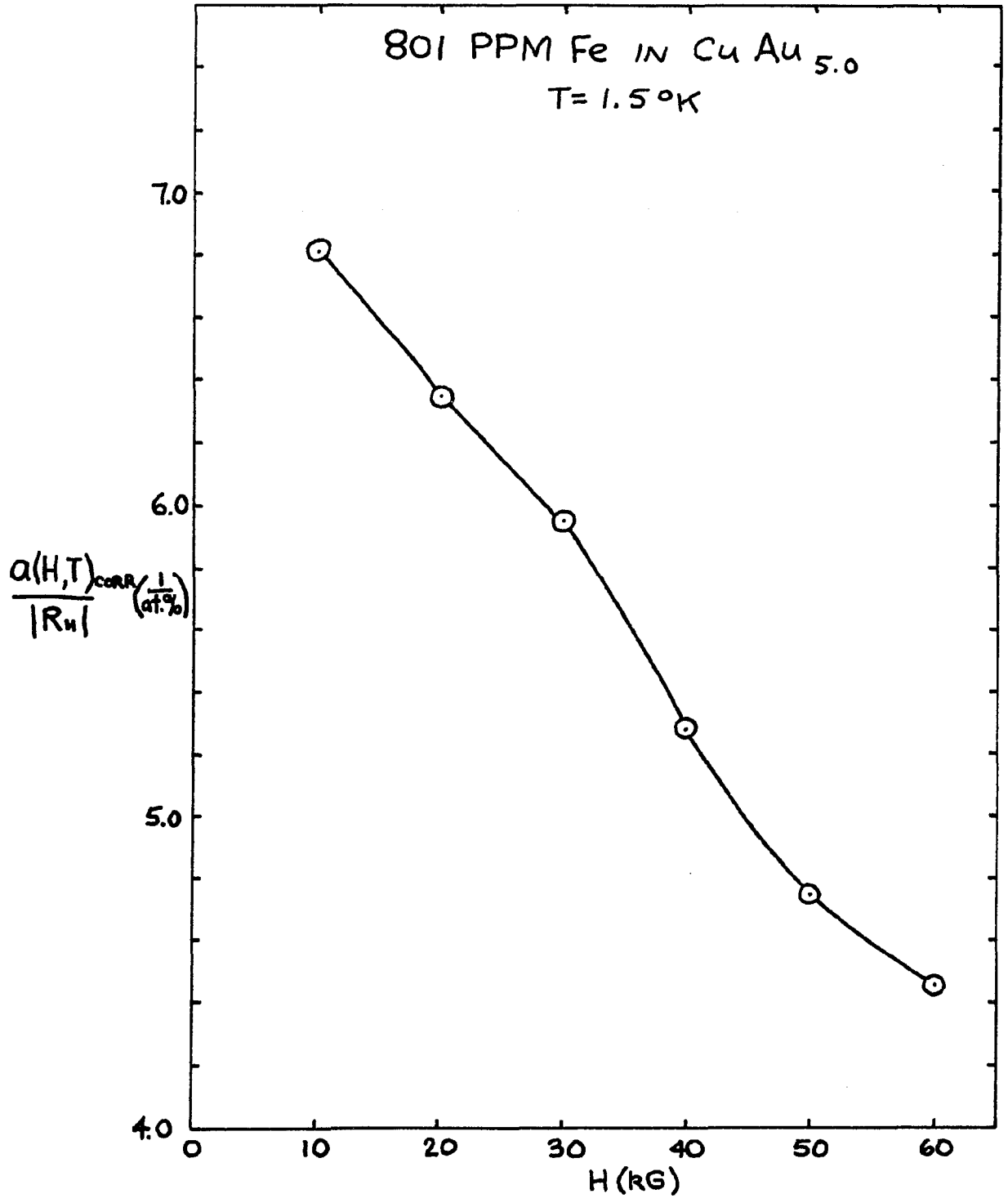
801 PPM Fe IN Cu Au 5.0
T= 1.5°K
7.0
6.0
5.0
4.0
$\frac{a(H,T)_{corr}}{|R_H|}\left(\frac{1}{at.\%}\right)$
0
10
20
30
40
50
60
H (kG)

FIGURE 32

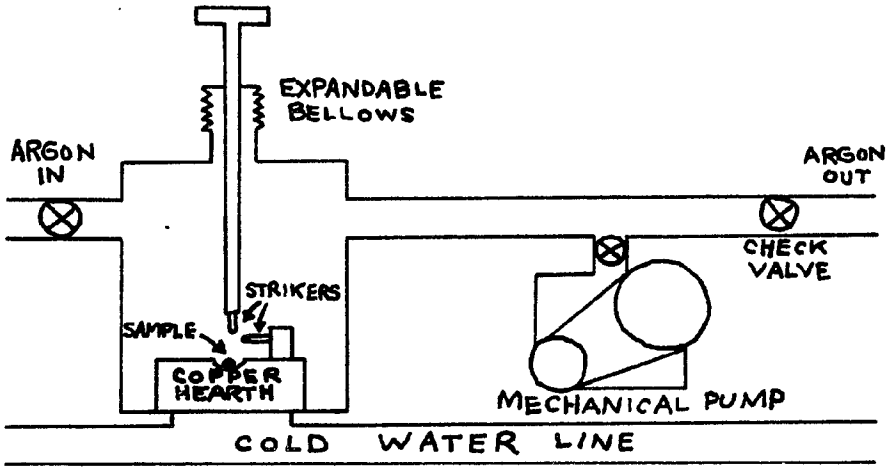

FIGURE 33

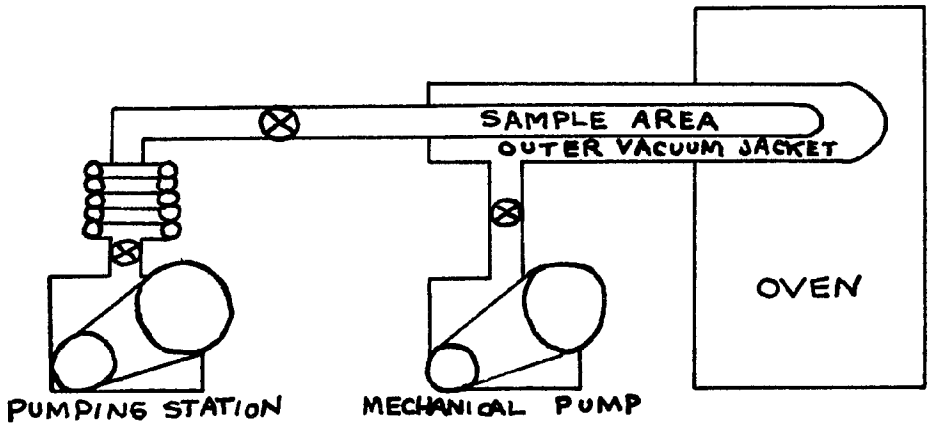

FIGURE 34

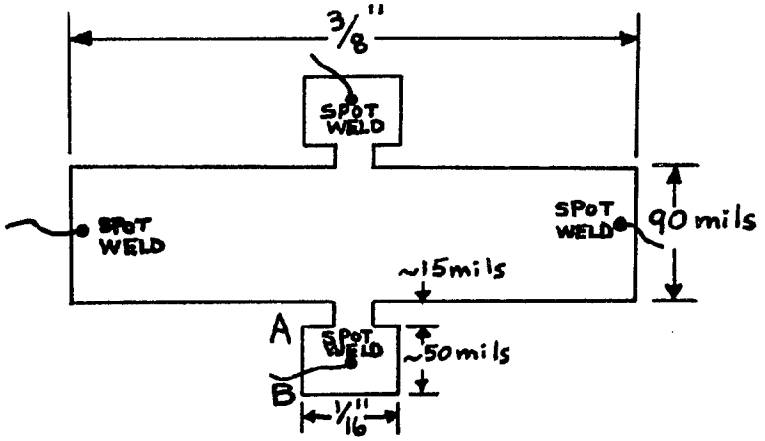

FIGURE 35

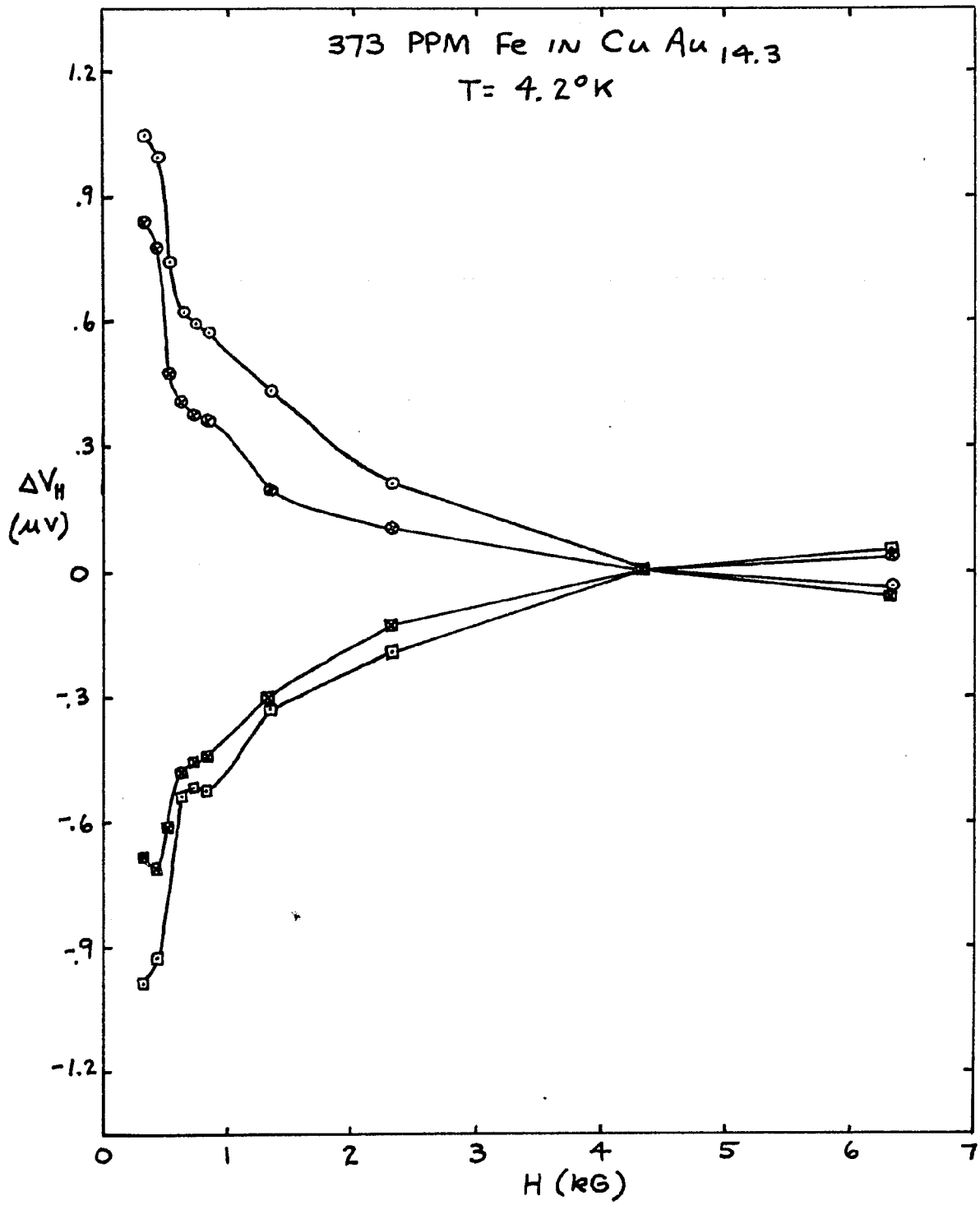

FIGURE 36

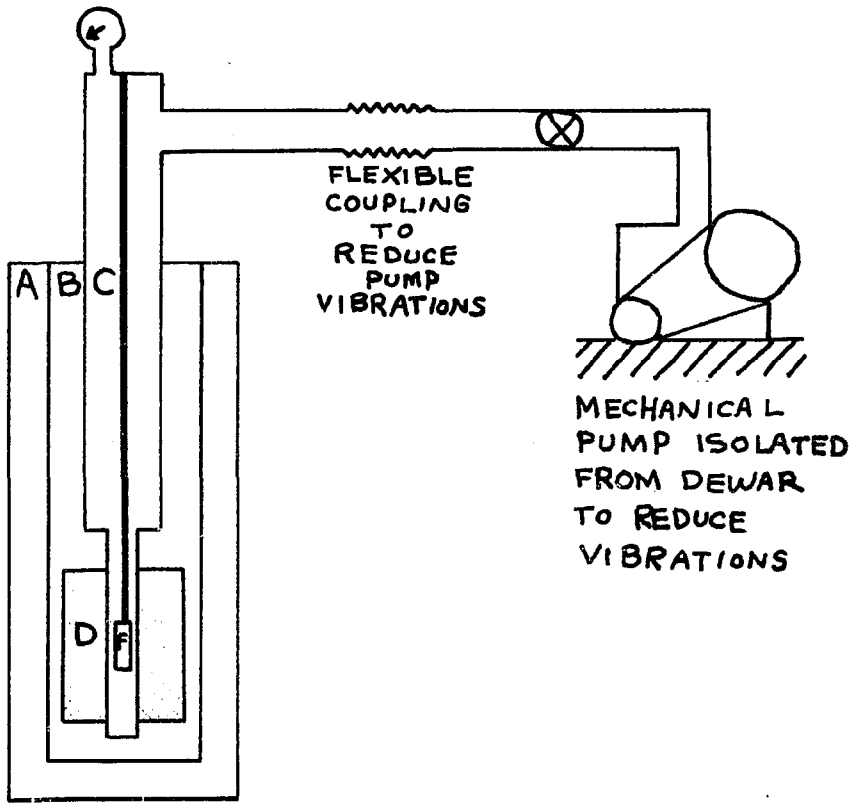

FIGURE 37

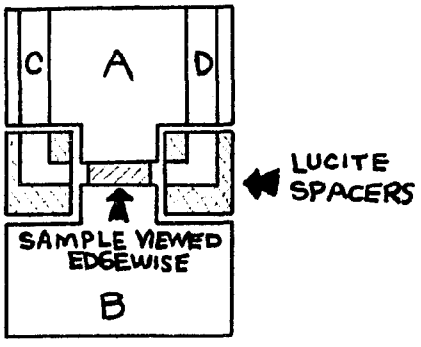

FIGURE 38

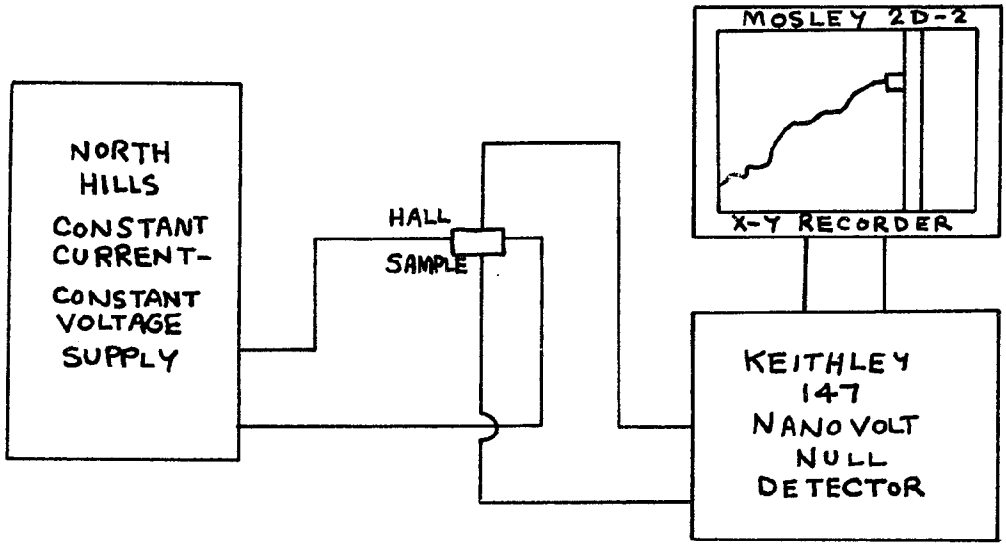

FIGURE 39

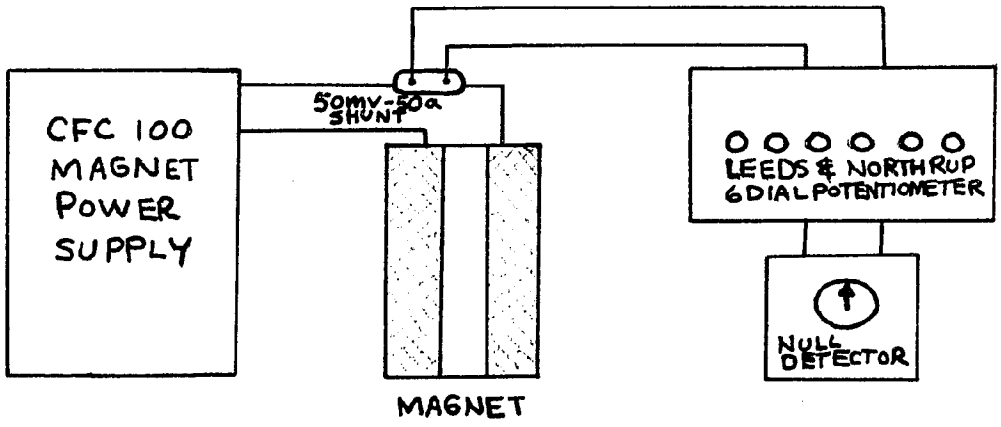

FIGURE 40

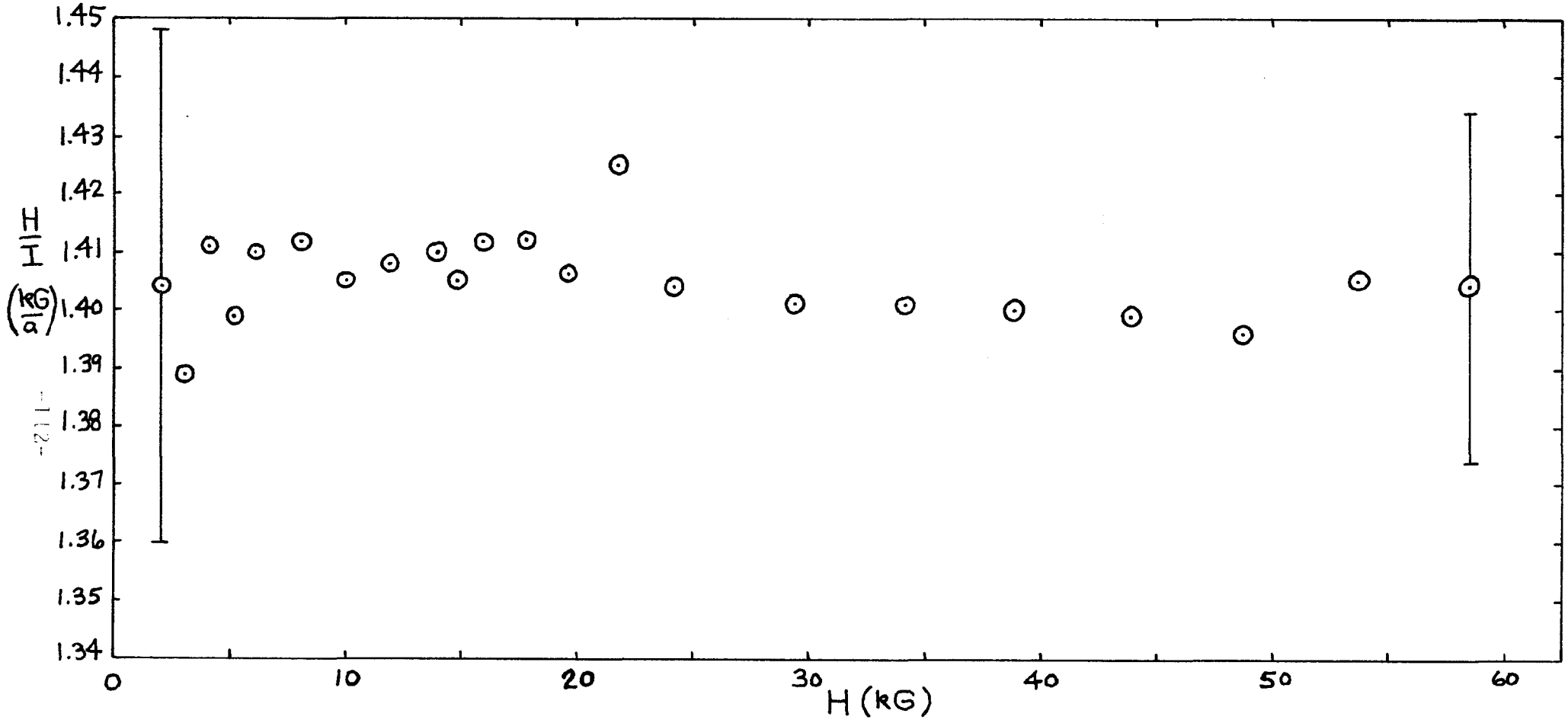
1.45
1.44
1.43
1.42
1.41
1.40
1.39
1.38
1.37
1.36
1.35
1.34
H/I (kG/a)
0
10
20
30
40
50
60
H (kG)

FIGURE 41

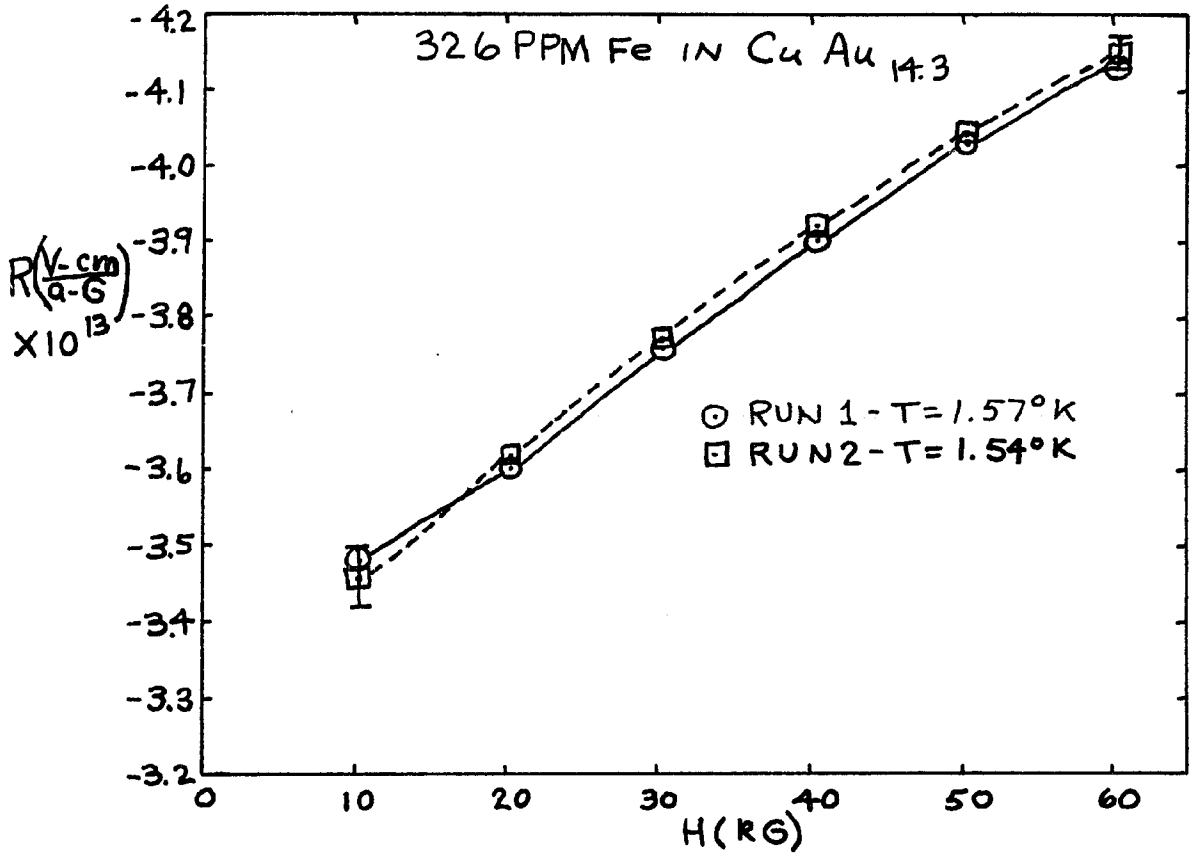

FIGURE 42

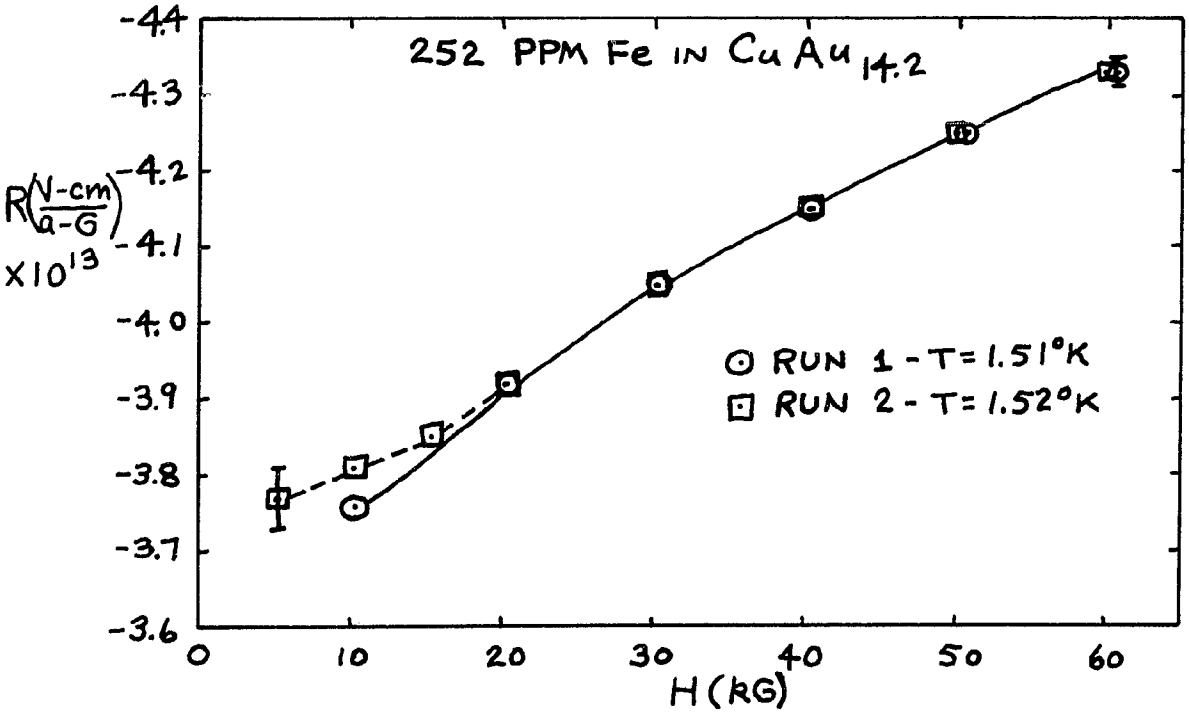

FIGURE 43

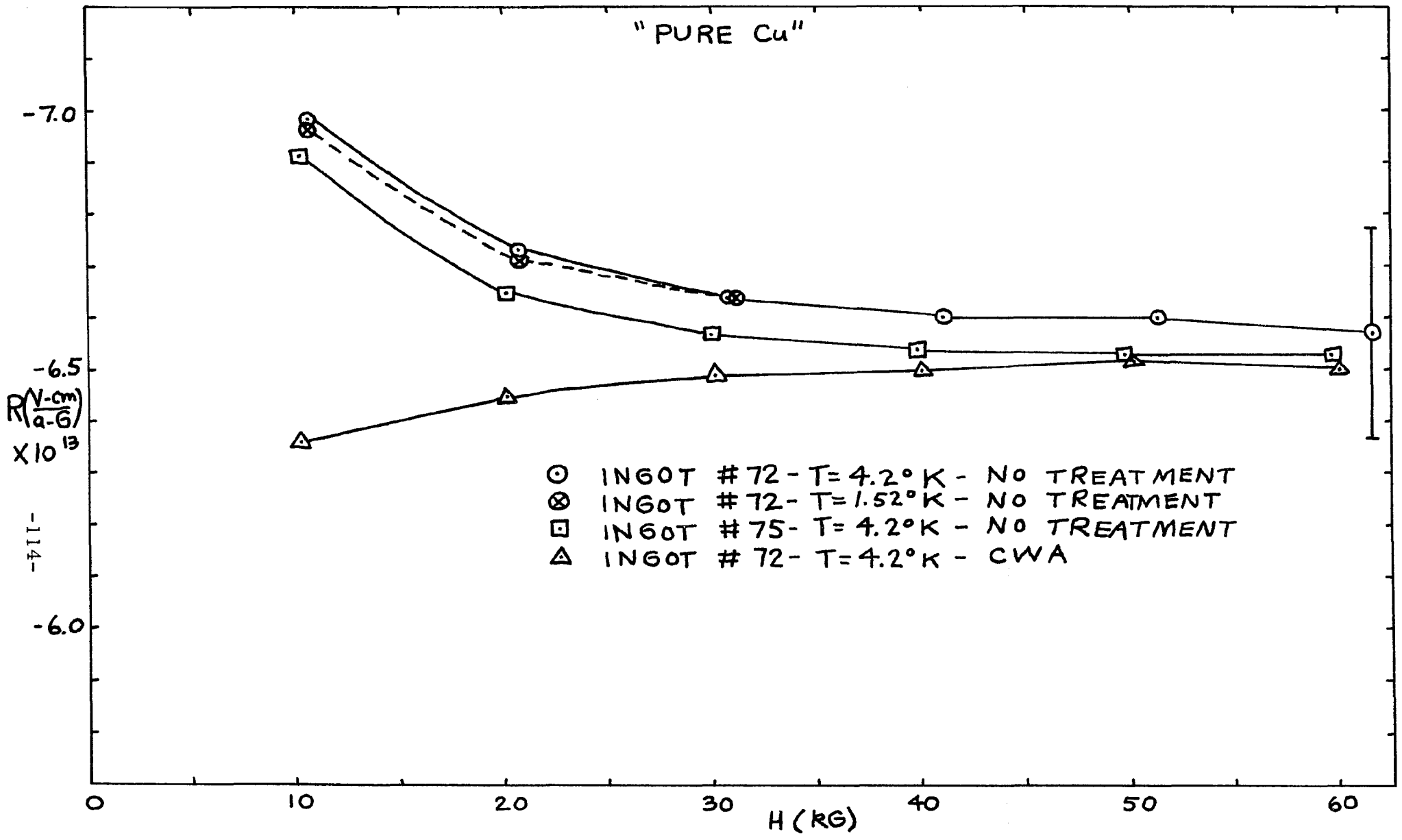
"PURE Cu"
-7.0
-6.5
-6.0
R(V-cm/a-G) X 10^13
0
10
20
30
40
50
60
H (KG)
INGOT #72 - T= 4.2° K - NO TREATMENT
INGOT #72 - T= 1.52° K - NO TREATMENT
INGOT #75 - T= 4.2° K - NO TREATMENT
INGOT #72 - T= 4.2° K - CWA

FIGURE 44

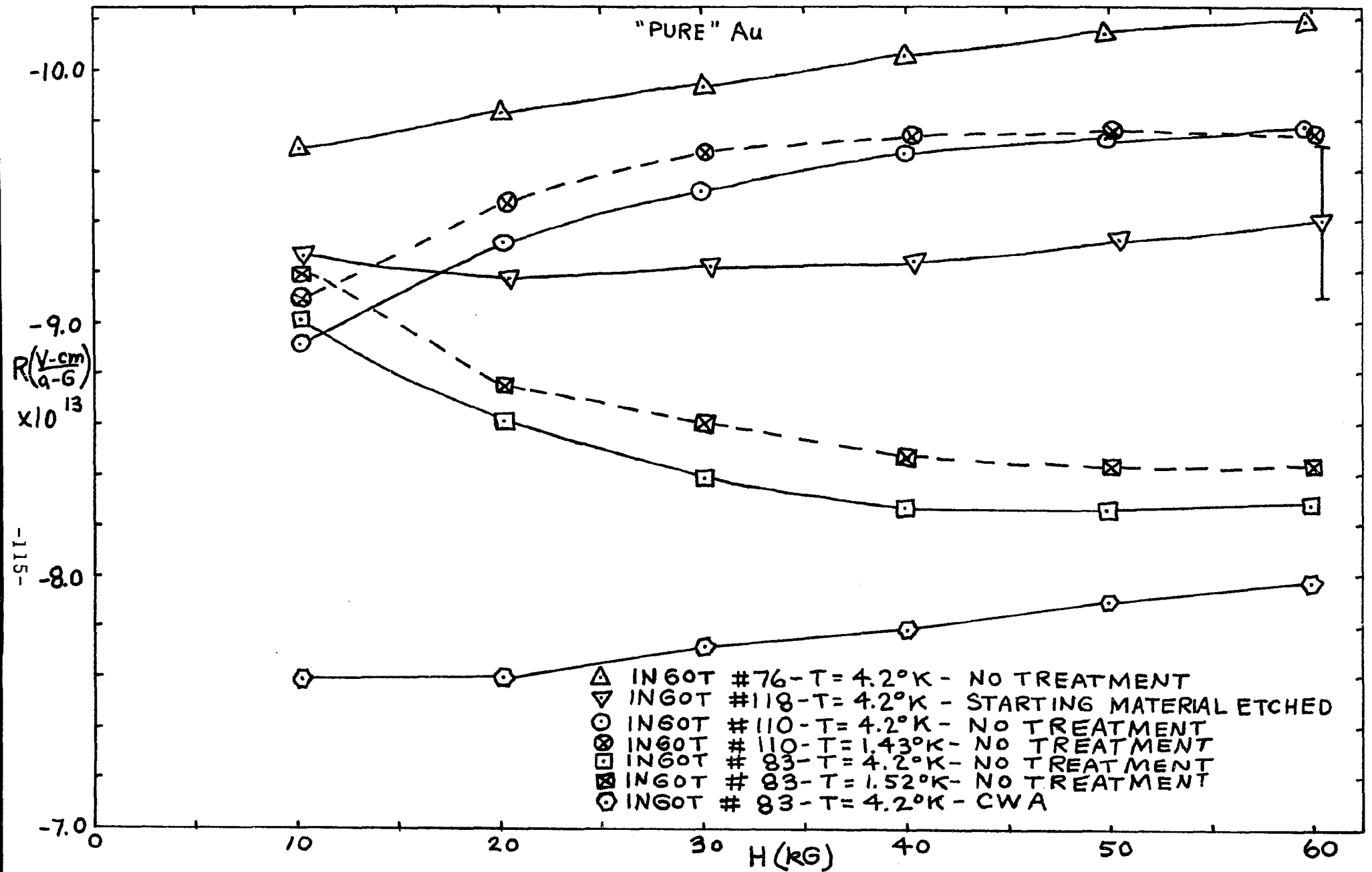
"PURE" Au
-10.0
-9.0
-8.0
-7.0
R(V-cm/a-G) x10^13
0
10
20
30
40
50
60
H(kG)
INGOT #76 - T = 4.2°K - NO TREATMENT
INGOT #118 - T = 4.2°K - STARTING MATERIAL ETCHED
INGOT #110 - T = 4.2°K - NO TREATMENT
INGOT #110 - T = 1.43°K - NO TREATMENT
INGOT # 83 - T = 4.2°K - NO TREATMENT
INGOT # 83 - T = 1.52°K - NO TREATMENT
INGOT # 83 - T = 4.2°K - CWA

FIGURE 45

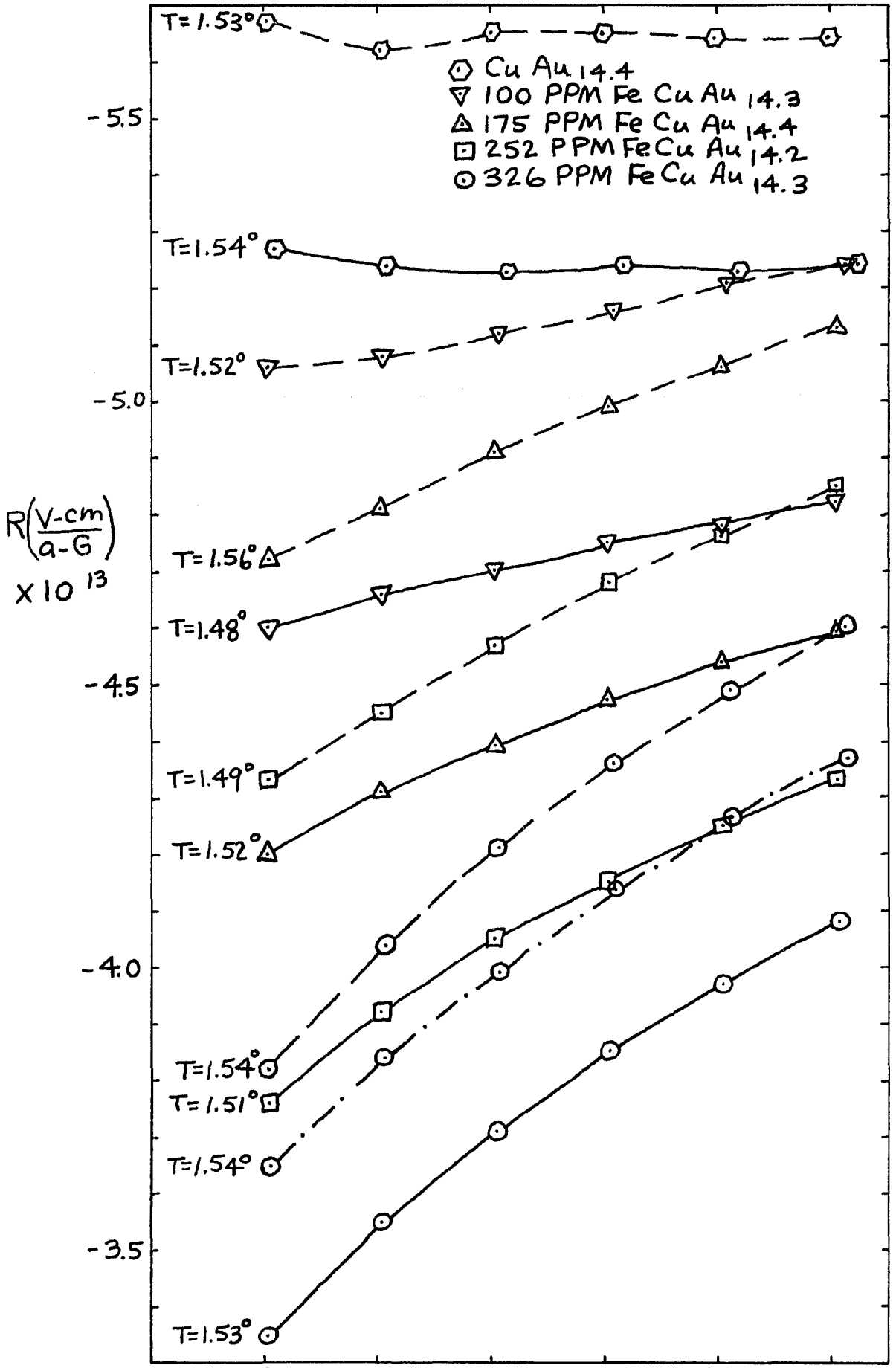
T= 1.53°
Cu Au 14.4
100 PPM Fe Cu Au 14.3
175 PPM Fe Cu Au 14.4
252 PPM Fe Cu Au 14.2
326 PPM Fe Cu Au 14.3
T=1.54°
T=1.52°
T=1.56°
T=1.48°
T=1.49°
T=1.52°
T=1.54°
T=1.51°
T=1.54°
T=1.53°
-5.5
-5.0
-4.5
-4.0
-3.5
R(V-cm/a-G) X 10 13
0
10
20
30
40
50
60
H(KG)

FIGURE 46

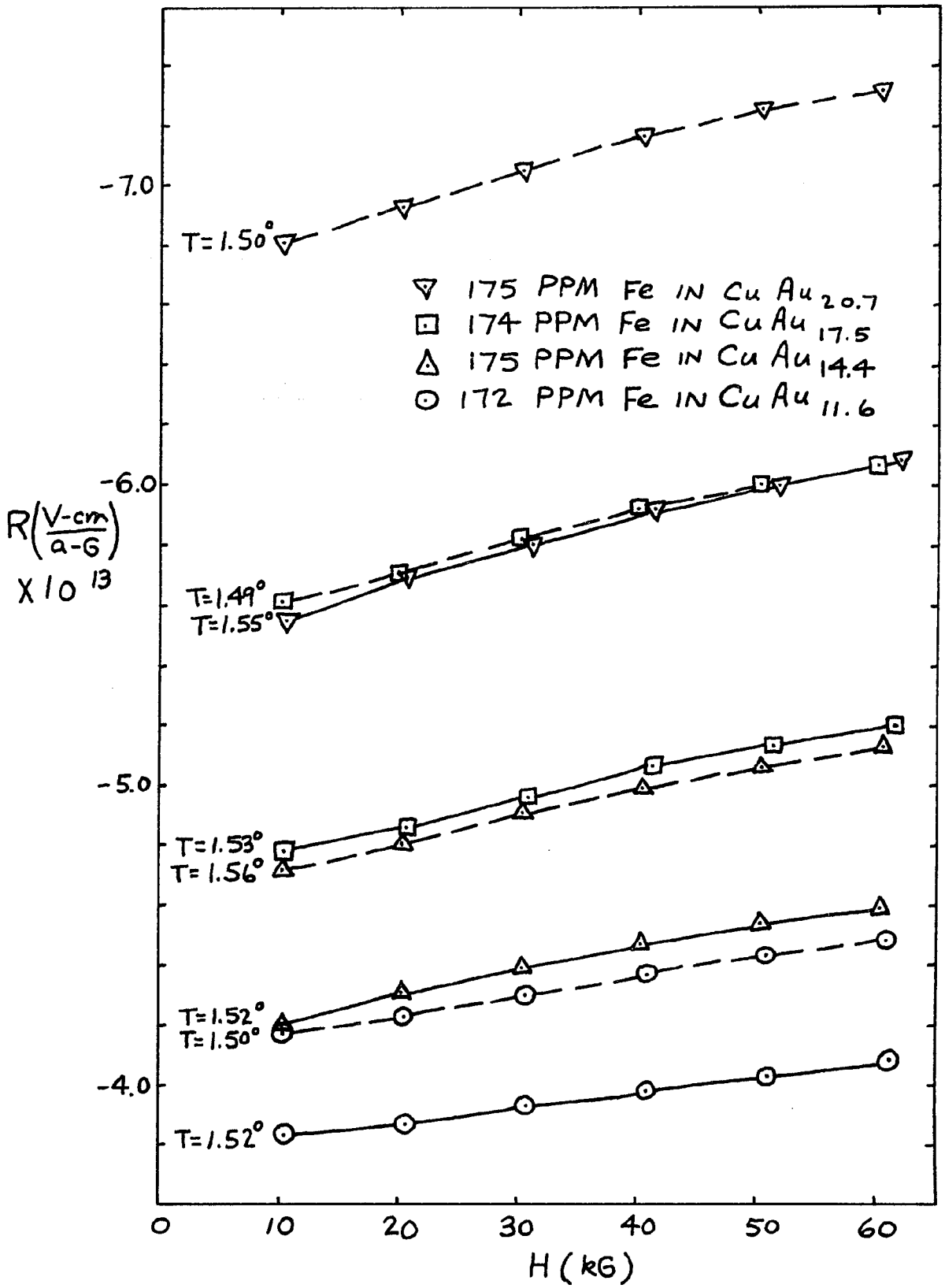
-7.0
-6.0
-5.0
-4.0
R(V-cm/a-G) X 10 13
T=1.50°
175 PPM Fe IN Cu Au 20.7
174 PPM Fe IN Cu Au 17.5
175 PPM Fe IN Cu Au 14.4
172 PPM Fe IN Cu Au 11.6
T=1.49°
T=1.55°
T=1.53°
T=1.56°
T=1.52°
T=1.50°
T=1.52°
0
10
20
30
40
50
60
H (kG)

FIGURE 47

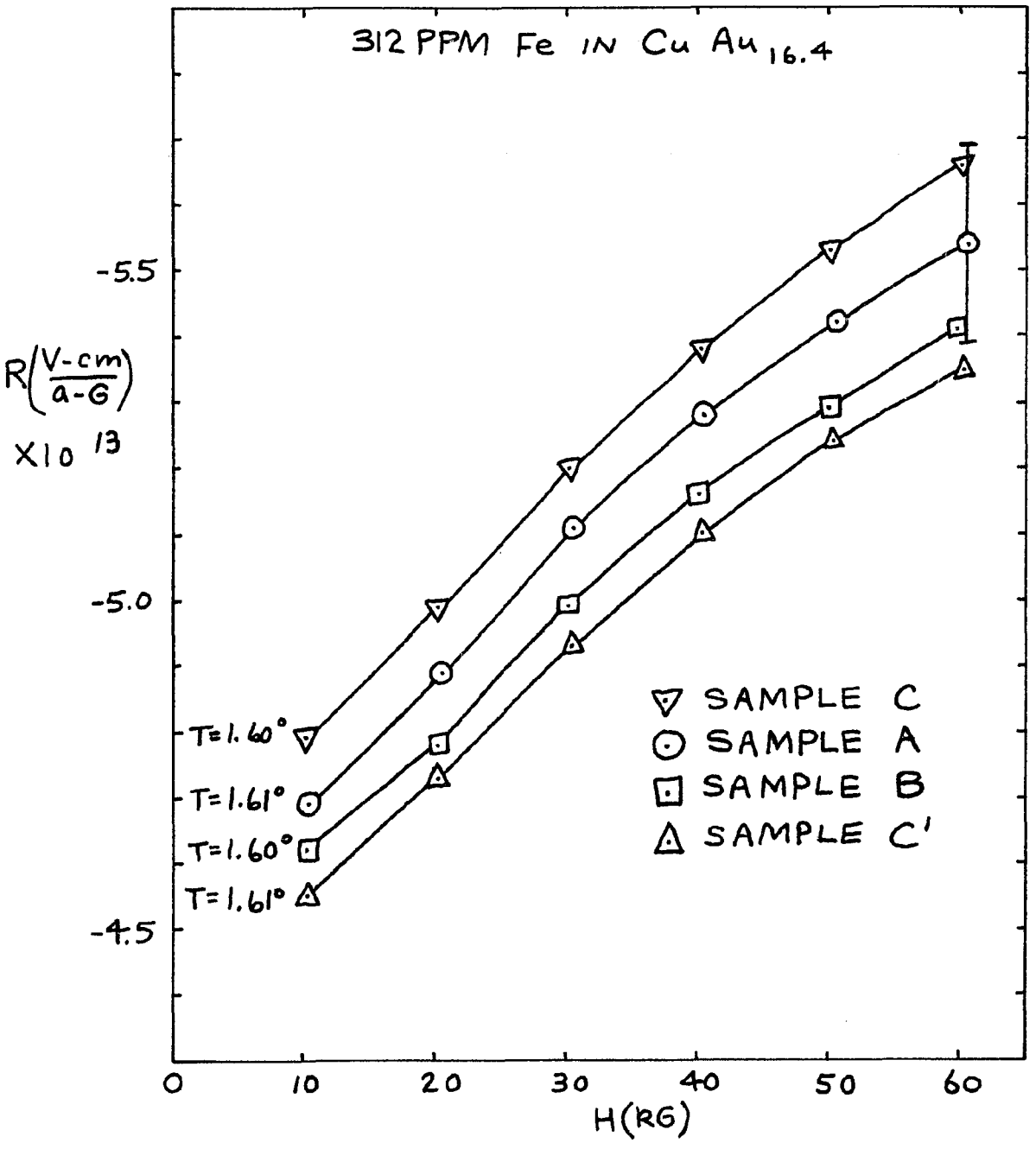
312 PPM Fe IN Cu Au 16.4
-5.5
R(V-cm/a-G)
X10 13
-5.0
-4.5
T=1.60°
T=1.61°
T=1.60°
T=1.61°
SAMPLE C
SAMPLE A
SAMPLE B
SAMPLE C'
0
10
20
30
40
50
60
H(KG)

FIGURE 48

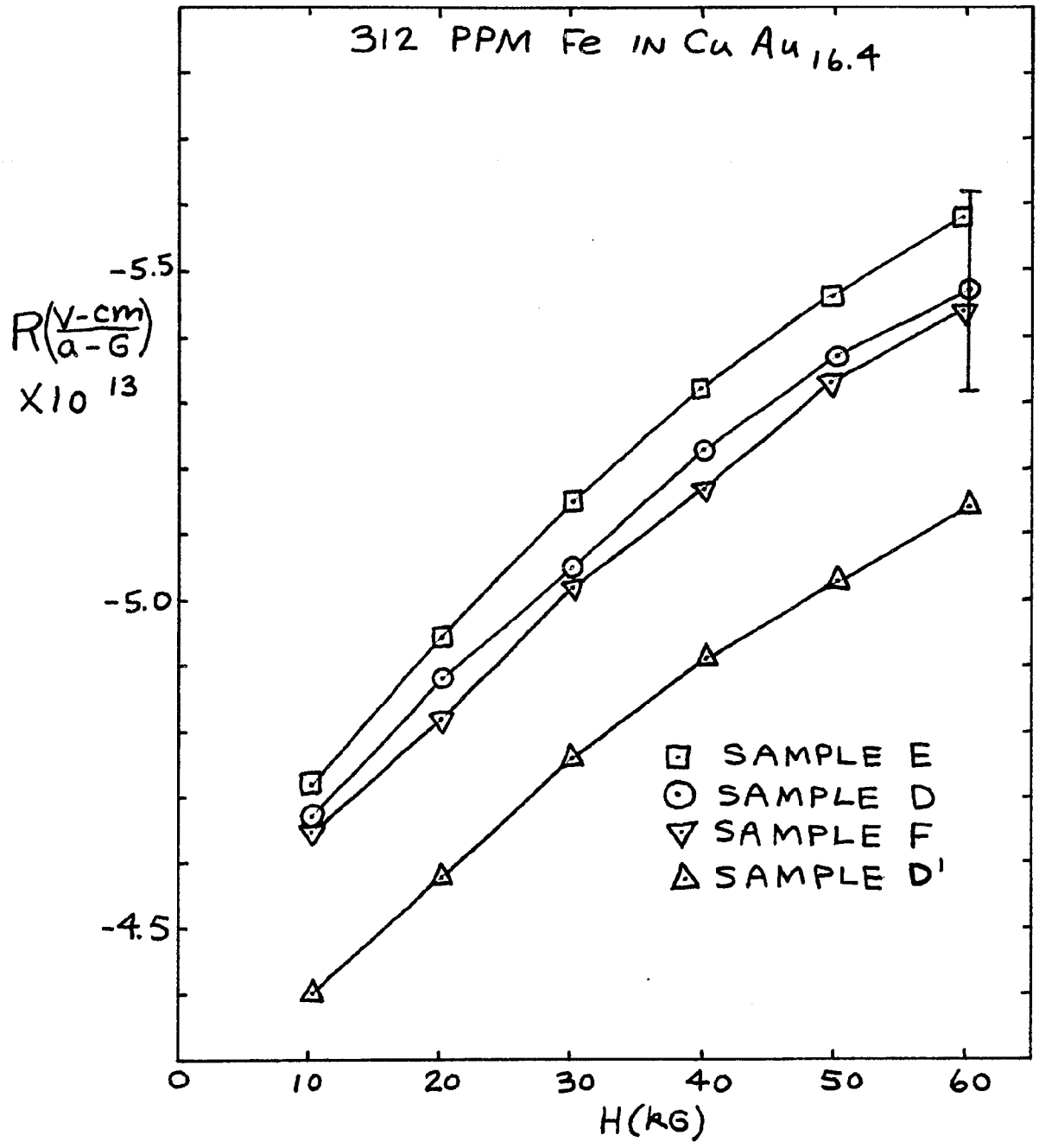
312 PPM Fe IN Cu Au 16.4
R(V-cm/a-G)
X10 13
-5.5
-5.0
-4.5
0
10
20
30
40
50
60
H(kG)
SAMPLE E
SAMPLE D
SAMPLE F
SAMPLE D'

FIGURE 49

	Cu	Ag	Au
$R_{observed} \times 10^{11}$ $m^3/a \cdot s$	-5.12	-8.81	-7.16
$R_{free\ electron} \times 10^{11}$ $m^3/a \cdot s$	-7.45	-10.65	-10.60

TABLE 1

Ingot Number	at. % Au	Nominal at. PPM Fe	Analyzed at. PPM Fe
72	0	0	1±.5 *
113	5.0	401	430±22
112	5.0	801	830±41
50	11.6	172	185±10
41	14.3	100	80±4
40	14.4	175	193±10
38	14.2	252	313±16
37	14.3	326	345±17
53	17.5	174	184±10
51	17.4	224	266±13
54	20.7	175	188±10
81	40.0	100	84±13
79	60.0	100	111±13
84	60.0	201	211±13
95	60.0	100	90±13
96	60.0	200	185±13
115	70.0	51	45±11 *
74	80.0	45	79±13
77	80.0	100	79±13
116	88.0	62	55±13 *
117	88.0	36	32±10 *
119	95.0	37	34±10 *
118	100.0	0	7±4 *

TABLE 2

Ingot Number	at. % Au	at. PPM Fe	RRR
72	0	0	460
75	0	0	420
114	5.0	0	1.83½
113	5.0	401	1.52
112	5.0	801	1.62
63	11.6	0	1.39
50	11.6	172	1.37
49	14.4	0	1.32
41	14.3	100	1.31½
40	14.4	175	1.31
38	14.2	252	1.30
37	14.3	326	1.30
61	17.5	0	1.28
53	17.5	174	1.27
51	17.4	224	1.26½
62	20.7	0	1.25
54	20.7	175	1.24
80	40.0	0	1.20
81	40.0	100	1.20
78	60.0	0	1.32½
79	60.0	100	1.27
84	60.0	201	1.34
109	60.0	0	1.28
95	60.0	100	1.23
96	60.0	200	1.25½
107	70.0	0	1.27
115	70.0	51	1.26
73	80.0	0	1.38
74	80.0	45	1.35
77	80.0	100	1.34½
111	88.0	0	1.57
116	88.0	62	1.55
117	88.0	36	1.55
85	95.0	0	2.26
119	95.0	37	2.21
83	100.0	0	108
110	100.0	0	86
118	100.0	0	86

TABLE 3

at. % Au	at. PPM Fe	s
5.0	801	0.75
11.6	172	0.56
14.4	175	0.52
14.2	252	0.55
17.5	174	0.51
17.5	224	0.55
20.7	175	0.52
40.0	100	0.56

TABLE 4

Pressure (mm)		T Pressure (^{o} K)		T Therm. (^{o} K)
atmos.		4.22		4.22
22.2		1.98		1.99
10.0		1.74		1.74
6.4		1.63		1.62
5.9½		1.61		1.60½
5.7½		1.60		1.60
5.2		1.58		1.58
5.0		1.57		1.56½
4.4		1.54		1.53½
4.0		1.52		1.51½
3.6½		1.50		1.50
3.3½		1.49		1.49
3.1		1.47		1.47½

TABLE 5

REFERENCE	$R(10^{-13}\ \frac{V\text{-}cm}{a - G})$
10	-6.7± .1
39	-6.2
42	-6.88
43	-6.9
44	-6.5± .04

TABLE 6

Sample		$\frac{R(2^{\circ}\,K) - R(T\ min)}{R(T\ min)}$		T min
A OUTER		.00073		$10\frac{1}{2}^{\circ}$ K
A INNER		.00481		17° K
B OUTER		.00420		$15\frac{1}{2}^{\circ}$ K
B INNER		.00422		16° K
C OUTER		.00400		$16\frac{1}{2}^{\circ}$ K
C INNER		.00439		$16\frac{1}{2}^{\circ}$ K
C' INNER		.00494		16° K

TABLE 7

BIBLIOGRAPHY.

1. Alderson, J.E.A., Farrell, T., Hurd, C.M., Phys. Rev. 1, 3904 B (1970).

2. Alderson, J.E.A., Farrell, T., Hurd, C.M., Phys. Rev. 174, 729 (1968).

3. Alderson, J.E.A., Hurd, C.M., J. Phys. Chem Solids 32, 2075 (1971).

4. Anderson, P.W., Phys. Rev. 124, 41 (1961).

5. Barnard, R.D., et. al., Phys. Rev. 176, 761 (1968).

6. Barnard, R.D., and Sumner, L., Phil. Mag. 20, 399 (1969).

7. Beal-Monod M.T., and Weiner, R.A., Phys. Rev. 3, B3056 (1971).

8. Beal-Monod, M.T., and Weiner, R.A., Phys. Rev. 3, B145 (1971).

9. Berg, G.J. Van den, in 'Progress in Low Temperature Physics' (G.J. Gorter Ed.) vol. 4 Chapt. 4. North Holland Publishing Company, Amsterdam (1964).

10. Berlincourt, T.G. Phys. Rev. 112, 381 (1958).

11. Blandin, A., and Friedel, J., J. Phys. Red. 20, 160 (1959).

12. Bloomfield, P.E., Hecht, R., and Sievert, P.R. Phys. Rev. 2, B 3714 (1970).

13. Chambers, R.G., Proc. Roy. Soc. (London) A238, 344 (1957).

14. Cracknell, A.P., Adv. Phys. 20, 1 (1971).

15. Daybell, M.D., and Steyert, W.A., Rev. Mod. Phys. 40, 380, (1968).

16. Dugdale, J.S., Firth, L.D., J. Phys. C. (Solid State Phys.) 2, 1272 (1969).

17. Fenton, E.W., Phys. Rev. 5, B3788 (1972).

18. Freidel, J., Nuovo Cimento Supplement 7, 287 (1958).

19. Freidel, J., 'Metallic Solid Solution' (J. Friedel and A. Guinier, Eds.) Benjamin, New York, (1963).

20. Hall, E.H., Am. J. Math. 2, 287 (1879).

21. Halse, M.R., Phil. Trans. R. Soc. 265, 507 (1969).

22. Heeger, A.J., 'Solid State Physics' (Seitz, F., Turnbull, D., Ehrenreich, H., Eds.) Vol. 23, p. 183, Academic Press, New York (1969).

23. Heine, V. Phil. Mag. 12, 53 (1965).

24. Huppmann W., Stangler, F., Phys. Stat. Sol 35, K 161 (1969).

25. Hurd, C.M., Phil. Mag. 12, 47 (1965).

26. Hurd, C.M. 'The Hall Effect in Metals and Alloys' Plenum Press, New York, 1972, pp. 184-189.

27. Isenberg, I.,Russel, B.R., Green, R.F., Rev. Sci. Inst. 19, 685 (1948).

28. Kondo, J. in 'Solid State Physics' F. Seitz, D. Turnbull, H. Ehrenreich, Eds.) Vol. 23, p. 183, Academic Press, New York, 1969.

29. Kondo, J. Prog. Theor. Phys. 32, 37 (1964).

30. Loram, J.W., Whall, T.E., Ford, P.J., Phys. Rev. 2,B857 (1970).

31. More, R., Solid State Comm. 7, 237 (1969), and R. More's Thesis.

32. Nagaoka, Y., Phys. Rev. 138, A1112 (1965).

33. Sarachik, M.P., J. Appl. Phys. 35, 1094 (1964).

34. Sarachik, M.P., Corenzwit, E., and Longinotti,L.D., Phys. Rev. 135, A1041 (1964).

35. Schrieffer, J., J. Appl. Phys. 38, 1143 (1967).

36. Seitz, F., Modern Theory of Solids , McGraw Hill, New York, 1940, p. 40.

37. Springford, M., Adv. Phys. 20, 493 (1971).

38. Ziman, J.M., Adv. Phys. 10, 1 (1961).